공학박사학위논문

Theoretical and Empirical Approaches to Fabricating Ultrahigh Strength Carbon Nanotube Yarns

초고강도 탄소나노튜브 섬유 제조를 위한 이론 및 실험적 연구

2018년 8월

서울대학교 대학원

재료공학부

정 연 수

Abstract

Theoretical and Empirical Approaches to Fabricating Ultrahigh Strength Carbon Nanotube Yarns

Yeonsu Jung

Department of Materials Science and Engineering

The Graduate School

Seoul National University

The purpose of this study is to fabricate ultrahigh-strength carbon nanotube yarns (CNTYs) for which the mechanical properties exceed those of conventional high-performance fibers through theoretical and empirical approaches for manufacturing high-strength CNTYs. Due to the inherently superb mechanical properties and high aspect ratios of CNTs, efforts to produce ultrahigh-strength CNTYs which properties that exceed those of conventional high-strength fibers such as carbon fibers have continued over the last few decades. As a result, a variety of CNTY fabrication methods have been developed since the early 2000s up to the present, and it is now possible to produce continuous CNTYs with these methods. Nevertheless, macroscale CNTYs still fail to exhibit the excellent mechanical performance of nanoscale

individual CNTs. To overcome these limitations, various attempts to improve the mechanical strength of CNTYs have recently been proposed. The mechanical and electrical properties of CNTs differ depending on certain aspects of the nanostructure, such as the length, number of walls, and the diameter of the nanotubes. In addition, the microstructure of the CNT assembly is closely related to the mechanical and electrical properties of the assembly. Therefore, the most important issue is to control the nanostructure of CNTs and the microstructure of the CNT assembly in order to fabricate ultrahigh-strength CNTYs.

Chapter 1 briefly describes the CNTYs and related factors that affect the mechanical properties of yarns. The purpose of this study is to review recent studies on improving these mechanical properties and to uncover issues and solutions that are thus far unresolved.

Chapter 2 introduces and presents the attempts made to derive the theoretical correlation between the structure and the CNTY strength based on the failure mechanism of CNTYs. First, the relationship between the structural parameters of the nanostructures of individual CNTs, the basic constituents of yarns, and the mechanical strength of the CNTYs is investigated. The effect of the microstructure of the CNT assembly on the strength of CNTYs is then theoretically considered.

Chapters 3 and 4 discuss the influence of the structural factors of CNTs as derived from chapter 2 on the yarn strength. The effect of the nanostructure of the carbon nanotubes on the mechanical properties of CNTYs is investigated by undertaking the synthesis CNTYs made of CNTs with various nanostructures, after which the effects of polymer chains on the internal structures of CNTYs and the yarn deformation behaviors are studied.

Finally, chapter 5 discusses developments related to ultrahigh-strength CNTYs through crosslinking considering the nanostructures and microstructures of CNTs based on the theoretical and empirical understanding presented in the previous chapter.

Keywords: carbon nanotube, yarn, ultrahigh strength, microstructure, nanostructure, mechanical property, structural material, crosslinking
Student Number: 2013-30186

Contents

List of Tables

List of Figures

Chapter 1 Introduction

1.1 Overview of carbon nanotube yarns (CNTYs)

Carbon nanotubes (CNTs), composed of a network of sp^2 hybridized carbons have shown outstanding thermal, electrical and mechanical properties. The excellent mechanical properties, viz. the theoretical tensile strength of 60 GPa and modulus of 1 TPa [1-3], and the one-dimensional morphological features with a high aspect ratio, are very attractive, particularly when considered as nano-reinforcements for nano-composites or as basic building blocks for high-performance CNT yarns (CNTYs) [4-13]. However, in practice, such unprecedented advantages of CNTs have not been realized regardless of CNTs have been applied, i.e., either in nano-composites or in CNTYs [14-17]. For example, in nanocomposites composed of a polymer matrix and CNTs, the tensile strength increased to 4.9 GPa with the amount of CNT loading up to 1~10 wt% but decreased soon after and acted as brittle materials. This was typically ascribed to the poor dispersion and weak interaction of CNTs with the polymer matrix [4-8, 13, 18-20]. In the case of CNTYs, on the other hand, the tensile strength ranged from 0.05 to 5.53 GPa, though this is far below the theoretical tensile strength of CNTs depending on the preparation process used.

1.2 Theoretical consideration of the tensile strength of CNTYs

Two theories have been the most typical and commonly accepted in order to understand the key parameters influencing the mechanical properties of CNTYs, although a few theoretical works have been carried out to predict the mechanical properties of CNTYs [21-23].

First, CNTY is commonly considered as a one-dimensional material composed of interlocked elementary fibers, i.e., CNTs [21, 24-26]. Thus, the tensile strength ratio of the yarn to the elementary fiber has been estimated by the classical yarn mechanics theory [22] described by equation (1.1),

$$\frac{\sigma_{yarn}}{\sigma_{fiber}} \approx cos^2\alpha[1-(k\ \mathrm{cosec}\ \alpha)] \quad (1.1)$$

where σ_{yarn} and σ_{fiber} are the strength of the CNTY and the elementary fiber, viz. CNT.

Fig. 1.1 shows the dependence of the yarn strength and the value of k on the twist angle (α) (Fig. 1.1a), and diameter (d) (Fig. 1.1b) of the elementary fibers (CNTs) according to equation (1.1). The term $cos^2\alpha$ describes a gradual decline of the yarn strength as the twist angle of the elementary fibers, α, increases. However, the second term *[1-(k cosec α)]* compensates for the drop-off effect of the yarn strength due to the increased transverse force by twisting. As the twist angle increases the distance between the CNTs become closer and the degree of yarn compaction becomes higher, resulting in the strengthening of the inter-tubular interactions. Here, the term

$k=(dQ/\mu)^{0.5}/3L$, where d is the diameter of elementary fiber, Q is the migration length of the fibers from the yarn surface to the inside, μ is the friction coefficient of the fiber with the neighboring fibers and L is the length of the fiber, describes a contribution factor of the unit length of elementary fibers. Equation (1.1) expresses that a smaller diameter, shorter migration length, higher friction coefficient and a longer length of the elementary fibers are beneficial requirements to make the stronger yarns.

Although equation (1.1) suggests that the longer and thinner the elementary CNTs are the stronger the CNTY would be, this equation does not appear to be feasible when applied to a practical CNTY due to two factors. The first is the dimensional difference and the second is the deformability of CNTs. Indeed, in the equation derived originally for cotton or woolen yarns, the elementary fibers, given their micron-sized diameters and lengths measurable in millimeters, were considered as non-deformable cylinders of a uniformly specific volume with a circular cross-section, whereas actual CNTs with nanometer-sized diameter and length of a few tens of microns are deformable, with the deformability depending on the structural parameters, in this case the diameter of the CNTs.

It should be noted that equation (1.1) suggests the importance of the shear strength and the length of the elementary CNTs when attempting to make CNTYs stronger, as reflected in the terms L, μ, and τ_F. As the shear strength of elementary CNTs in a practical CNTY is a function of the contact area between the neighboring CNTs, which is again a function of multiple variables, such as the length, tortuosity, surface roughness, orientation, twist angle, and degree of crosslinking, among others, it is necessary when attempting to realize stronger CNTYs to gain a deep understanding of the influence of these parameters on how the strength of CNTYs is improved.

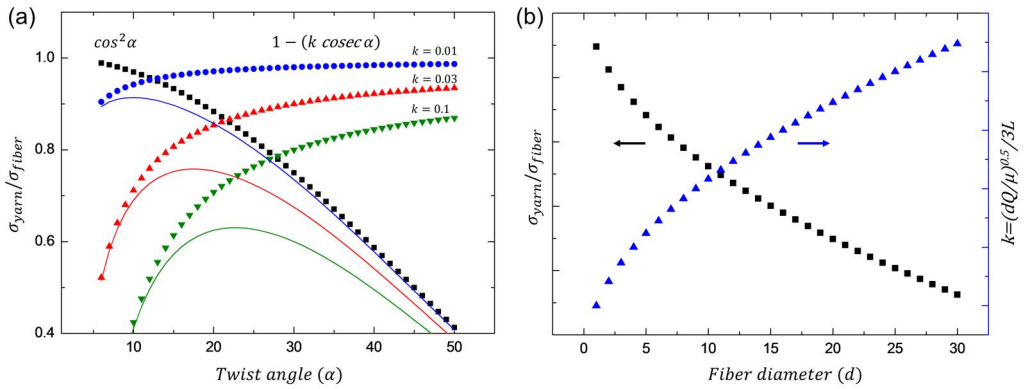

Fig. 1.1. Theoretical dependence of the strength ratio of yarn to fiber (solid line) on (a) the twist angle (symbols denote the influence of the twist angle on each term) and (b) the fiber diameter according to equation (1.1).

1.3 The state-of-the-art tensile performance of CNTYs

1.3.1 Effect of different yarn formation processes on tensile performance of CNTYs

CNTYs are prepared typically through fiber spinning processes including rotary spinning as in the formation of cotton yarn and extrusion spinning as in the wet or melt spinning of polymeric materials. A typical form of the wet-spinning of CNTYs, reported by Ericson et al. in 2004 [27], involved the extrusion of a spinning dope composed of a high concentration of single-walled CNTs (SWCNTs) in a 102 % sulfuric acid solution, which behaved as liquid crystal. Dry-spun CNTYs can be prepared either by spinning vertically grown CNT arrays [24, 28, 29] or by directly spinning in-situ grown CNTs via the floating-catalyst chemical-vapor-deposition (FCCVD) process [30-32]. Fig. 1.2 illustrates the typical processes used to form CNTYs.

The tensile performance capabilities of CNTYs vary in widely with different yarn formation processes because the intrinsic structural characteristics of elementary CNTs, e.g., the length and diameter, among others, and the extrinsic structural features of CNTYs such as orientation, twist angle, and type of bundling are all different depending on the yarn formation process adapted. This is shown in Table 1.1, which illustrates the variations in the structural parameters of CNTs and the resulting tensile performance parameters of CNTYs. It is not obvious from Table 1.1 if there are any clear correlations between the tensile performances of CNTY and the structural parameters. In other words, although the theories considered above suggest that longer and thinner CNTs would lead to the formation of stronger CNTYs, the actual data do not appear to show such a correlation clearly. This implies that it is necessary to look

into the details of the influence of each parameter and to determine if there would be other factors, such as the degree of compaction of the CNTs, which influence the tensile performance capabilities of CNTYs.

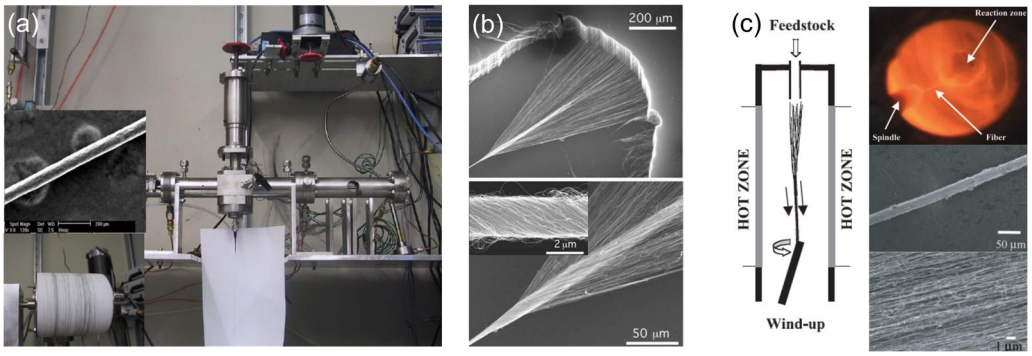

Fig. 1.2. CNTY formation process: (a) Wet spinning from [1]. (b) Dry spinning from vertically grown CNT array from [2]. (c) In-situ Direct spinning by FCCVD from [30]. (a-c) Reprinted with permission from AAAS.

Table 1.1. Variations of the structural parameters of CNTs and the resulting tensile performances of CNTY with different types of yarn formation processes.

Ref	Process	Structural parameter				Mechanical performance		
	Spinning method	Length (μm)	Diameter (nm)	Number of walls	Alignment* / Twist angle (°)	Strength (GPa) / Specific strength (GPa/(g cm^{-3}))	Modulus (GPa)/Specific modulus (GPa/(g cm^{-3}))	Strain (%)
[27]	Liquid crystal	-	-	1	- / -	0.12 / -	120 / -	-
[33]	Liquid crystal	4.3	2-4	2-3	0.99 / -	1.0 / 0.77	120 / 92.3	1.4
[34]	Liquid crystal	100	50	>50**	0.92 / -	0.15 / -	69 / -	2.5
[35]	CNT array	260	≤6	≥17	- / 15-20	1.17 / -	53.5 / -	~3
[36]	CNT array	650	~10	~9	- / 21	1.91 / -	330 / -	7.02
[37]	CNT array	2100	~40	~30	- / 25	0.77 / 0.62	51.1 / 41.2	~2
[38]	CNT array	250	~15	~15**	- / 7.7~9.2	1.6 / -	110 / -	~1.4
[39]	Direct spinning	-	4-10	2	~0.8 / -	0.86 / 0.95***	357 / 397	4-8
[40]	Direct spinning	-	-	1	- / -	- / 0.85	- / 37.4	~5
[41]	Direct spinning	-	2-7	≥2	0.81 / -	0.36 / -	- / -	22-25
[31]	Direct spinning	-	8-10	2	0.86 / -	1.25 / 0.75	~66.8 / ~40	~18

*Degree of alignment determined by XRD diffractograms
**Calculated assuming an interlayer distance of 0.34 nm
***Average values measured with a gauge length of 20 mm

1.3.2 Effect of elementary CNT structure on CNTY strength

1.3.2.1 Length of CNTs

In the theories to predict the tensile strength of CNTYs one of the most influential parameters is the interaction energy between the CNTs that dissipates the crack propagation energy based on the slippage failure mechanism. For this reason there have been many efforts to synthesize long CNTs so as to increase the interaction forces by extending the contact area between the CNTs with weak shear strength [28, 36, 42-44]. For example, CNT arrays 2.2 cm [45] or 4.7 mm [28] long were successfully synthesized, but only CNTs in the range of 0.5~1.5 mm could be spun into a yarn. Zhang et al. [36] and Ghemes et al. [37] prepared CNT arrays with lengths in the range of 0.3~2 mm which were spun into yarns. Fig. 1.3 clearly illustrates that the strength of the CNTY increases linearly with the length of the elementary CNTs with an additional effect on this increase by a post-twisting step.

It is crucial to note here that despite a clear correlation, the strength of the resulting CNTYs from millimeter-long CNTs as shown in Fig. 1.3b, is lower than that of micrometer-long CNTs as presented in Fig. 1.3a. This result indicates that if structural characteristics other than the length of the elementary CNTs are identical, a linear correlation becomes true. In other words, there operate other structural parameters such as the tube diameter and the number of walls which affect the evolution of the strength of CNTYs.

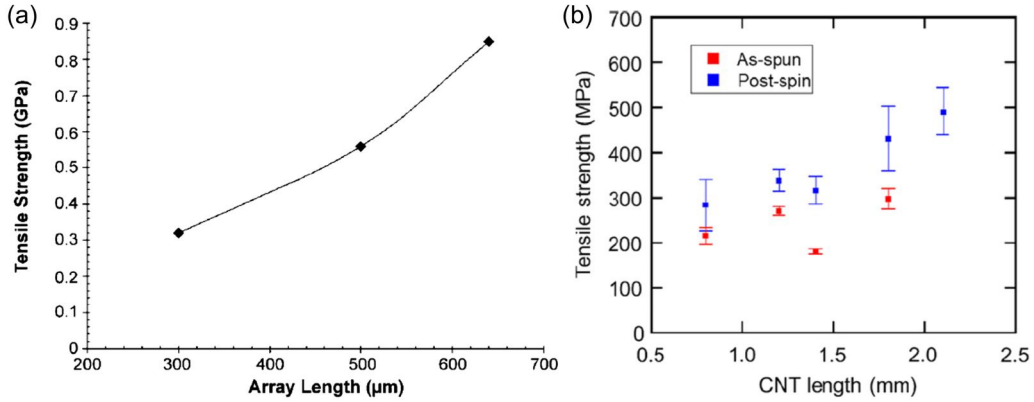

Fig. 1.3. Dependence of tensile strengths of MWCNTYs on the length of elementary CNTs: (a) in micron scale [36, 37] and (b) in millimeter scale [35], Reproduced with permission. Copyright 2012, Elsevier.

1.3.2.2 Diameter and number of walls of CNTs

Given the length of elementary CNTs, the strength of the resulting CNTYs varies significantly with the diameter and the number of walls of the CNTs, thus determining the extent of inter-tubular interactions. Jia et al. [35] elaborately controlled the synthesis conditions in their effort to synthesize CNT arrays with different numbers of walls ranging from a few walls (2-3) to multiple walls (>15) and lengths in the range of 260~1000 μm. They tested the strength of the resulting CNTYs with controlled diameters of 10-15 μm and twist angles of 15-20°.

From Table 1.2, it is clear that the highest strength of CNTYs is achieved when the elementary CNTs have the smallest diameters and fewest walls. Using the data in Table 1.2, we calculated the parameters in equations (1.1), i.e., L/D, and $L/D^{0.5}$, and plotted them in relation to the yarn strength as shown in Fig. 1.4.

According to classical yarn mechanics, equation (1), and theories pertaining to fiber-reinforced composites, the strength depends on $L/D^{0.5}$ or the aspect ratio, L/D, of elementary CNTs. However, Fig. 1.4 clearly shows that both models failed to describe the relationship between the structural features of the elementary CNTs and the resultant CNTY strength.

Table 1.2. Effect of diameter and number of walls of elementary CNTs on the tensile strength of resulting CNTYs. Adapted from ref. [35]. Copyright 2011, Elsevier.

Carbon source	C_2H_2- I	C_2H_2- II	C_2H_4	C_2H_2-CM
Tube diameter (nm)	8-10	8-10	< 6	> 17
Number of walls	8-10	~ 6	2-3	> 15
I_G/I_D	0.88	0.99	1.27	1.65
Length (μm)	320	320	260	1000
Strength (MPa)	689	866	1170	383
Modulus (GPa)	10.1	16.0	53.5	6.5

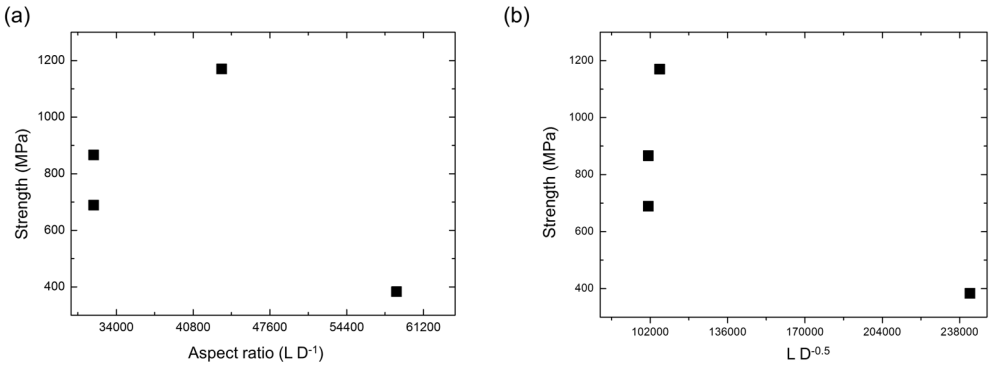

Fig. 1.4. Yarn strength as a function of the different variables of L/D and $L/D^{0.5}$. Here, the data in Table 1.2 were used to calculate the value of each variable.

1.3.2.3 Alignment of CNTs

Apart from the intrinsic structural characteristics of elementary CNTs, there are other factors influencing the strength of CNTYs, as indicated well by conventional yarn mechanics. Those include the orientation and twist angle of the elementary CNTs along the loading axis, which crucially influence the compaction of the elementary CNTs, viz. the load-bearing efficiency.

During the wet spinning of CNTY, the orientation of elementary CNTs can be enhanced by using a spinning dope, where CNTs form a lyotropic-nematic liquid crystalline-like phase [10, 25, 45]. During the direct spinning process, CNTs assemble in-situ in a gas phase into a yarn form. Alemán et al. [40] demonstrated a means of controlling the alignment of the elementary CNTs in the resulting yarn by diluting the concentration of the CNTs in a reactor as shown in Fig. 1.5. The concentration of CNTs in the reactor critically determines the draw ratio of the CNT aerogel and the orientation of the elementary CNTs in the resulting CNTYs. With a low feed rate of the carbon source for CNT synthesis and a high draw ratio up to 18 the specific strength of the resulting CNTYs was improved from 0.3 to 1 GPa/SG [40].

The winding speed of the yarn is also an effective variable when attempting to control the alignment of elementary CNTs in the yarn [39] as shown in Fig. 1.6. By controlling the winding speed, an extremely high specific strength of 10 N/tex (equivalent to 10 GPa/SG), of CNTYs was obtained at a short gauge length of 1 mm.

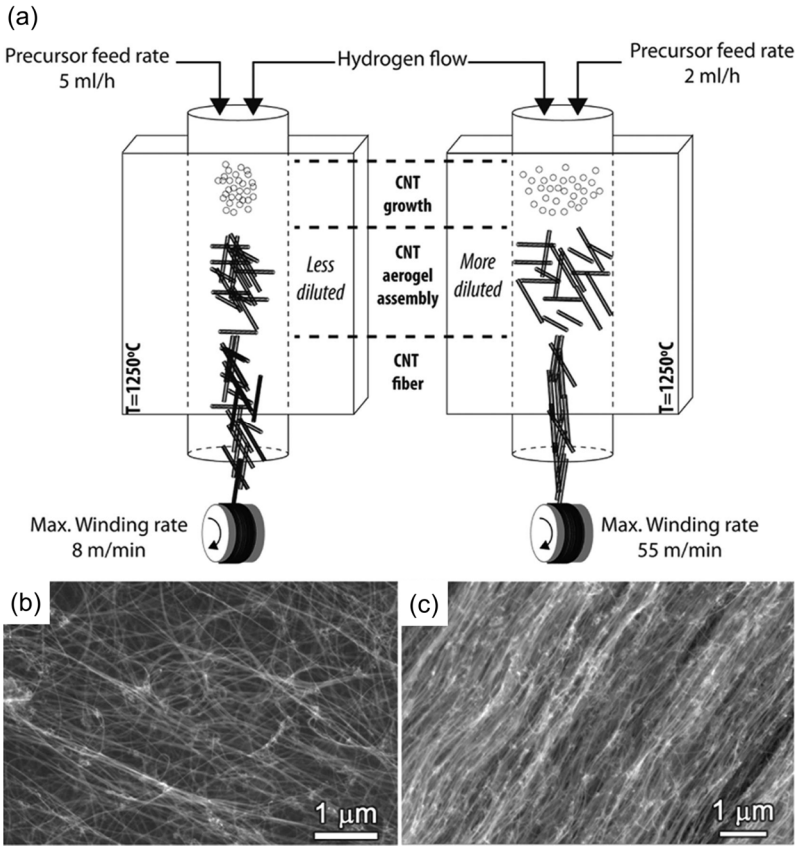

Fig. 1.5. A way of controlling the alignment of CNTs in a direct CNTY formation by diluting the concentration of CNTs in a reactor (a) a schematic representation of the direct CNTY spinning process showing the effect of aerogel dilution on the orientability of the final fibers, and scanning electron micrographs of (b) nonoriented and (c) oriented CNTYs. Reproduced with permission.[40] Copyright 2015, ACS Publications.

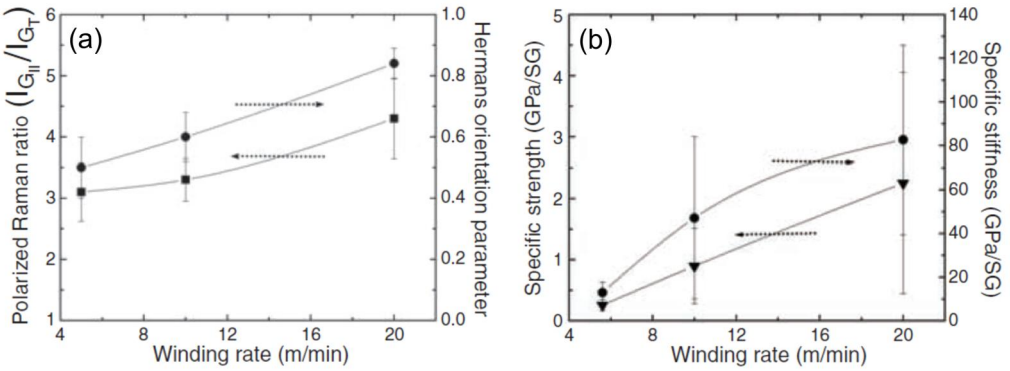

Fig. 1.6. Effect of winding rate on (a) the orientation and (b) the average specific strength and stiffness of CNTYs at 2-mm gauge length. From ref. [39]. Reprinted with permission from AAAS.

1.3.2.4 Twist angle of CNTs

Along with the alignment or orientation of elementary CNTs, the twist angle also plays a very important role in the evolution of the CNTY strength because it increases the interlocking of CNTs to form a continuous long yarn. In principle, to increase the helix angle by twisting is mechanically unfavorable as the orientation of the CNTs moves off of the yarn axis, the direction of load bearing as theoretically discussed in the previous section. There is thus a trade-off between the interlocking effect and the off-axis effect of elementary CNTs by twisting. Indeed, Zhao et al. [25] controlled this using a custom-made apparatus as shown in Fig. 1.7. This relies on the twist angle of the elementary CNTs according to the ratio of V_d/V_t, where V_d is the yarn drawing speed and V_t is the twisting speed. They examined the effect of this ratio on the tensile strength of CNTYs.

They showed that the strength peak of CNTYs appears at the twist angle in a broad range from 10 to 40˚ [25, 29, 35-37], far broader than the optimum angle which ranges from 15 to 25˚, as reported for traditional yarns. For conventional textile yarns, the highest strength of a yarn generally appears only once at the optimum twist angle of 15~25˚. It is however interesting to note that there are two peaks each for the strength and modulus, one of which appears in the range of 15~25˚ and the other being a new peak at around 30˚ regardless of the diameter of the CNTY as shown in Fig. 1.8. They explained that the first peak arises from simple interlocking effects between CNTs and the second peak from the further interlocking of transversely flattened CNTs. This additional interlocking effect by the flattened CNTs due to twisting and confirmed experimentally via the Raman peak shift at 1610 cm^{-1} based on the qualitative continuum model [25].

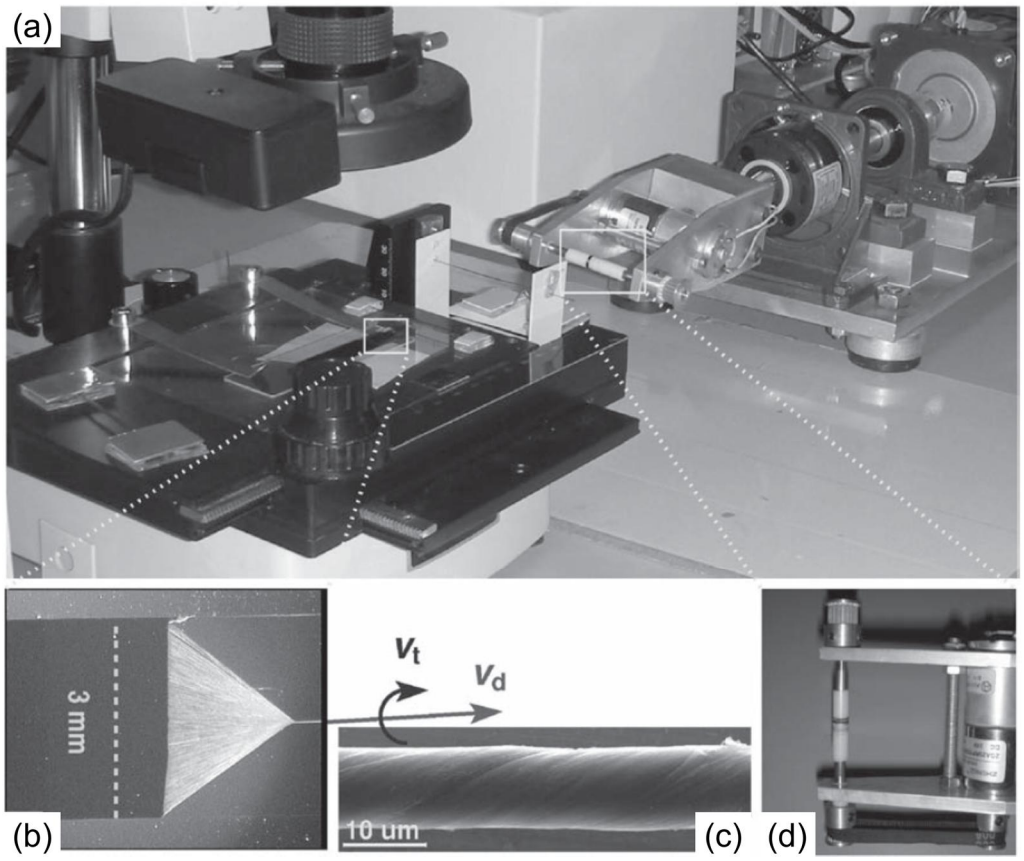

Fig. 1.7. (a) A home-made CNTY formation apparatus, (b-d) Draw and twist of elementary CNTs during yarn formation from the CVD grown CNT forest Reproduced with permission.[25] Copyright 2010, Wiley-VCH.

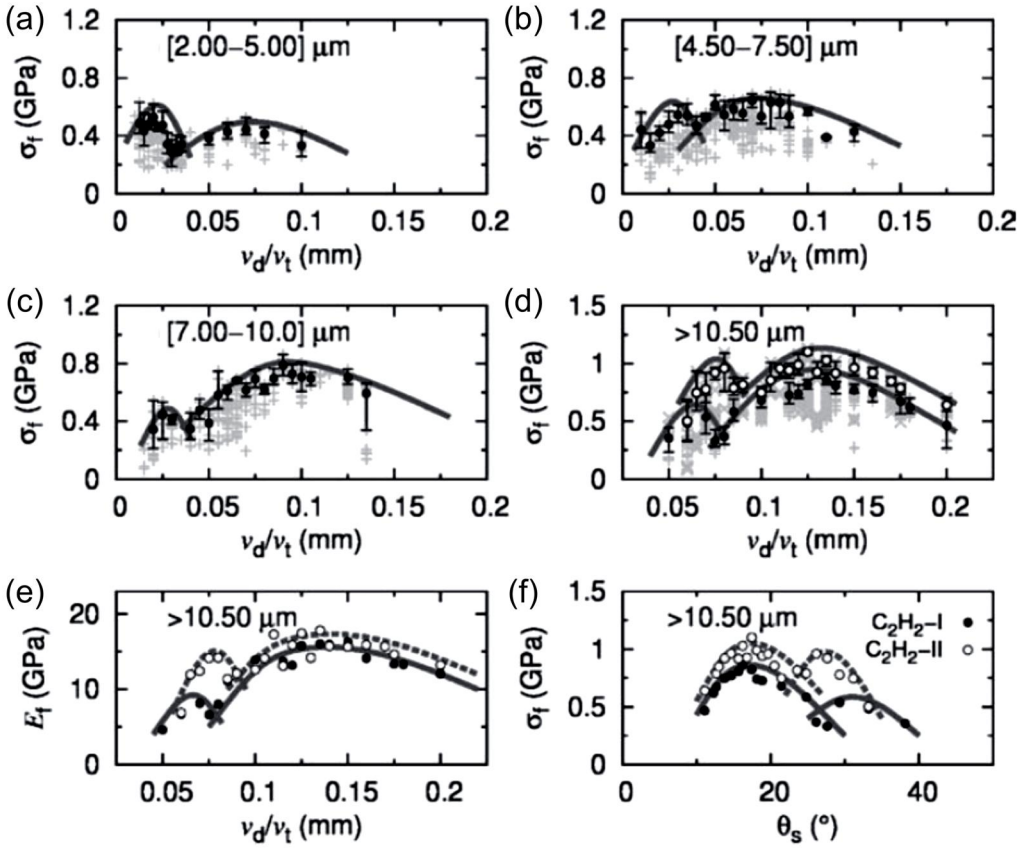

Fig. 1.8. Tensile strength and modulus dependence on the twist angle in different windows of CNTY diameter. Reproduced with permission.[25] Copyright 2010, Wiley-VCH.

1.3.3 Routes to improving the tensile strength of CNTYs

1.3.3.1 Physical densification

The improvement of the strength of CNTY can be achieved essentially by two approaches: reducing the cross-sectional area of the CNTYs under a given load and increasing the load-bearing capacity by increased the inter-tubular interactions under a given cross-sectional area of the yarn. In this vein, any effort to maximize the inter-tubular interactions can be effective not only to reduce the effective cross-sectional area of the CNTY but also to increase the load bearing capability through enhanced interactions.

One of the most commonly adopted methods to reduce the cross-sectional area of CNTYs is by solvent densification [29, 31, 32, 46, 47]. Among the various types of solvents, i.e., non-polar, polar protic and polar aprotic ethylene glycol was reported as the most effective when used to densify CNTYs, implying that polarity is the key factor due to the dipole-induced interaction among CNTs. Fig. 1.9 shows the improvements of the average strength and electrical conductivity of CNTYs after solvent densification.

Mechanical densification means, such as pressing CNTYs between rollers as shown in Fig. 1.10, has also been reported to have great potential to improve the tensile strength of CNTYs [41, 48-50]. Indeed, Wang et al. [41] demonstrated that the average tensile strength of CNTY can be improved by up to 4.34 GPa after mechanical densification by the synergetic effect of the reduced cross-sectional area by a factor of ~10 with an increase in the load-bearing capacity by 120 % through enhanced inter-tubular interactions. Table 1.3 shows the effectiveness of mechanical pressure when utilized to increase the packing density and mechanical performance of CNTY.

It is however clear that there is an upper limit with regard to the compaction of elementary CNTs in a CNTY, as the density of CNTY cannot surpass the density of graphite, 2.23 g/cm^3, even if the elementary CNTs are fully collapsed and flattened without any inter-tubular space.

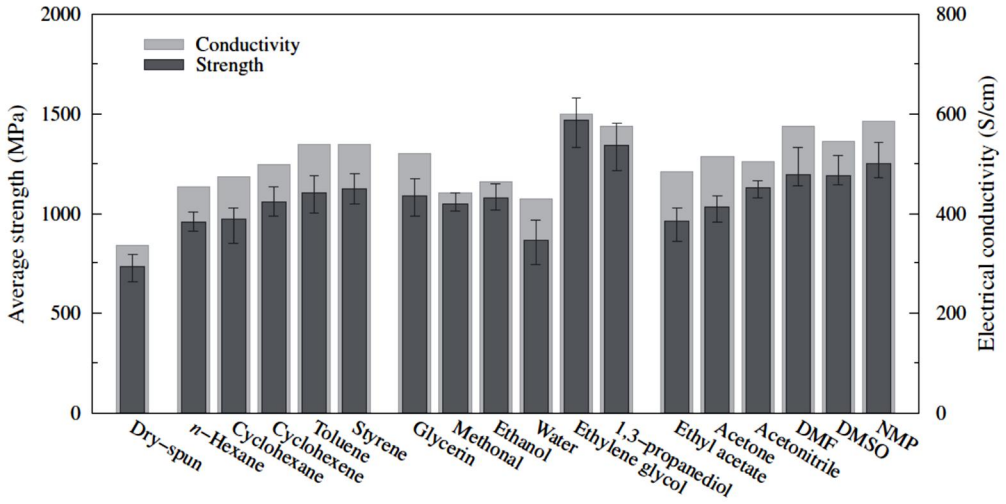

Fig. 1.9. Tensile strength and electrical conductivity of CNTYs after solvent densification. Reproduced with permission.[47] Copyright 2012, Elsevier.

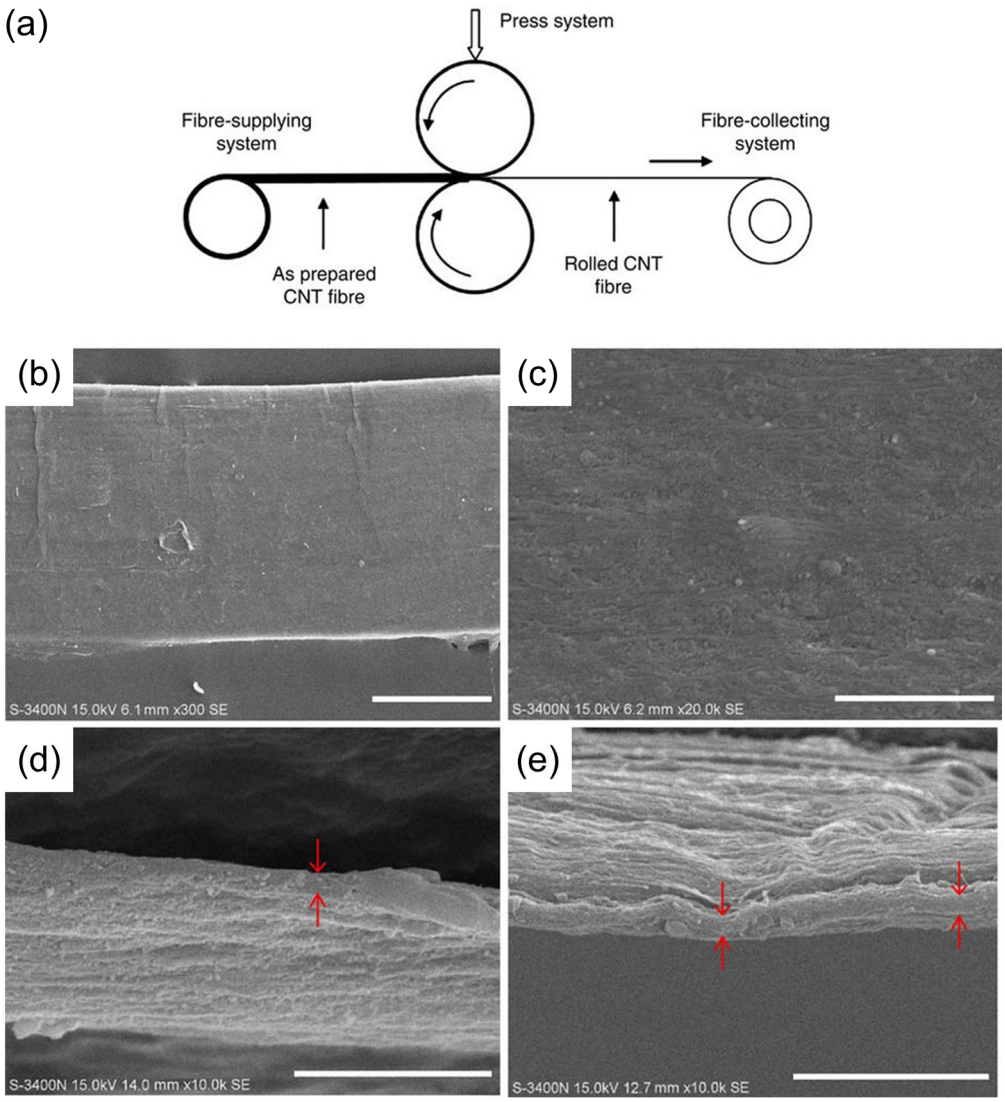

Fig. 1.10. (a) A schematic representation of mechanical densification of CNTY, (b~e) SEM micrographs after rolling, showing a smooth surface morphology. Scale bars, 100 mm (b), 2 mm (c) and 5 mm (d,e). Reproduced with permission.[41] Copyright 2014, Nature Publishing Group.

Table 1.3. Mechanical densification effect on the tensile strength of cylindrical and ribbon-like SWCNTYs. Reproduced with permission.[48] Copyright 2016, Royal Society of Chemistry.

Sample	Diameter/width × thickness (μm)	Apparent density (g/cm^3)	Breaking elongation (%)	Tensile strength (MPa)	Young's modulus (GPa)	Treatment pressure (GPa)
Cylindrical fiber 1	Φ: 280	0.68	13.7	17	0.35	-
Cylindrical fiber 2	Φ: 300	0.53	27	18	0.30	-
Ribbon-like fiber 1	800 × 36	1.11	4.8	300	6.5	0.9
Ribbon-like fiber 2	1500 ×13	1.53	1.5	700	50	2.1
Ribbon-like fiber 3	1600 × 13	1.54	1.8	720	72	2.7
Ribbon-like fiber 4	1800 × 8	1.66	1.2	960	81	3.7

1.3.3.2 Polymeric or carbon mediator

Based on the slippage failure mechanism the strength of CNTYs can basically be ascribed to the shear strength between the elementary CNTs. There have thus been many efforts to improve the shear strength by infiltrating mediating materials such as polymers or carbon materials into the inter-tubular spaces. For example, Ma et al. [51] experimentally demonstrated that the load-transfer efficiency between elementary CNTs improves greatly from 0.045 to 0.4 by infiltrating polymers, e.g. polyvinyl alcohol (PVA) [46, 47, 51-53].

Apart from linear chain polymers, cross-linkable polymers such as epoxy and bismaleimide (BMI) have also been widely adopted for CNTY strengthening [47, 51, 54-57]. Ryu et al. [56] introduced mussel-inspired catecholamine polymer (PEI-C) infiltrated CNTYs, realizing strength levels which exceeded 2 GPa.

Carbon-coated CNTYs are another route to achieving higher strength. For example, Hahm et al. [58] showed a dramatically enhanced tensile strength level of CNTYs, in that case an increase from 0.068 to 0.80 GPa, when using a core of CNTY and a glassy carbon shell as shown in Fig. 1.11a. Similarly, Ryu et al. [59] also showed greatly increased tensile strength up to 4.0 GPa, which is nearly 400 % higher than that of pure CNTY, by fabricating CNTYs with a carbonized polydopamine (PDA) coating as shown in Fig. 1.11b.

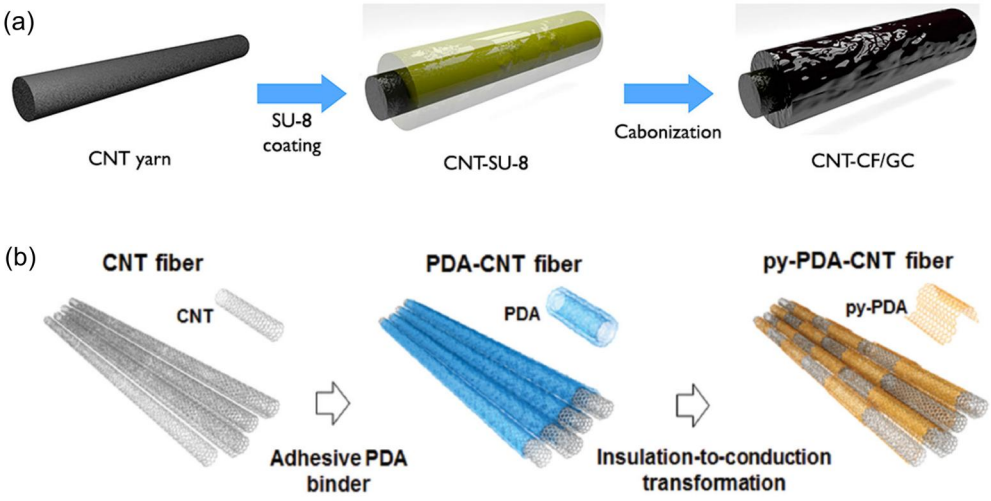

Fig. 1.11. The fabrication process of (a) CNTY/GC core/shell type yarns, (b) PDA-CNTY and py-PDA-CNTY. Reproduced with permission.[58, 59] Copyright 2013, ACS Publications and Copyright 2015, Wiley-VCH.

1.3.3.3 Surface modification of CNTs

As chemically strengthened CNTYs were produced mostly by wet-process, chemical modification methods can be classified into three types on the basis of the functional groups attached onto the surfaces of the elementary CNTs.

The first method is to enhance the van der Waals interaction without the attachment of further functional groups. Impurities and defects such as sp^3 carbons are usually considered as an obstacle for π-π interaction. Thus, the elimination of impurities and the restoration of sp^2 carbon can help to increase the interaction force between the elementary CNTs [60-63]. A typical example can be found in the work of Choi et al. [60], which reported CNTYs with an improved strength value of 420 MPa after removal of defects in a sp^2 conjugated system of CNT walls through intramolecular cross-dehydrogenative coupling (ICDC), which converts sp^3 carbons into sp^2 carbons. As a result of the recovery of sp^2 carbons, which improves the van der Waals interaction, the elementary CNTs become more closely packed, structure resulting in a slight decrease of the yarn diameter as shown in Fig. 1.12.

The strength of as-spun CNTY is relatively low due to the weak inter-tubular interaction between CNTs which is van der Waals interaction or π-π interaction between CNTs. It is reasonable to enhance the inter-tubular interaction by introducing additional strong bonds instead of the existing π-π interaction so as to realize enhanced mechanical performance of CNTYs hence the second method involves the introduction of functional groups that induce ionic or hydrogen bonding as compared to π-π interaction [34, 64, 65]. For instance, Park et al. [64] doped CNTs with nitrogen by the thermal decomposition of an ionic liquid and successfully induced hydrogen bonds

between the CNTs so as to obtain the resultant CNTY, which in their case showed an increased specific strength from 0.32 GPa/SG to 0.65 GPa/SG.

The third improvement method involves grafting a polymer onto the surfaces of the CNTs [65, 66]. Indeed, Naraghi et al. [66] reported a CNTY grafted with PMMA oligomer, achieving a shear strength value of 400 MPa between CNTs due to the increased interlocking of the PMMA oligomers (Fig. 1.14).

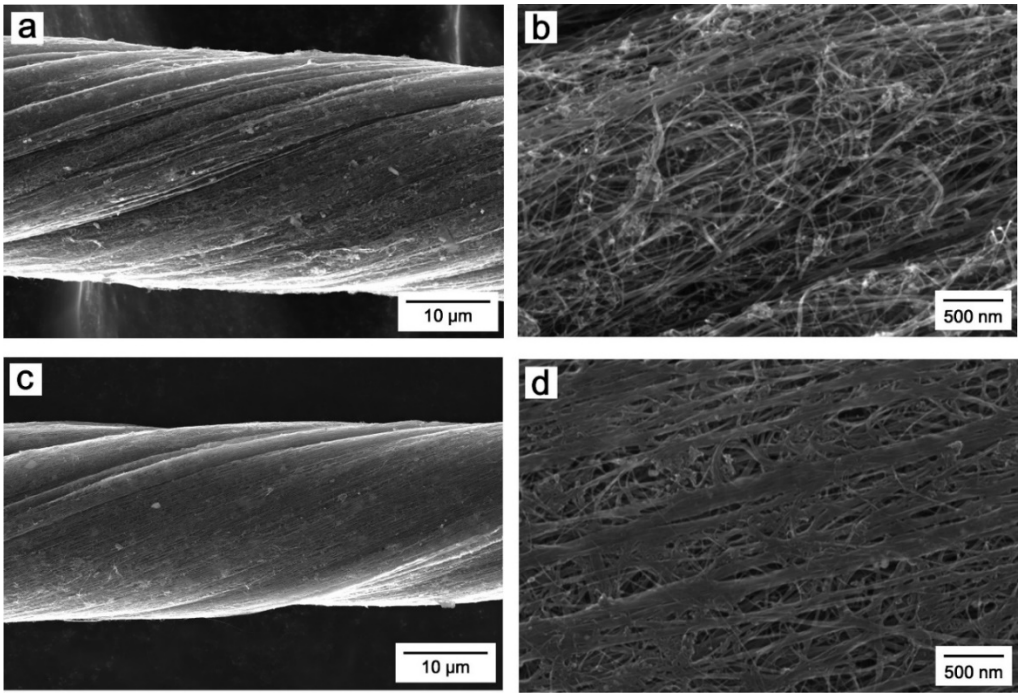

Fig. 1.12. SEM micrographs of (a, b) before and (c, d) after ICDC reaction on CNTYs. Reproduced with permission.[60] Copyright 2013, ACS.

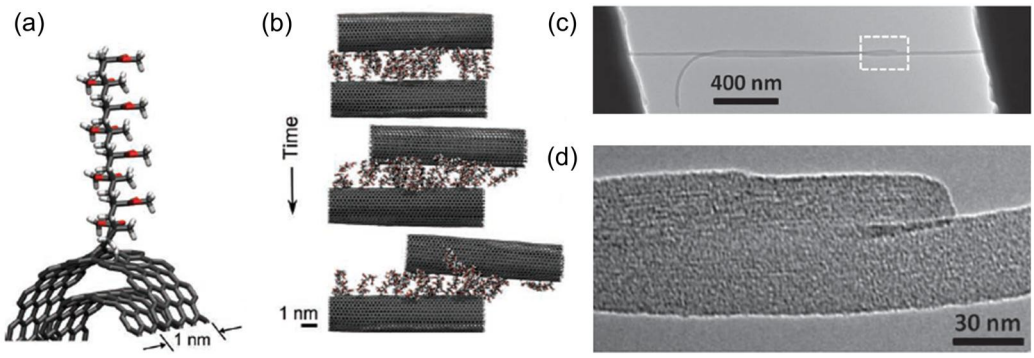

Fig. 1.13. A schematic representation of (a) PMMA grafted CNT and (b) shearing between oligomer grafted CNTs, (c) TEM micrograph of two overlapping CNTs, and (d) High-resolution TEM micrograph of the end of the oligomer grafted CNTs. Reproduced with permission.[66] Copyright 2013, Wiley-VCH.

The aforementioned methods enhance the mechanical performance of CNTYs via non-covalent interactions viz. van der Waals interaction, hydrogen interaction, and physical interlocking. The ductile property of CNTY was preserved even after chemical modification, those interactions could be prolonged until the breakage of CNTY. As a result, not only the tensile strength but also the toughness (energy to failure) of CNTY was simultaneously improved as shown in Fig. 1.14.

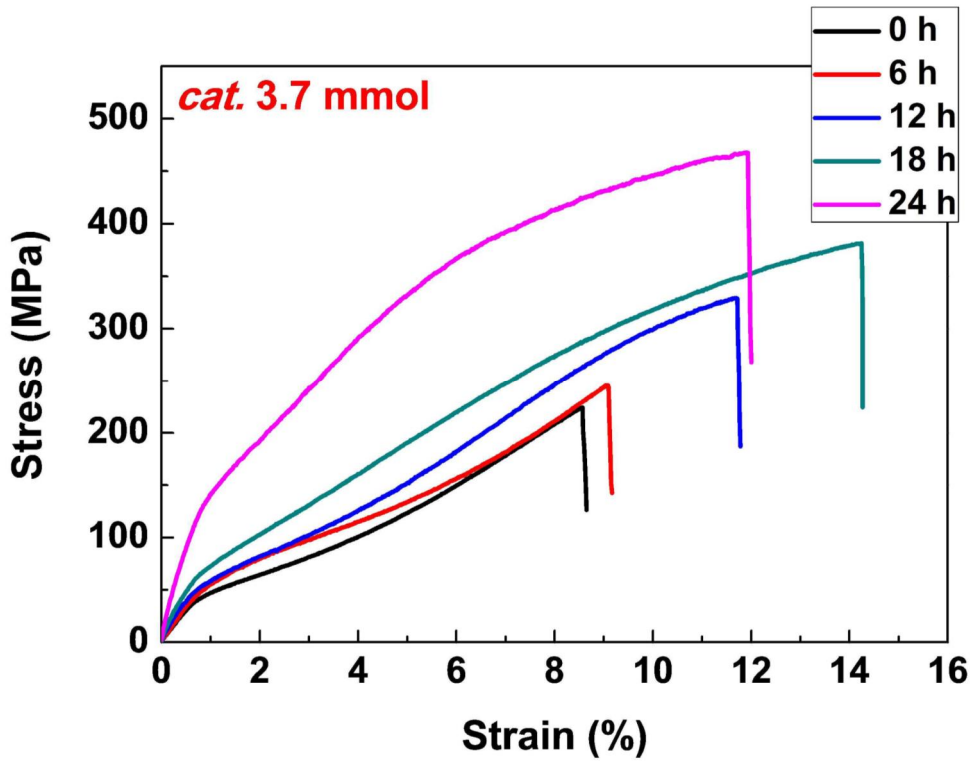

Fig. 1.14. Changes of S-S curves of CNTYs with increasing ICDC reaction time. Reproduced with permission.[65] Copyright 2013, ACS

1.3.3.4 Crosslinking between CNTs

An extreme means of maximizing the inter-tubular interaction is to bond CNTs together covalently. In order to obtain the highest strength of CNTYs, the chemical crosslinking of CNTs has thus been commonly considered. Cornwell and Welch [67] suggested a model of directly cross-linked CNTY as shown in Fig. 1. 15a and b, that is expected to exhibit yarn strength levels as high as 60 GPa, which is very close to the theoretical strength of CNTs. If this is realized, the CNTY would fail due not to slippage but due instead to the rupture of the CNTs. To realize this model, Filleter et al. [68] reported through in situ TEM tensile testing that an e-beam irradiated CNT bundle showed the strength of 17 GPa, though this remains below the theoretically predicted value. In this case, despite the direct crosslinking between CNTs, the dramatic destruction of the outer wall of the CNTs as shown in Fig. 1.15c, was found to be a limiting factor with reference to the strength.

To avoid any structural deterioration of CNTs while preserving the crosslinking of CNTs, several linker molecules have been introduced such as aliphatic diols [70], aromatic diamines [71], reactive polymeric molecules [72], etc. as schematically shown in Fig. 1. 16. Given that as-produced CNTs do not possess any functional groups on the surface, the functionalization of CNTs is required prior to chemical crosslinking. For example, the pre-oxidation of CNTs was adopted to introduce carboxylic groups, which can participate in the crosslinking process through subsequent reactions such as esterification [70] and amidation [72]. Further, diazotization of CNTs using either 4-carboxybenzenediazonium salts or p-phenylenediamine was found to be effective for the crosslinking of CNTs through the subsequent amidation of the CNTs.

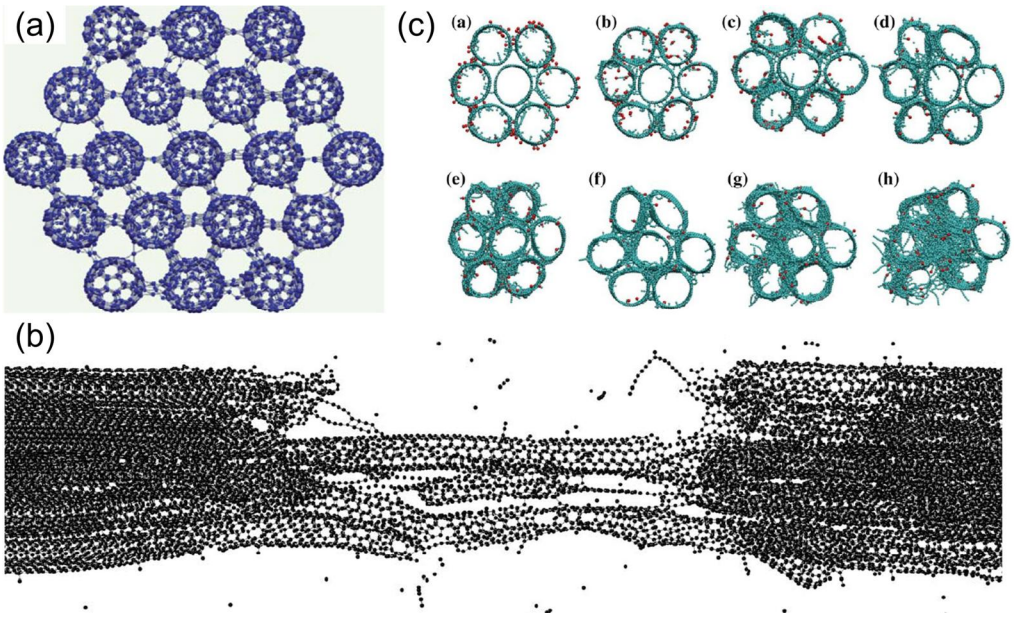

Fig. 1.15. Schematic representative of (a) directly cross-linked CNTs, (b) failure of the cross-linked CNT and (c) e-beam irradiated CNTs yarn. Reproduced with permission.[67, 69] Copyright 2011, AIP publishing and Copyright 2013, Elsevier.

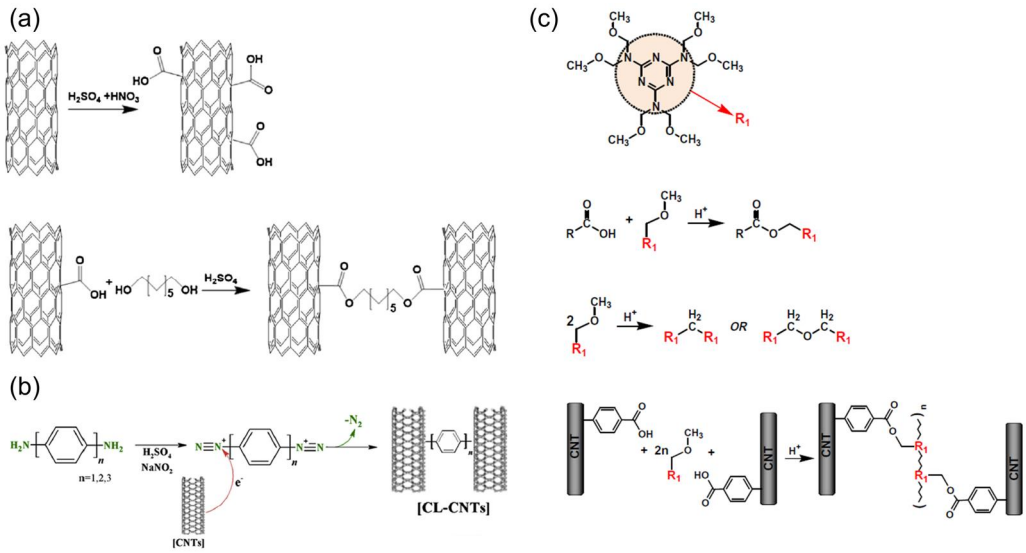

Fig. 1.16. CNT cross-linking by various chemical reagents. Reproduced with permission.[70-72] Copyright 2017, Elsevier, Copyright 2017, Elsevier and Copyright 2013, Elsevier.

It is important to note that although the strength of CNTYs could be enhanced remarkably via the chemical crosslinking of CNTs, the current state of research remains far from the theoretically predicted value. This implies that there should be further works to find possible routes either crosslink CNTs directly without structural deterioration or increase the degree of crosslinking between CNTs.

1.4 Aim and scope of this study

The aim of this study is to design and fabricate ultrahigh-strength CNTY through both theoretical and empirical approaches based on a state-of-the-art analysis and an overview of CNTYs. CNT is the most attractive materials in the structural materials fields, but the CNT assembly shows very poor mechanical performance on the macroscopic scale compared to the strength of individual CNTs on the nanoscale. As discussed in the section on state-of-the-art approaches, previous works based on conventional yarn mechanics does not provide a theoretical and empirical guideline or insight into the development of high-strength CNTY. This study attempts to discern possible correlations between the intrinsic and extrinsic structural parameters of elementary CNTs and the specific strength of the resulting CNTYs.

The theoretical approach related to the specific strength of CNTYs will be considered in chapter 2. On the basis of the failure mechanism, CNT slippage, of CNTYs, an equation describing the specific strength of CNTYs is derived by carrying out a calculation of the total shear force and the linear density while relying on the intrinsic structure of CNTs. In particular, the structural parameters of the length, diameter and the number of tube walls are considered as key factors affecting the specific strength of CNTYs, and the relationship between the specific strength of CNTYs and the nanostructures of the component CNTs is discussed by reviewing theoretical studies. In addition, the dependence of the CNTY strength on the CNT assembly structure and the basic load-bearing element is addressed.

The reliability of the theoretical approach will be verified by comparing the specific strengths of CNTYs made of various nanostructured CNTs in chapter 3. CNTYs with different nanostructured CNTs are prepared by a direct spinning method, and the

synthesis condition is manipulated for nanostructural control of the elemental CNTs. The specific strength of CNTYs with different nanostructures is theoretically predicted based on the structural parameters of each CNT, and the estimated strength levels are compared with experimental results.

In chapter 4, the effect of the microstructure of the CNT assembly is investigated through polymer infiltration, which is a typical means of CNTY strengthening. Usually, polyvinyl alcohol (PVA) is adapted to enhance the CNTY strength. However, PVA is not compatible with CNTs, and a strengthening mechanism by PVA has yet to be developed. Therefore, CNTYs are impregnated with various polymers with different affinities toward CNTs in this study. Modifications of the internal CNTY microstructure are analyzed and the relationship between the microstructure and specific strength of CNTYs is assessed in order to provide insight into the roles of polymer chains in CNTYs.

A major issue regarding the improvement of the CNTY strength is to develop an efficient means of chemical crosslinking. To resolve this issue, methods of polymeric material grafting selectively onto the double-walled CNT assembly, a favorable nanostructure, in CNTYs and an effective chemical crosslinking method are proposed with the goal of preparing ultrahigh-strength CNTY. The advanced CNTY performance will be compared to crosslinked CNTYs by a common method and compared also to conventional high-performance fibers in chapter 5.

1.5 References

[1] Yu MF, Files BS, Arepalli S, Ruoff RS. Tensile loading of ropes of single wall carbon nanotubes and their mechanical properties. Phys. Rev. Lett. 2000, 84, 5552-5.

[2] Yu M-F, Lourie O, Dyer MJ, Moloni K, Kelly TF, Ruoff RS. Strength and breaking mechanism of multiwalled carbon nanotubes under tensile load. Science 2000, 287, 637-40.

[3] Dai H, Wong EW, Lieber CM. Probing electrical transport in nanomaterials: Conductivity of individual carbon nanotubes. Science 1996, 272, 523-6.

[4] Kim SW, Kim T, Kim YS, Choi HS, Lim HJ, Yang SJ, et al. Surface modifications for the effective dispersion of carbon nanotubes in solvents and polymers. Carbon 2012, 50, 3-33.

[5] Coleman JN, Khan U, Blau WJ, Gun'ko YK. Small but strong: A review of the mechanical properties of carbon nanotube–polymer composites. Carbon, 2006, 44, 1624-52.

[6] Spitalsky Z, Tasis D, Papagelis K, Galiotis C. Carbon nanotube–polymer composites: chemistry, processing, mechanical and electrical properties. Prog. Polym. Sci. 2010, 35, 357-401.

[7] Bauhofer W, Kovacs JZ. A review and analysis of electrical percolation in carbon nanotube polymer composites. Compos. Sci. Technol. 2009, 69, 1486-98.

[8] Gojny FH, Wichmann MHG, Köpke U, Fiedler B, Schulte K. Carbon nanotube-reinforced epoxy-composites: enhanced stiffness and fracture toughness at low nanotube content. Compos. Sci. Technol. 2004, 64, 2363-71.

[9] Allaoui A, Bai S, Cheng HM, Bai JB. Mechanical and electrical properties of a MWNT/epoxy composite. Compos. Sci. Technol. 2002, 62, 1993-8.

[10] Oh JY, Yang SJ, Park JY, Kim T, Lee K, Kim YS, et al. Easy preparation of self-assembled high-density buckypaper with enhanced mechanical properties. Nano Lett. 2015, 15, 190-7.

[11] Oh JY, Kim YS, Jung Y, Yang SJ, Park CR. Preparation and exceptional mechanical properties of bone-mimicking size-tuned graphene oxide@carbon nanotube hybrid paper. ACS Nano 2016, 10, 2184-92.

[12] Oh JY, Jung Y, Cho YS, Choi J, Youk JH, Fechler N, et al. Metal–phenolic carbon nanocomposites for robust and flexible energy-storage devices. ChemSusChem 2017, 10, 1675-82.

[13] Oh JY, Choi YS, Yang SJ, Kim J, Choi HS, Choi GD, et al. Effect of microstructure and morphological properties of carbon nanotubes on the length reduction during melt processing. Compos. Sci. Technol. 2015, 112, 42-9.

[14] Jeong YC, Lee K, Kim T, Kim JH, Park J, Cho YS, et al. Partially unzipped carbon nanotubes for high-rate and stable lithium-sulfur batteries. J. Mater. Chem. A 2016, 4, 819-26.

[15] Jung Y, Jeong YC, Kim JH, Kim YS, Kim T, Cho YS, et al. One step preparation and excellent performance of CNTY based flexible micro lithium ion batteries. Energy Storage Mater. 2016, 5, 1-7.

[16] Lee J, Kim T, Jung Y, Jung K, Park J, Lee D-M, et al. High-strength carbon nanotube/carbon composite fibers via chemical vapor infiltration. Nanoscale 2016, 8, 18972-79.

[17] Kim YS, Oh JY, Kim JH, Shin MH, Jeong YC, Sung SJ, et al. Crucial role of oxidation debris of carbon nanotubes in subsequent end-use applications of carbon nanotubes. ACS Appl. Mater. Interfaces 2017, 9, 17552-64.

[18] Sung SJ, Kim T, Yang SJ, Oh JY, Park CR. New insights into the oxidation of

single-walled carbon nanotubes for the fabrication of transparent conductive films. Carbon 2015, 81, 525-34.

[19] Meng J, Zhang Y, Song K, Minus ML. Forming crystalline polymer-nano interphase structures for high-modulus and high-tensile/strength composite fibers. Macromol. Mater. Eng. 2014, 299, 144-53.

[20] Liu Y, Kumar S. Polymer/carbon nanotube nano composite fibers–a review. ACS Appl. Mater. Interfaces 2014, 6, 6069-87.

[21] Vilatela JJ, Elliott JA, Windle AH. A model for the strength of yarn-like carbon nanotube fibers. ACS Nano 2011, 5, 1921-7.

[22] J. W. S. Hearle, P. Grosberg, Stanley Backer. Structural mechanics of fibers, yarns, and fabrics. vol. 1 New York: Wiley, 1969.

[23] Beese AM, Wei X, Sarkar S, Ramachandramoorthy R, Roenbeck MR, Moravsky A, et al. Key factors limiting carbon nanotube yarn strength: exploring processing-structure-property relationships. ACS Nano 2014, 8, 11454-66.

[24] Zhang M, Atkinson KR, Baughman RH. Multifunctional carbon nanotube yarns by downsizing an ancient technology. Science 2004, 306, 1358-61.

[25] Zhao J, Zhang X, Di J, Xu G, Yang X, Liu X, et al. Double-peak mechanical properties of carbon-nanotube fibers. Small 2010, 6, 2612-7.

[26] Miao M. The role of twist in dry spun carbon nanotube yarns. Carbon 2016, 96, 819-26.

[27] Ericson LM, Fan H, Peng H, Davis VA, Zhou W, Sulpizio J, et al. Macroscopic, neat, single-walled carbon nanotube fibers. Science 2004, 305, 1447-50.

[28] Li QW, Zhang XF, DePaula RF, Zheng LX, Zhao YH, Stan L, et al. Sustained growth of ultralong carbon nanotube arrays for fiber spinning. Adv. Mater. 2006, 18, 3160-3.

[29] Kai L, Yinghui S, Ruifeng Z, Hanyu Z, Jiaping W, Liang L, et al. Carbon nanotube yarns with high tensile strength made by a twisting and shrinking method. Nanotechnology 2010, 21, 045708.

[30] Li Y-L, Kinloch IA, Windle AH. Direct spinning of carbon nanotube fibers from chemical vapor deposition synthesis. Science 2004, 304, 276-8.

[31] Zhong X-H, Li Y-L, Liu Y-K, Qiao X-H, Feng Y, Liang J, et al. Continuous multilayered carbon nanotube yarns. Adv. Mater. 2010, 22, 692-6.

[32] Jung Y, Kim T, Park CR. Effect of polymer infiltration on structure and properties of carbon nanotube yarns. Carbon 2015, 88, 60-9.

[33] Behabtu N, Young CC, Tsentalovich DE, Kleinerman O, Wang X, Ma AWK, et al. Strong, light, multifunctional fibers of carbon nanotubes with ultrahigh conductivity. Science 2013, 339, 182-6.

[34] Zhang S, Koziol KKK, Kinloch IA, Windle AH. Macroscopic fibers of well-aligned carbon nanotubes by wet spinning. Small 2008, 4, 1217-22.

[35] Jia J, Zhao J, Xu G, Di J, Yong Z, Tao Y, et al. A comparison of the mechanical properties of fibers spun from different carbon nanotubes. Carbon 2011, 49, 1333-9.

[36] Zhang X, Li Q, Tu Y, Li Y, Coulter JY, Zheng L, et al. Strong carbon-nanotube fibers spun from long carbon-nanotube arrays. Small 2007, 3, 244-8.

[37] Ghemes A, Minami Y, Muramatsu J, Okada M, Mimura H, Inoue Y. Fabrication and mechanical properties of carbon nanotube yarns spun from ultra-long multi-walled carbon nanotube arrays. Carbon 2012, 50, 4579-87.

[38] Liu K, Zhu F, Liu L, Sun Y, Fan S, Jiang K. Fabrication and processing of high-strength densely packed carbon nanotube yarns without solution processes. Nanoscale 2012, 4, 3389-93.

[39] Koziol K, Vilatela J, Moisala A, Motta M, Cunniff P, Sennett M, et al. High-performance carbon nanotube fiber. Science 2007, 318, 1892-5.

[40] Alemán B, Reguero V, Mas B, Vilatela JJ. Strong Carbon nanotube fibers by drawing inspiration from polymer fiber spinning. ACS Nano 2015, 9, 7392-8.

[41] Wang JN, Luo XG, Wu T, Chen Y. High-strength carbon nanotube fibre-like ribbon with high ductility and high electrical conductivity. Nat Commun 2014, 5, 3848.

[42] Zhang S, Zhu L, Minus M, Chae H, Jagannathan S, Wong C-P, et al. Solid-state spun fibers and yarns from 1-mm long carbon nanotube forests synthesized by water-assisted chemical vapor deposition. J. Mater. Sci. 2008, 43, 4356-62.

[43] Hill FA, Havel TF, Hart AJ, Livermore C. Enhancing the tensile properties of continuous millimeter-scale carbon nanotube fibers by densification. ACS Appl. Mater. Interfaces 2013, 5, 7198-207.

[44] Zhang X, Li Q, Holesinger TG, Arendt PN, Huang J, Kirven PD, et al. Ultrastrong, stiff, and lightweight carbon-nanotube fibers. Adv. Mater. 2007, 19, 4198-201.

[45] Cho W, Schulz M, Shanov V. Growth and characterization of vertically aligned centimeter long CNT arrays. Carbon 2014, 72, 264-73.

[46] Liu K, Sun Y, Lin X, Zhou R, Wang J, Fan S, et al. Scratch-resistant, highly conductive, and high-strength carbon nanotube-based composite yarns. ACS Nano 2010, 4, 5827-34.

[47] Li S, Zhang X, Zhao J, Meng F, Xu G, Yong Z, et al. Enhancement of carbon nanotube fibres using different solvents and polymers. Compos. Sci. Technol. 2012, 2, 1402-07.

[48] Hou G, Wang G, Deng Y, Zhang J, Nshimiyimana JP, Chi X, et al. Effective enhancement of the mechanical properties of macroscopic single-walled carbon

nanotube fibers by pressure treatment. RSC Adv. 2016, 6, 97012-7.

[49] Tran TQ, Fan Z, Liu P, Myint SM, Duong HM. Super-strong and highly conductive carbon nanotube ribbons from post-treatment methods. Carbon 2016, 99, 407-15.

[50] Xu W, Chen Y, Zhan H, Wang JN. High-strength carbon nanotube film from improving alignment and densification. Nano Lett. 2016, 16, 946-52.

[51] Ma W, Liu L, Zhang Z, Yang R, Liu G, Zhang T, et al. High-strength composite fibers: realizing true potential of carbon nanotubes in polymer matrix through continuous reticulate architecture and molecular level couplings. Nano Lett. 2009, 9, 2855-61.

[52] Wu ML, Chen Y, Zhang L, Zhan H, Qiang L, Wang JN. High-prformance carbon nanotube/polymer composite fiber from layer-by-layer deposition. ACS Appl. Mater. Interfaces 2016, 8, 8137-44.

[53] Liu W, Zhang X, Xu G, Bradford PD, Wang X, Zhao H, et al. Producing superior composites by winding carbon nanotubes onto a mandrel under a poly(vinyl alcohol) spray. Carbon 2011, 49, 4786-91.

[54] Boncel S, Sundaram RM, Windle AH, Koziol KKK. Enhancement of the mechanical properties of directly spun CNT fibers by chemical treatment. ACS Nano 2011, 5, 9339-44.

[55] Zu M, Li Q, Zhu Y, Dey M, Wang G, Lu W, et al. The effective interfacial shear strength of carbon nanotube fibers in an epoxy matrix characterized by a microdroplet test. Carbon 2012, 50, 1271-9.

[56] Ryu S, Lee Y, Hwang J-W, Hong S, Kim C, Park TG, et al. High-Strength Carbon Nanotube Fibers Fabricated by Infiltration and Curing of Mussel-Inspired Catecholamine Polymer. Adv. Mater. 2011, 23, 1971-5.

[57] Tran TQ, Fan Z, Mikhalchan A, Liu P, Duong HM. Post-treatments for multifunctional property enhancement of carbon nanotube fibers from the floating catalyst method. ACS Appl. Mater. Interfaces 2016, 8, 7948-56.

[58] Hahm MG, Lee J-H, Hart AHC, Song SM, Nam J, Jung HY, et al. Carbon nanotube core graphitic shell hybrid fibers. ACS Nano 2013, 7, 10971-7.

[59] Ryu S, Chou JB, Lee K, Lee D, Hong SH, Zhao R, et al. Direct insulation-to-conduction transformation of adhesive catecholamine for simultaneous increases of electrical conductivity and mechanical strength of CNT fibers. Adv. Mater. 2015, 27, 3250-5.

[60] Choi Y-M, Choo H, Yeo H, You N-H, Lee DS, Ku B-C, et al. Chemical method for improving both the electrical conductivity and mechanical properties of carbon nanotube yarn via intramolecular cross-dehydrogenative coupling. ACS Appl. Mater. Interfaces 2013, 5, 7726-30.

[61] Tran TQ, Headrick RJ, Bengio EA, Myo Myint S, Khoshnevis H, Jamali V, et al. Purification and dissolution of carbon nanotube fibers spun from the floating catalyst method. ACS Appl. Mater. Interfaces 2017, 9, 37112-9.

[62] Sundaram RM, Windle AH. One-step purification of direct-spun CNT fibers by post-production sonication. Mater. Design 2017, 126, 85-90.

[63] Gspann TS, Smail FR, Windle AH. FD173: Spinning of carbon nanotube fibres using the floating catalyst high temperature route: purity issues and the critical role of sulphur. Faraday Discuss. 2014, 173, 47-65.

[64] Park O-K, Kim HJ, Hwang JY, Kim SM, Jeong Y, Lee JK, et al. Effects of nitrogen doping from pyrolyzed ionic liquid in carbon nanotube fibers: enhanced mechanical and electrical properties. Nanotechnology 2015, 26, 075706.

[65] Beese AM, Sarkar S, Nair A, Naraghi M, An Z, Moravsky A, et al. Bio-inspired

carbon nanotube–polymer composite yarns with hydrogen bond-mediated lateral interactions. ACS Nano 2013, 7, 3434-46.

[66] Naraghi M, Bratzel GH, Filleter T, An Z, Wei X, Nguyen ST, et al. Atomistic investigation of load transfer between DWNT bundles "Crosslinked" by PMMA oligomers. Adv. Funct. Mater. 2013, 23, 1883-92.

[67] Cornwell CF, Welch CR. Very-high-strength (60-GPa) carbon nanotube fiber design based on molecular dynamics simulations. J. Chem. Phys. 2011, 134, 204708.

[68] Filleter T, Bernal R, Li S, Espinosa HD. Ultrahigh strength and stiffness in cross-linked hierarchical carbon nanotube bundles. Adv. Mater. 2011, 23, 2855-60.

[69] O'Brien NP, McCarthy MA, Curtin WA. Improved inter-tube coupling in CNT bundles through carbon ion irradiation. Carbon 2013, 51, 173-84.

[70] Im Y-O, Lee S-H, Kim T, Park J, Lee J, Lee K-H. Utilization of carboxylic functional groups generated during purification of carbon nanotube fiber for its strength improvement. Appl. Surf. Sci. 2017, 392, 342-9.

[71] Park O-K, Choi H, Jeong H, Jung Y, Yu J, Lee JK, et al. High-modulus and strength carbon nanotube fibers using molecular cross-linking. Carbon 2017, 118, 413-21.

[72] Min J, Cai JY, Sridhar M, Easton CD, R. Gengenbach T, McDonnell J, et al. High performance carbon nanotube spun yarns from a crosslinked network. Carbon 2013, 52, 520-27.

Chapter 2 Theoretical Approach to High-Specific Strength CNTYs

2.0 Major symbols

n: $Number\ of\ walls$

τ: $Shear\ strength\ (MPa)$

σ: $Specific\ strength\ of\ CNTY\ (N/tex, GPa/(g \cdot cm^{-3}))$

D_o: $Outer\ diameter\ of\ CNT\ (nm)$

D_i: $Inner\ diameter\ of\ CNT\ \ (nm)$

ρ: $Density\ of\ graphite\ (g/cm^3)$

L: $Length\ of\ CNT\ (\mu m)$

E: $Flexural\ rigidity\ of\ graphene\ (J)$

γ: $Surface\ energy\ of\ CNT\ (J/m^2)$

N: Number of CNT layer of bundle

2.1 Introduction

There has been remarkable progress with regard to the fabrication of yarns based on high-performance CNTs. However, the theoretically predicted tensile strength of CNTs has yet to be realized in practical CNTYs or CNT-reinforced composites.

Although equation (1.1) is commonly used to predict the CNTY strength [1-3], and it suggests that longer and thinner elementary CNTs lead to stronger CNTYs, this equation does not appear to be feasible when applied to a practical CNTY for two reasons. The first of these is the dimensional difference and the second is the deformability of CNTs [4-6]. Indeed, in the equation, derived originally for cotton or wool yarns, elementary fibers given their micron-sized diameters and lengths measurable in millimeters were considered as non-deformable cylinders of a uniformly specific volume with a circular cross-section, whereas actual CNTs with nanometer-sized diameters and lengths of a few tens of microns are deformable, with the deformability depending on the structural parameters, in this case the number of walls and the diameter of the CNTs [4-6].

To overcome the limitations of equation (1.1), this study introduces a proper theoretical approach which considers that failures of CNTYs consisting of millions of elementary CNTs are governed not by the rupture of the elementary CNTs but by pull-out due to the weak interaction between the CNTs and the unique hierarchical structure of the CNTY. The goal is to find rational routes based on fundamental theories to improve the specific strength further and thus hopefully realize the theoretical performance capabilities of CNTYs.

2.2 CNTY model

Many researchers have attempted to develop a CNTY model in order to predict the strength of yarn-like CNT fibers and enhance the mechanical properties of CNTY through a clear understanding of the deformation behaviors of CNTYs [1-4, 7-12]. Although these efforts provide helpful suggestions pertaining to favorable nanostructures of the component CNTs to improve the CNTY strength, the models were limited, only describing the strength of the CNT bundle rather than the strength of the CNTY. In addition, smaller bundles are theoretically considered to offers better CNTY strength, but the most common empirical means of CNTY strengthening, in this case the densification and compaction of the CNTYs leading to a larger bundle and thus stronger CNTYs, implies contradictory results with regard to theoretical predictions [7, 8, 13-16]. Thus, we attempt to describe the hierarchical level of the CNTY structure more accurately in this study, unlike earlier simple models with three hierarchic levels and CNT-bundled yarn, in order to resolve the contradiction between the theoretical and empirical results.

The goals of CNTY structure modeling are to find the failure point at which slippage mainly occurs and to provide a guideline for CNTY strengthening. CNTY has a hierarchical structure, similar to wool fibers [17]. The structure of wool fiber has many hierarchic levels, as shown in Fig. 2.1. The basic elements are α-helix molecules, and assembled molecules form what is termed a protofibril (~2nm). Seven protofibrils form a microfibril (7~8 nm), which again produce a macrofibril (~400 nm). CNTY also has similar hierarchic levels (Fig. 2.2). The basic components of CNTY are individual CNTs, and they form a primary CNT bundle, termed a microbundle in this study. Component CNTs are assumed such that they are perfectly aligned along the yarn axis

and randomly stacked in a microbundle. The primary CNT bundle, the microbundle, forms a reticulated structure, and overlapped regions can be considered as secondary bundles, each of which is called a macrobundle (Fig. 2.3). The reticulated structure is highly beneficial with regard to high load-transfer efficiency from a load-bearing element to adjacent elements [12].

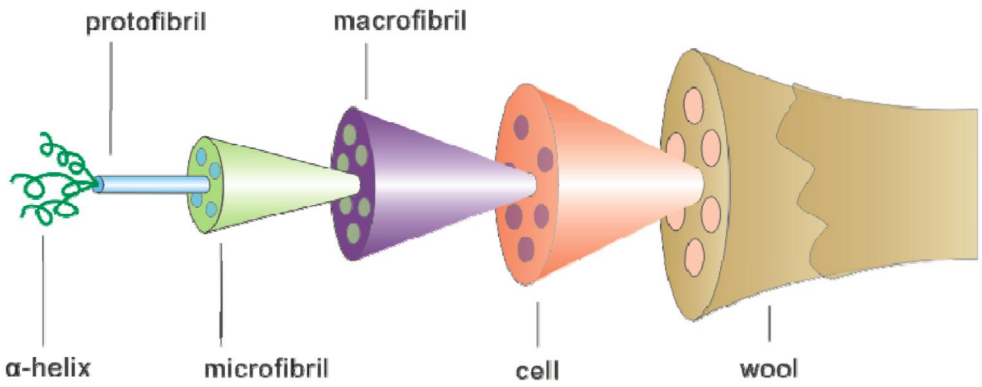

Fig. 2.1. Hierarchical structure of wool fiber.

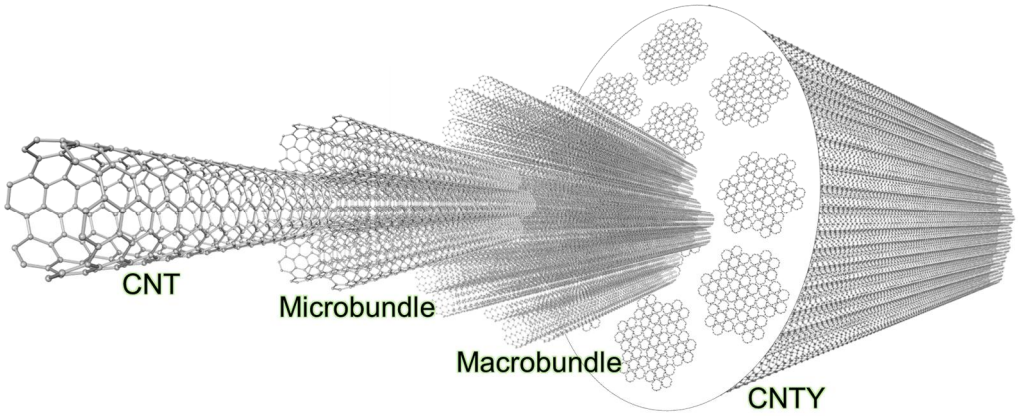

Fig. 2.2. Proposed hierarchical structure of CNTY.

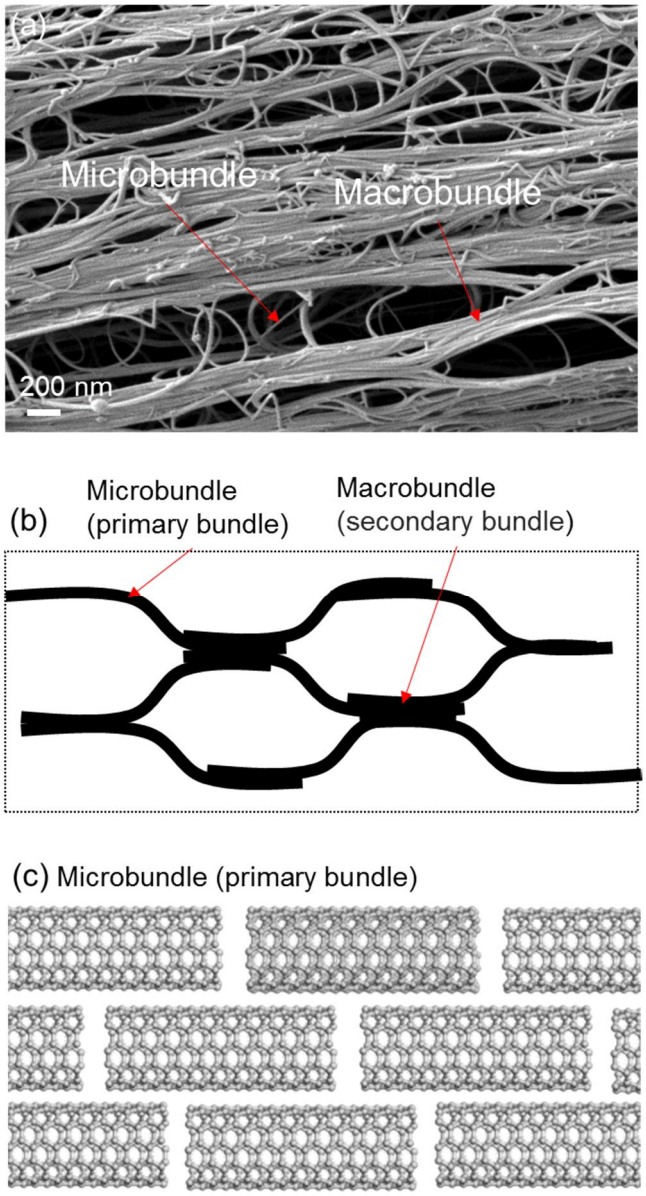

Fig. 2.3. (a) SEM image of as-prepared CNTY before densification, (b) a simple model of the hierarchical structure of CNTY, and (c) model of a CNT microbundle.

The CNTYs prepared in this study also showed typical yarn-like pullout failure, as shown in Fig. 2.4, and it was found that failure of the CNTY was generated by slippage rather than by the fracturing of the component CNTs. Considering the large number of pores and spaces between the macrobundles (Fig. 2.3a and Fig. 2.5), it is reasonable to assume that the CNTY strength depends on the CNT macrobundle strength. Two possible causes of CNTY failures can be considered. First, all CNT-CNT interfaces in a macrobundle contribute to the load-bearing capacity evenly regardless of the microbundle size or the total number of tubes. In this case, the specific strength of CNTY can be calculated from the surface area, the shear strength between individual CNTs, and the linear density of the component CNTs. The second cause is slippage which arises between the microbundles in a macrobundle. However, it is difficult to distinguish the two failure cases when slippage arises in the fractography results of CNTYs (Fig. 2.4). Therefore, both cases are theoretically addressed to determine the dependency of the specific strength on the tube nanostructure and bundle structure.

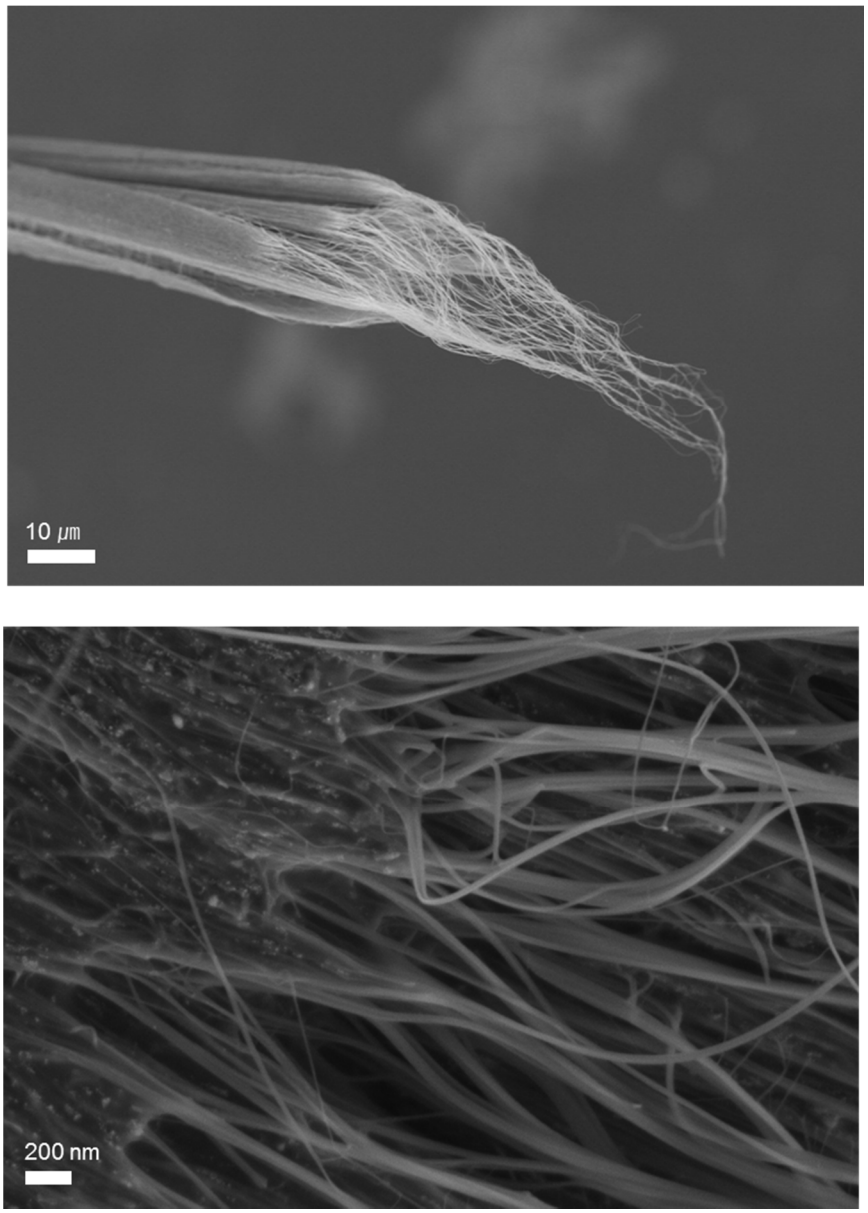

Fig. 2.4. SEM images of the end of CNTY after breakage under low and high magnification.

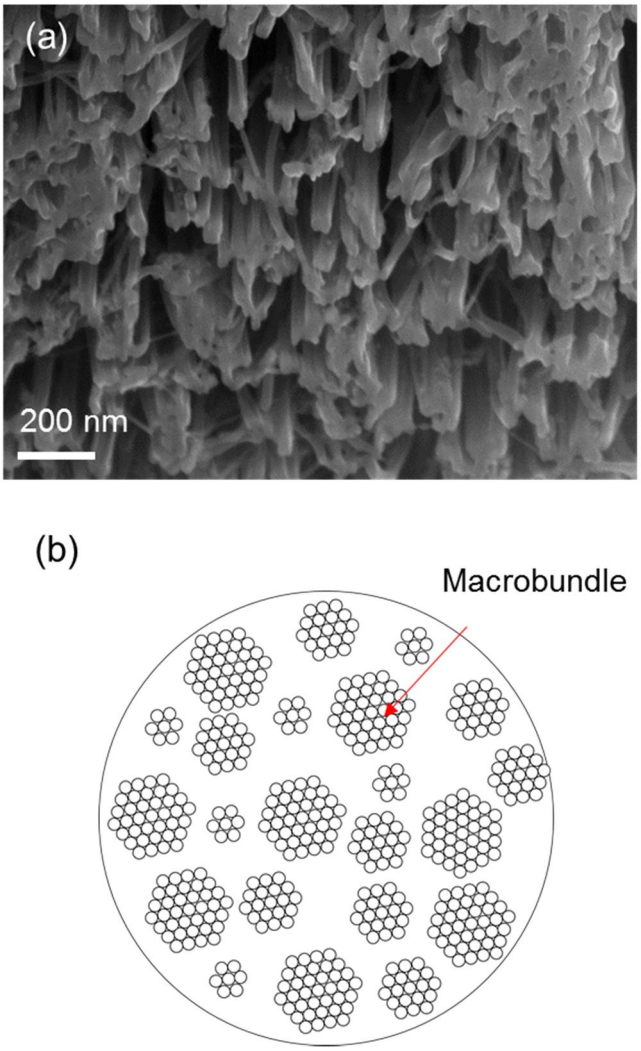

Fig. 2.5. (a) SEM images of a FIB cut cross-section of CNTY and (b) corresponding simple model.

2.3 Effect of the nanostructure on the CNTY strength

If we assume that all CNTs in a macrobundle evenly contribute to the ability to withstand force applied to the CNTY and failures caused by intertubular sliding, the specific strength of CNTY can be derived from the total shear force divided by the linear density. The total shear force (*F*) can be simply calculated using the total surface area of the CNT and the shear strength between the CNTs, as follows:

$$F\ (nN) = \frac{\pi D_o L}{4} \times \tau \quad (2.1)$$

Here, 1/4 denotes the mean length of the overlap between the CNTs and the interface of two surfaces. Moreover, the mass per unit length linear density (tex, g/km) of CNTs can be determined by the density of graphite and the structural parameters of the nanotubes, in this case the diameter and number of walls, via the following equation (2.2).

$$Linear\ density\ (tex, g/km) = 10^{-9} \times \frac{\pi}{4}(D_o^2 - D_i^2) \cdot \rho \quad (2.2)$$

Hence, the specific strength of CNTY can be determined as follows:

$$\sigma\ (GPa/(g \cdot cm^{-3}), N/tex) = \frac{D_o}{(D_o^2 - D_i^2)} \times \frac{\tau L}{\rho} \quad (2.3)$$

Here, σ is the specific strength of CNTY in GPa/(g cm^{-3}) or N/tex (numerically equivalent).

According to equation (2.3), which describes the specific strength of CNTY, the length and shear strength levels between the CNTs should be maximized to realize the ideal strength of individual CNTs in macroscopic CNTYs. This result is in good agreement with those in previous works on, for instance, classical yarn mechanics and other theories. The former term, k_1, in equation (2.3) is evidence of a favorable nanostructure of CNTs.

$$\frac{D_o}{(D_o^2 - D_i^2)} = k_1 \quad (2.4)$$

The inner diameter, D_i, of CNT can be expressed with the outer diameter, D_o, and the number of walls, n, of the CNT using the following equation (2.5), given that the distance between the tube walls is 0.34 nm.

$$D_i = D_0 - (2n \times 0.34) \quad (2.5)$$

As a result, the value of k_1 gradually decreases with an increase in both the outer diameter and number of walls of the nanotubes. This indicates that single-walled CNTs with a smaller diameter offers the advantage of better specific strength as a basic component of the CNTY, which break due to the pullout failure mechanism as opposed to the fracturing of single CNTs. Fig. 2.6 shows dependence of the value of k_1 on the number of walls and the outer diameter of the CNTs. This calculation method is typically used to determine the critical lengths of fillers in composite materials, and Vilatela et al. [4] used it to predict the CNTY strength. The meaning of the value of k_1 is nearly identical to that associated with the Ω_1 value suggested in the literature in relation to individual CNTs.

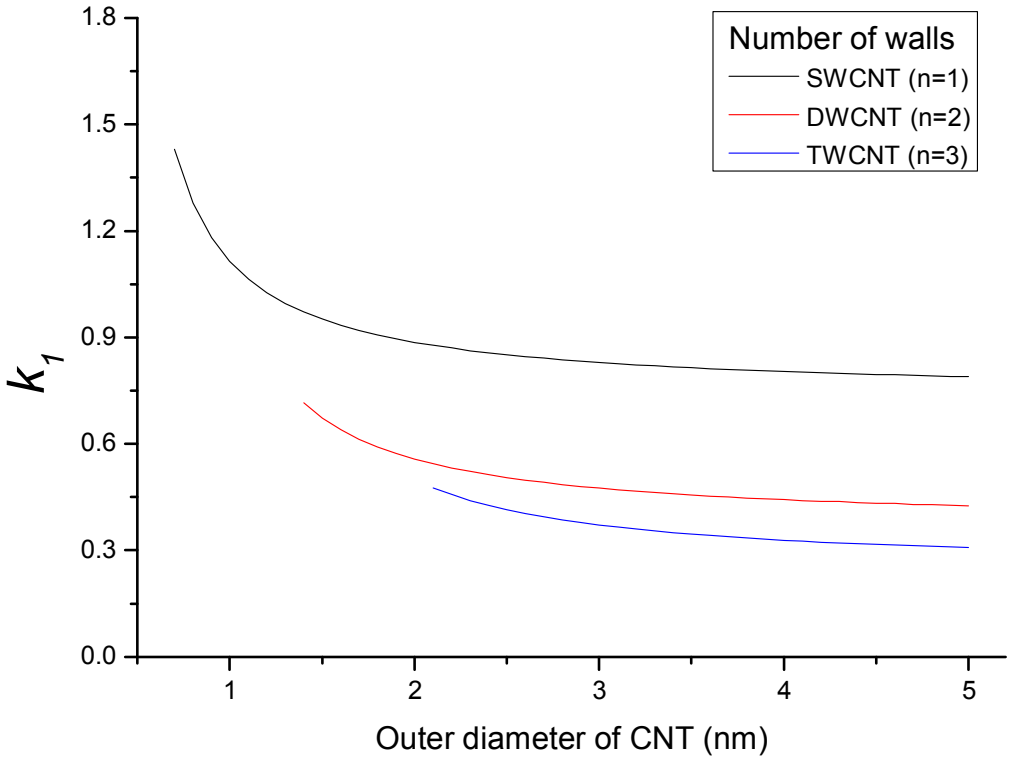

Fig. 2.6. Dependence of the value of k_1 on the nanotube diameter and number of walls.

The specific strength of the CNTY was predicted from the surface area, shear strength and linear density of CNTs assuming that all surfaces of the CNTs contribute to the load-bearing capacity. However, considering the actual contact area of CNTs, equation (2.3) overestimates the total shear force, as nanotubes have a round cross-section and because it is nearly impossible for all tube surfaces to be in contact with neighboring CNTs. Therefore, the fraction of the tube surface area in contact should be defined to estimate the actual specific strength of the CNTYs. Vilatela et al. [4] derived the proportion of the CNT surface area in contact with neighboring CNTs using classical elasticity theory [5, 18-20], expressed as the total energy of the tubes considering the surface energy and the flexural rigidity of the contact and non-contact areas of nanotubes in contact. This method can provide a significant means of determining a favorable nanostructure for better mechanical performance of CNTYs. The fraction of the perimeter in contact can be expressed as follows:

$$\Omega_2 = 1 - \frac{1}{R}\sqrt{\frac{nE_b}{2\gamma}} = 1 - \frac{1}{D_o}\sqrt{\frac{2nE_b}{\gamma}} \tag{2.6}$$

In this equation, r denotes the radius of curvature.

Fig. 2.7 presents the Ω_2 value against the structural parameters of the nanotubes with the surface energy and flexural rigidity set to 0.13 J/m^2 and 2.21 x 10^{-19} J, respectively, from the literature [18-20].

A larger diameter and fewer walls are prerequisites for a high specific strength of CNTYs due to the increase in the proportion of the effective surface area of the CNTs, as shown in Fig. 2.7. However, two values, k_1 and Ω_2, showed contradictory trends with regard to the diameters of the CNTs (Figs. 2.6 and 7). Fig. 2.8 shows the dependency of the combined value, $k_1\Omega_2$, on the nanotube diameter and number of walls, suggesting theoretically that SWCNTs with tubes with larger diameters are more appropriate to ensure better specific strength of the CNTYs.

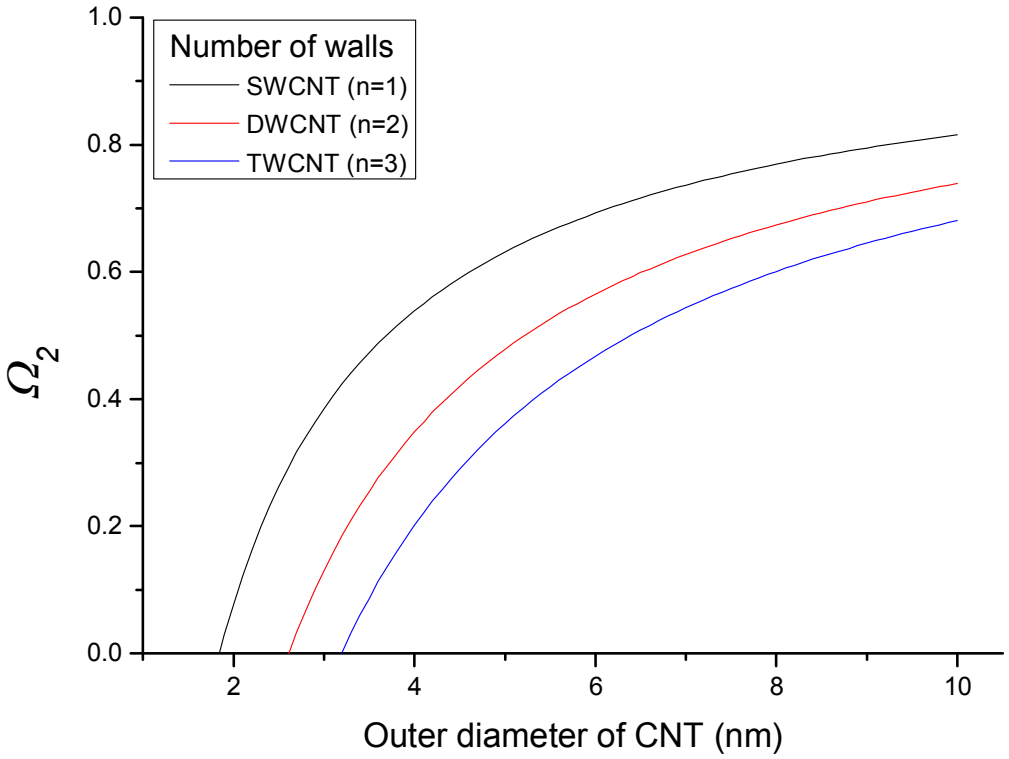

Fig. 2.7. The proportion of the surface area of the nanotubes in contact with other CNTs according to the outer diameter and number of walls.

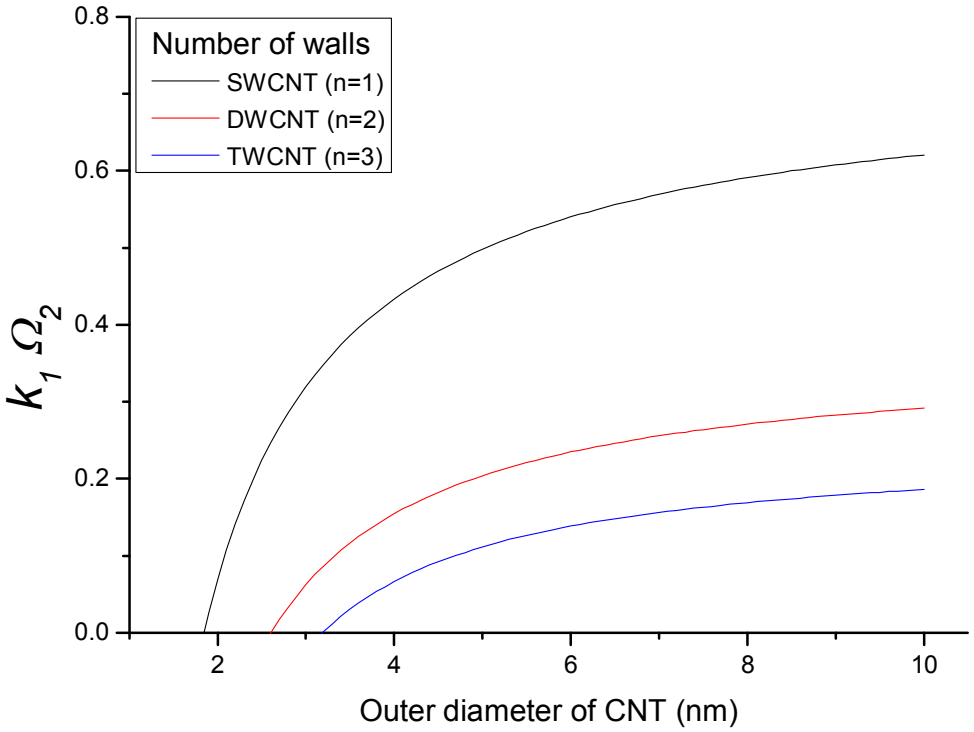

Fig. 2.8. Tendency of the $k_1\Omega_2$ value considering the diameters of the CNTs and number of walls.

2.4 Effect of the bundle size on the CNTY strength

The sizes of the microbundle and macrobundles of CNTs are among the key factors determining the strength of the CNTY. Recently, it was found by Yu et al. [16] and others [21, 22] that a relatively low CNTY strength was caused by inter-bundle sliding. These studies reported that only tubes on the perimeters of the bundles carried the load according to tensile testing of CNT bundles. Moreover, Vilatela et al. [4] found that Ω_1 will decrease greatly, leading to poor mechanical performance with an increase of the bundle size, i.e., the total number of tubes in a bundle, when the basic element for stress transfer in the CNTY is a bundle, as only the perimeter tubes contribute to the load-bearing capacity [16].

On the other hand, many empirical approaches aimed to fabricate closely packed CNTYs, meaning larger bundles, using methods such as solvent densification and mechanical rolling [23-27]. In such cases, the surfaces of inner tubes in contact with each other contribute to shear stress, while the outer surfaces of the perimeter CNTs in the assembly exposed to air do not contribute to the load-bearing capacity. Thus, larger CNT bundles are advantageous because they increase the faction of the CNT surface area in contact with neighboring CNTs, resulting in a greater capacity to withstand an applied load.

Considering the CNTY model suggested in this study, the earlier CNT bundles, smaller is better for greater mechanical performance of the CNTY, correspond to the microbundle. The latter bundles, larger bundles are favorable, are likely to be the macrobundle in this study. However, it is difficult to express the effect of each bundle size with regard to the specific strength of CNTYs quantitatively in

the form of an equation due to the complicated nature of assembled CNT structures.

2.5 Conclusion

The CNTY structure is described as having many hierarchical levels, similar to wool fibers, and the effects of the tube nanostructure and bundle size on the specific strength were discussed here. The key to improving the mechanical performance of CNTY is how effectively to utilize the CNT-CNT interface for better load-bearing capacity when applied to CNTYs. Single-walled CNTs with large diameters offer more potential to realize the ideal strength of CNTs in macroscopic CNTYs. In a previous model of the CNTY structure, the CNT-bundle yarn could not explain the contradiction between the theoretical and empirical results with regard to the effect of the bundle size on the strength. The hierarchical CNTY model proposed in this study showed the opposite tendency of the CNTY strength on the bundle size of micro- and macro-bundles. While a smaller size of low-level CNT bundles, i.e., microbundles, was helpful, a larger size of the bundle at the highest level, the macrobundle, was more effective for realizing better CNTY strength.

Despite the attempts to gain insight into the CNTY strength, actual CNTYs are more complicated than the level suggested in this study, and other parameters not dealt with here should be considered in order to estimate the specific strength of actual CNTYs more accurately.

2.6 References

[1] Zhang M, Atkinson KR, Baughman RH. Multifunctional carbon nanotube yarns by downsizing an ancient technology. Science 2004, 306, 1358-61.

[2] Zhao J, Zhang X, Di J, Xu G, Yang X, Liu X, et al. Double-peak mechanical properties of carbon-nanotube fibers. Small 2010, 6, 2612-7.

[3] Miao M. The role of twist in dry spun carbon nanotube yarns. Carbon 2016, 96, 819-26.

[4] Vilatela JJ, Elliott JA, Windle AH. A model for the strength of yarn-like carbon nanotube fibers. ACS Nano 2011, 5, 1921-7.

[5] Chopra NG, Benedict LX, Crespi VH, Cohen ML, Louie SG, Zettl A. Fully collapsed carbon nanotubes. Nature 1995, 377, 135.

[6] Elliott JA, Sandler JKW, Windle AH, Young RJ, Shaffer MSP. Collapse of single-wall carbon nanotubes is diameter dependent. Phys. Rev. Lett. 2004, 92, 095501.

[7] Naraghi M, Filleter T, Moravsky A, Locascio M, Loutfy RO, Espinosa HD. A multiscale study of high performance double-walled nanotube–polymer fibers. ACS Nano 2010, 4, 6463-76.

[8] Filleter T, Yockel S, Naraghi M, Paci JT, Compton OC, Mayes ML, et al. Experimental-computational study of shear interactions within double-walled carbon nanotube bundles. Nano Lett. 2012, 12, 732-42.

[9] O'Brien NP, McCarthy MA, Curtin WA. Improved inter-tube coupling in CNT bundles through carbon ion irradiation. Carbon 2013, 51, 173-84.

[10] Beese AM, Wei X, Sarkar S, Ramachandramoorthy R, Roenbeck MR, Moravsky A, et al. Key factors limiting carbon nanotube yarn strength: Exploring processing-structure-property relationships. ACS Nano 2014, 8, 11454-66.

[11] Paci JT, Furmanchuk Ao, Espinosa HD, Schatz GC. Shear and friction between carbon nanotubes in bundles and yarns. Nano Lett. 2014, 14, 6138-47.

[12] Ma W, Liu L, Zhang Z, Yang R, Liu G, Zhang T, et al. High-strength composite fibers: Realizing true potential of carbon nanotubes in polymer matrix through continuous reticulate architecture and molecular level couplings. Nano Lett. 2009, 9, 2855-61.

[13] Lee J, Kim T, Jung Y, Jung K, Park J, Lee D-M, et al. High-strength carbon nanotube/carbon composite fibers via chemical vapor infiltration. Nanoscale 2016, 8, 18972-9.

[14] Jung Y, Kim T, Park CR. Effect of polymer infiltration on structure and properties of carbon nanotube yarns. Carbon 2015, 88, 60-9.

[15] Oh JY, Yang SJ, Park JY, Kim T, Lee K, Kim YS, et al. Easy preparation of self-assembled high-density buckypaper with enhanced mechanical properties. Nano Lett. 2015, 15, 190-7.

[16] Yu MF, Files BS, Arepalli S, Ruoff RS. Tensile loading of ropes of single wall carbon nanotubes and their mechanical properties. Phys. Rev. Lett. 2000, 84, 5552-5.

[17] Fan J, Liu JF, He JH. Hierarchy of wool fibers and fractal dimensions. Int. J. Nonlin. Sci. Num. Simul. 2011, 9, 293.

[18] Kudin KN, Scuseria GE, Yakobson BI. C_2F, BN, and C nanoshell elasticity from ab initio computations. Phys. Rev. B 2001, 64, 235406.

[19] Gülseren O, Yildirim T, Ciraci S. Systematic ab initio study of curvature effects in carbon nanotubes. Phys. Rev. B 2002, 65, 153405.

[20] Qiang L, Marino A, Rui H. Elastic bending modulus of monolayer graphene. J. Phys. D: Appl. Phys. 2009, 42, 102002.

[21] Qian D, Liu WK, Ruoff RS. Load transfer mechanism in carbon nanotube ropes. Comp. Sci. Technol. 2003, 63, 1561-9.

[22] Naraghi M, Bratzel GH, Filleter T, An Z, Wei X, Nguyen ST, et al. Atomistic investigation of load transfer between DWNT bundles "Crosslinked" by PMMA oligomers. Adv. Funct. Mater. 2013, 23, 1883-92.

[23] Liu K, Sun Y, Lin X, Zhou R, Wang J, Fan S, et al. Scratch-resistant, highly conductive, and high-strength carbon nanotube-based composite yarns. ACS Nano 2010, 4, 5827-34.

[24] Kai L, Yinghui S, Ruifeng Z, Hanyu Z, Jiaping W, Liang L, et al. Carbon nanotube yarns with high tensile strength made by a twisting and shrinking method. Nanotechnol. 2010, 21, 045708.

[25] Cho H, Lee H, Oh E, Lee S-H, Park J, Park HJ, et al. Hierarchical structure of carbon nanotube fibers, and the change of structure during densification by wet stretching. Carbon 2018, 136, 409-16.

[26] Wang JN, Luo XG, Wu T, Chen Y. High-strength carbon nanotube fibre-like ribbon with high ductility and high electrical conductivity. Nat. Commun. 2014, 5, 3848.

[27] Li S, Zhang X, Zhao J, Meng F, Xu G, Yong Z, et al. Enhancement of carbon nanotube fibres using different solvents and polymers. Comp. Sci. Technol. 2012, 72, 1402-7.

Chapter 3 Empirical Approach 1: Effects of the Nanostructure Characteristics of Individual Component CNTs on the CNTY Strength

3.1 Introduction

Carbon nanotubes (CNTs) are most attractive as a filler material for fiber-reinforced composites (FRCs) and as a component in super-strong fibers due to their outstanding mechanical strength and high aspect ratio [1-5]. In the early 2000s, mainly manufacturing methodologies of CNTYs were studied and introduced. These methods of producing CNTYs included liquid crystalline spinning, CNT array spinning, and direct spinning [6-9]. Morphological features such as the degree of CNT alignment on the yarn axis and the twist angle were widely investigated to improve the mechanical properties of CNTYs [10-15].

CNTs are generally classified according to the number of walls, and there are a wide variety of mechanical and electrical properties depending on this factor. For instance, single-walled CNTs (SWCNTs) are either semiconducting or metallic depending on the chirality, while multi-walled CNTs (MWCNTs) show only a metallic property [16-19]. In addition, a high aspect ratio of CNTs is considered to be the most important feature to realize the ideal strength of CNTs, which can be as high as 60 GPa in macroscopic CNTYs. According to the theoretical approach introduced in chapter 2, the number of

walls and the diameter, however, are the key factors to consider when attempting to enhance the specific strength of CNT yarns (CNTYs), as opposed to the aspect ratio given the deformability of CNTs.

In this chapter, various CNTYs with nanostructures different from those of SWCNTs and MWCNTs are synthesized in order to confirm the reliability of the theoretical approach and investigate the effects of the nanostructure characteristics of individual CNTs on the mechanical performance of CNTYs. In general, SWCNTs are assumed to be highly promising materials to achieve high-strength materials and yarns. Unlike common expectations, however, CNTYs with double-walled CNTs (DWCNTs) exhibit both the highest engineering and highest true specific strength levels. The true specific strength of each CNTY showed tendencies very similar to that of the theoretically predicted strength in chapter 2.

3.2 Experimental

Spinning the CNTYs

CNTs with various nanostructures, from single-walled to multi-walled carbon nanotubes, were synthesized by means of floating-catalyst chemical vapor deposition at 1200 °C using a previously reported method [20-22]. Ferrocene, thiophene, methane and hydrogen were added to the reactor and the composition was varied according to the desired nanostructure of the nanotubes. As-synthesized component CNTs were spun into a continuous yarn using a water bath at the bottom of a vertical furnace (Fig. 3.1).

Characterization of CNTs and CNTYs

The linear densities (tex, g/km) of the CNTYs were measured by weighing 50 m of each sample. A thermal gravimetric analysis (TGA, SDT-Q600, TA Instruments) was used to determine the purity of the CNTYs between room temperature and 1000 °C in an air atmosphere. The number of walls and the diameters of the synthesized CNTs were observed via high-resolution TEM (JEM-2100F, JEOL). The mechanical properties were measured using a CNTY length of 10 mm at a strain rate of 3 mm/min on a tensile stage (TST350, Linkam). The crystallinity of the CNTs was evaluated using Raman spectroscopy with a 532nm laser (RAMANplus, Nanophoton).

Measurement of CNT length

As-synthesized CNTYs were purified using the following method. The CNTYs were heat-treated in an air atmosphere at 500 °C for one hour and washed with HCl several times to remove the amorphous carbon and iron catalyst in the CNTYs. The purified CNTYs were then neutralized with DI water and dried in a vacuum oven at 80 °C. They were subsequently dissolved in chlorosulfonic acid with a concentration of 0.05 mg/ml, and droplets were dropped onto a wafer. Isolated CNTs were successfully deposited on the wafer, and the lengths were measured by a FE-SEM (MERLIN Compact, ZEISS) image analysis.

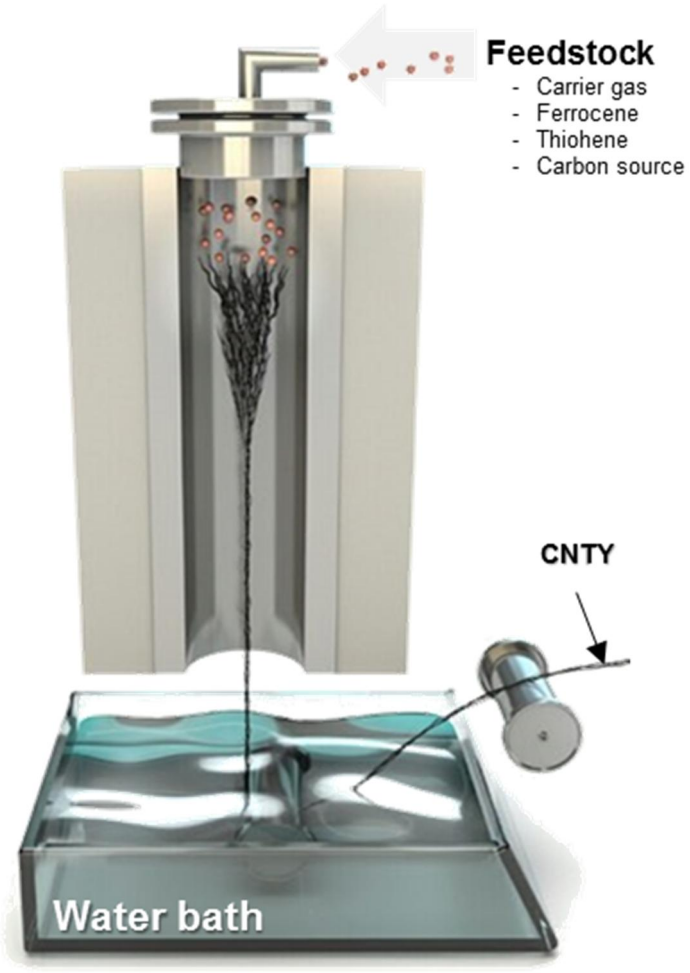

Fig. 3.1. Schematic illustration of the CNTY fabrication process by direct spinning.

3.3 Results and discussion

Despite the fact that a number of works have revealed the role of the promotor thiophene, the synthesis mechanism of CNTs by direct spinning has not been clarified to date. Sulfur critically affects the formation of CNTs during the chemical vapor deposition process [7, 23-25]. Although the mechanisms by which sulfur influences this process have been explained, these mechanisms are not completely understood. They include deactivation of the catalysts by the blocking of active sites, a decrease in the melting point of the catalysts, and interaction with growing CNTs. Sulfur is generally regarded as a promotor as it causes the carbon atoms produced by the decomposition of carbon sources to diffuse rapidly into an iron catalyst due to the iron sulfide which forms on the catalyst [20, 23, 26-28]. In spite of the unclear CNT growth mechanism, it has been experimentally found that the nanostructures of CNTs can be varied according to the feedstock composition. Reguero et al. [29] and Lee et al. [25] reported that altering the promotor concentration allowed control of the catalyst particle formation and the number of tube walls.

In this study, SWCNTs tended to be synthesized with low thiophene levels and carbon source feed rates, while MWCNTs were produced at higher thiophene and carbon source concentration levels. As shown in the TEM images in Fig. 3.2a-c in the Raman spectra (Fig. 3.2d), SWCNTs, DWCNTs, and MWCNTs were successfully synthesized in order to investigate the effects of tube nanostructure on the mechanical strength capabilities of CNTYs. Typical radial-breathing-mode (RBM) peaks, which indicate the presence of SWCNTs, appeared in the Raman spectra at low wavenumbers (100~500 cm^{-1}) [20, 30, 31].

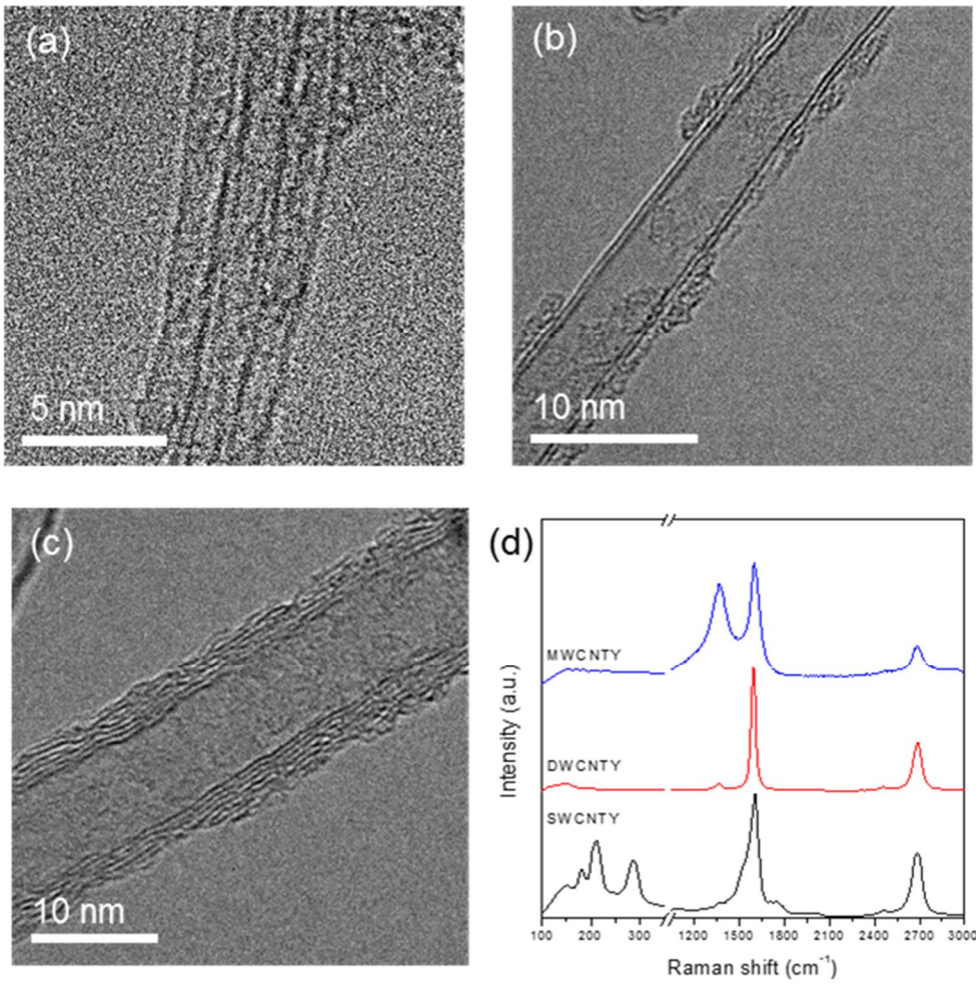

Fig. 3.2. TEM images of (a) SWCNTs, (b) DWCNTs, and (c) MWCNTs, and (d) Raman spectra of each CNT.

The length of each CNT was measured from SEM images of isolated CNTs (Fig. 3.3). CNTs were separated into individual CNTs using the method described in the experimental section. CNTs synthesized by direct spinning were much shorter compared to other CNTs which are used to manufacture CNTYs by liquid crystalline and CNT array spinning [6, 14, 32, 33]. The numbers of walls and the diameters of the CNTs were observed by TEM. All structural parameters, i.e., the diameters, the numbers of walls and length of each CNT, along with the theoretical values, k_1 and Ω_2, are summarized in Table 3.1. The theoretical value, k_1, was highest for the SWCNTs, as high as 0.88 among the CNTs in this study, as expected from chapter 2 because all layers contribute to the load-bearing capacity.

Despite the lowest number of walls and the highest value of k_1 of the SWCNTs, the DWCNTYs showed the highest $k_1\Omega_2$ value among the samples, as the value, Ω_2, which indicates the deformability in the radial direction of the tubes for DWCNTs, is much higher than that of the SWCNTs, as high as 0.48 in this case. This outcome suggests that the proportion of the surface area in contact with neighboring CNTs for the DWCNTs synthesized in this work was highest among the samples considering theoretical approaches used based on the structural parameters. In addition, the DWCNTYs are predicted to store or dissipate the tensile stress applied to the CNTYs most effectively, resulting higher mechanical performance.

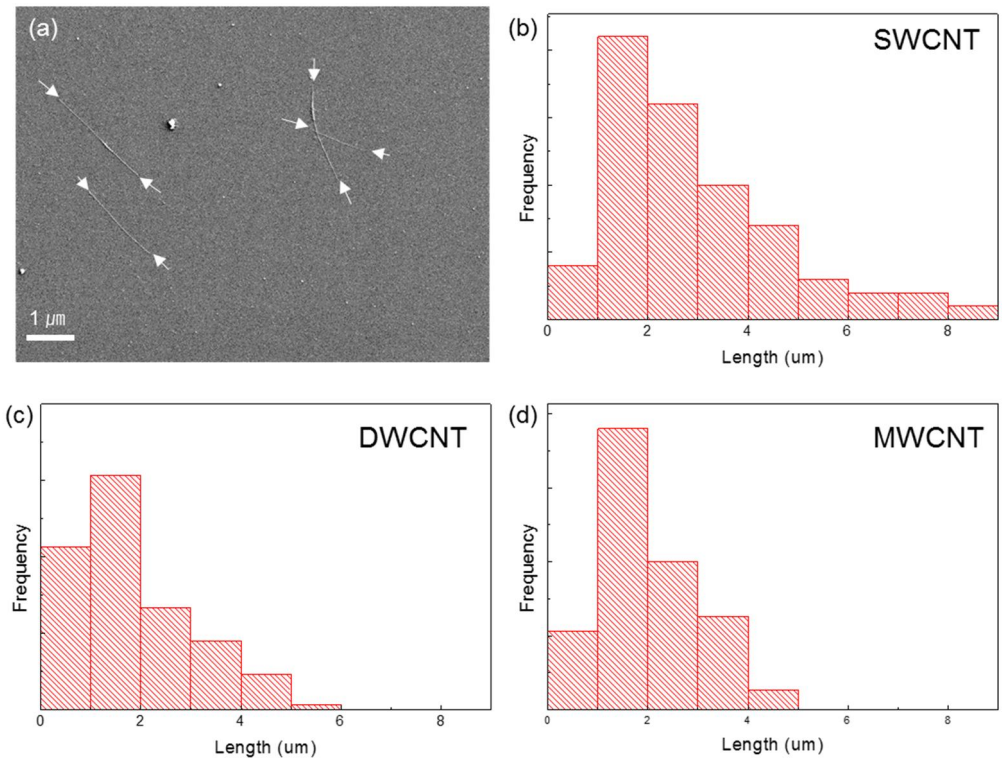

Fig. 3.3. (a) SEM images of isolated individual CNTs and (b-d) length distribution of each CNT. (white arrows indicate the ends of the CNTs)

	SWCNT	DWCNT	MWCNT
Structural parameters			
Diameter (nm)	~2.1	~5	~10.5
Number of walls	1	2	~7
Average length (um)	2.72	1.90	1.98
Theoretical values			
k_1	0.88	0.43	0.14
Ω_2	0.12	0.48	0.54
$k_1 \cdot \Omega_2$	0.11	0.21	0.08

Table 3.1. Structural parameters and theoretical values of each CNT.

Directly spun CNTYs contain inherent impurities, amorphous carbon, and iron catalyst as these CNTYs were not purified after the synthesis process (Fig. 3.4). The CNT purity rate was quantitatively analyzed because impurities are not considered as load-bearing elements, as shown in Fig. 3.5. Amorphous carbon is normally burned out below the temperature of CNT pyrolysis, and CNTs become fully decomposed at 1000 °C [26, 35]. Quantitative analysis results of the amorphous carbon, residue catalyst and the CNTs are summarized in Table 3.2. A large amount of the iron catalyst in an inactivated state was found in the SWCNTs, and the purity levels of the CNTs were approximately 52.5 %, 73.8 %, and 71.7 % for the SWCNTs, DWCNTs, and MWCNTs, respectively. In order to compare the true mechanical strength with the theoretically predicted strength, the engineering strength of each CNTY was changed to the true strength based on each purity (Table 3.3). The true specific strength in this study is the specific strength assuming that the applied force (tensile stress) is withstood by only the CNTs, not by other impurities considering the load-bearing elements. DWCNTYs showed the highest mechanical performance in terms of both the engineering and true specific strength due to their favorable structure and high purity.

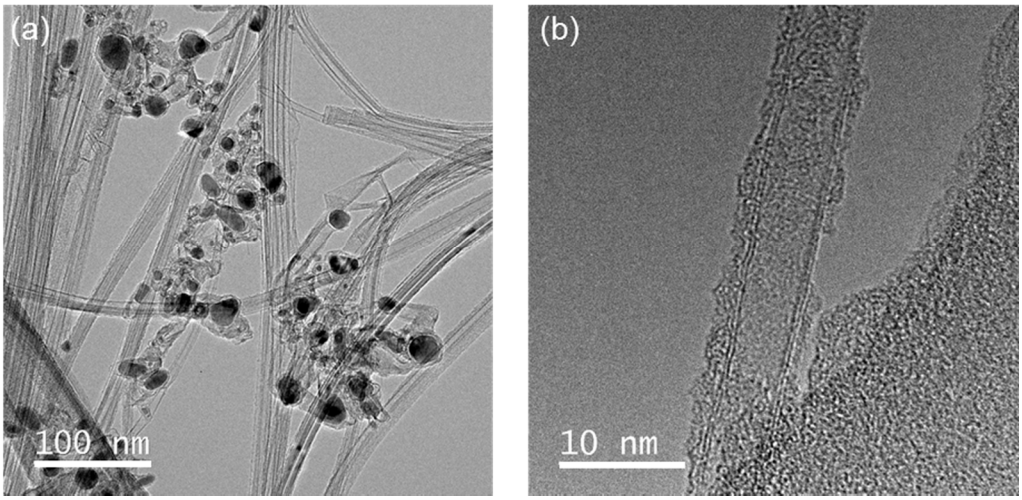

Fig. 3.4. TEM images of (a) the catalyst used and (b) amorphous impurities in CNTYs.

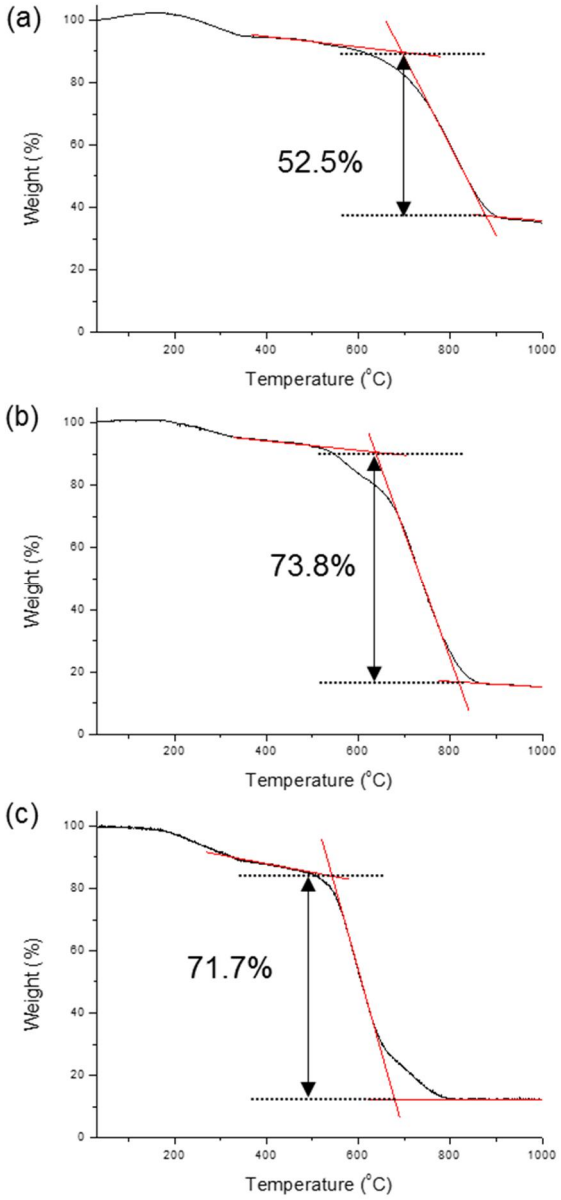

Fig. 3.5. Quantitative analysis of each CNT by TGA: (a) SWCNTs, (b) DWCNTs, and (c) MWCNTs.

Table 3.2. Quantitative analysis results of amorphous carbon, residue catalyst and the CNTYs for each CNT.

wt%	SWCNT	DWCNT	MWCNT
Amorphous carbon	10.2	9.4	16.1
Residue catalyst	37.3	16.8	12.2
CNT	52.5	73.8	71.7

Table 3.3. Engineering and true strength results of CNTYs.

	SWCNTY	DWCNTY	MWCNTY
Engineering specific strength (GPa/(g cm^{-3}), N/tex)	1.15 ± 0.18	1.79 ± 0.22	0.79 ± 0.04
True specific strength (GPa/(g cm^{-3}), N/tex)	2.19 ± 0.34	2.42 ± 0.30	1.10 ± 0.06

The theoretical specific strength was plotted against the tube diameter for each case considering the number of tube walls, i.e., single-, double- and seven-walled CNTs, according to equation (2.13) in Fig. 3.6, the following are assumed: flexural rigidity of the wall $E = 2.21 \times 10^{-19} J$, surface energy of the tube $\gamma = 0.13 J/m^2$, shear strength between CNTs $\tau = 14 MPa$, and density $\rho = 2.23 g/cm^3$. The filled symbols in Fig. 3.6 denote the practically synthesizable diameter range of the CNTs considering the cases of different numbers of tube walls in previous reports. The experimental results, i.e., the true specific strengths, of each CNTY are indicated by the red symbols in the plot of the theoretical prediction, and they are well matched with the estimated values. Although CNTYs made up of SWCNTs with a large diameter have more of a potential to be theoretically much stronger, it has not been reported that CNTs with a diameter larger than 2.5 nm for CNTYs could be practically synthesized. DWCNTs generally have a diameter range from 3 to 10 nm, whereas that for MWCNTs exceeds 5 nm [32, 36, 37]. Moreover, having considered the purity of each CNT, the DWCNTYs are practically most promising for high-strength CNTYs.

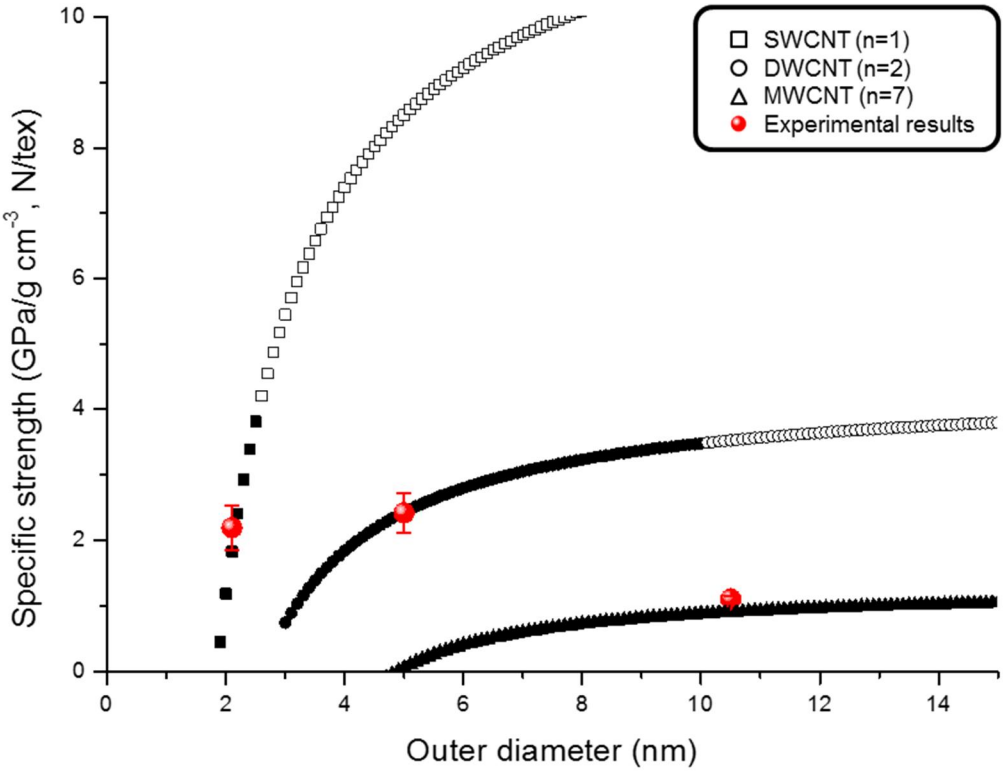

Fig. 3.6. Theoretical specific strength and true specific strength outcomes of SWCNTs, DWCNTs, and MWCNTs (n=7). (Filled symbols are plots of the practically synthesizable diameter of each CNT type.)

`

3.4 Conclusion

Three different CNTYs with different nanostructured CNTs were prepared by direct spinning in order to confirm the validity of theoretical approaches. The purity of DWCNTs was highest, and the DWCNTYs presented both the highest engineering and true specific strength levels. The true specific strengths of three CNTYs were in good agreement with the values estimated by theoretical predictions. Although SWCNTs with larger diameters are likely to be much more capable of utilizing the excellent mechanical properties of individual CNTs in macroscopic-scale CNTYs, DWCNTYs were found to be experimentally the strongest among them due to the practical limitation of the synthesis of large-diameter SWCNTs.

3.5 References

[1] Coleman JN, Khan U, Blau WJ, Gun'ko YK. Small but strong: A review of the mechanical properties of carbon nanotube–polymer composites. Carbon 2006, 44, 1624-52.

[2] Yu MF, Files BS, Arepalli S, Ruoff RS. Tensile loading of ropes of single wall carbon nanotubes and their mechanical properties. Phys. Rev. Lett. 2000, 84, 5552-5.

[3] Vigolo B, Pénicaud A, Coulon C, Sauder C, Pailler R, Journet C, et al. Macroscopic fibers and ribbons of oriented carbon nanotubes. Science 2000, 290, 1331-4.

[4] Yu M-F, Lourie O, Dyer MJ, Moloni K, Kelly TF, Ruoff RS. Strength and breaking mechanism of multiwalled carbon nanotubes under tensile load. Science 2000, 287, 637-40.

[5] Demczyk BG, Wang YM, Cumings J, Hetman M, Han W, Zettl A, et al. Direct mechanical measurement of the tensile strength and elastic modulus of multiwalled carbon nanotubes. Mater. Sci. Eng. A 2002, 334, 173-8.

[6] Ericson LM, Fan H, Peng H, Davis VA, Zhou W, Sulpizio J, et al. Macroscopic, neat, single-walled carbon nanotube fibers. Science 2004, 305, 1447-50.

[7] Li Y-L, Kinloch IA, Windle AH. Direct spinning of carbon nanotube fibers from chemical vapor deposition synthesis. Science 2004, 304, 276-8.

[8] Zhang M, Atkinson KR, Baughman RH. Multifunctional carbon nanotube yarns by downsizing an ancient technology. Science 2004, 306, 1358-61.

[9] Zhu HW, Xu CL, Wu DH, Wei BQ, Vajtai R, Ajayan PM. Direct synthesis of long single-walled carbon nanotube strands. Science 2002, 296, 884-6.

[10] Koziol K, Vilatela J, Moisala A, Motta M, Cunniff P, Sennett M, et al. High-

performance carbon nanotube fiber. Science 2007, 318, 1892-5.

[11] Xu W, Chen Y, Zhan H, Wang JN. High-strength carbon nanotube film from improving alignment and densification. Nano Lett. 2016, 16, 946-52.

[12] Alemán B, Reguero V, Mas B, Vilatela JJ. Strong carbon nanotube fibers by drawing inspiration from polymer fiber spinning. ACS Nano 2015, 9, 7392-8.

[13] Miao M. Yarn spun from carbon nanotube forests: Production, structure, properties and applications. Particuology 2013, 11, 378-93.

[14] Zhao J, Zhang X, Di J, Xu G, Yang X, Liu X, et al. Double-peak mechanical properties of carbon-nanotube fibers. Small 2010, 6, 2612-7.

[15] Miao M. The role of twist in dry spun carbon nanotube yarns. Carbon 2016, 96, 819-26.

[16] Kataura H, Kumazawa Y, Maniwa Y, Umezu I, Suzuki S, Ohtsuka Y, et al. Optical properties of single-wall carbon nanotubes. Synth. Met. 1999, 103, 2555-8.

[17] Bachilo SM, Strano MS, Kittrell C, Hauge RH, Smalley RE, Weisman RB. Structure-assigned optical spectra of single-walled carbon nanotubes. Science 2002, 298, 2361-6.

[18] Strano MS, Dyke CA, Usrey ML, Barone PW, Allen MJ, Shan H, et al. Electronic structure control of single-walled carbon nanotube functionalization. Science 2003, 301, 1519-22.

[19] Hirschmann TC, Araujo PT, Muramatsu H, Zhang X, Nielsch K, Kim YA, et al. Characterization of bundled and individual triple-walled carbon nanotubes by resonant Raman spectroscopy. ACS Nano 2013, 7, 2381-7.

[20] Jung Y, Song J, Huh W, Cho D, Jeong Y. Controlling the crystalline quality of carbon nanotubes with processing parameters from chemical vapor deposition synthesis. Chem. Eng. J. 2013, 228, 1050-6.

[21] Jung Y, Kim T, Park CR. Effect of polymer infiltration on structure and properties of carbon nanotube yarns. Carbon 2015, 88, 60-9.

[22] Choi J, Jung Y, Yang SJ, Oh JY, Oh J, Jo K, et al. Flexible and robust thermoelectric generators based on all-carbon nanotube yarn without metal electrodes. ACS Nano 2017, 11, 7608-14.

[23] Motta MS, Moisala A, Kinloch IA, Windle AH. The Role of Sulphur in the synthesis of carbon nanotubes by chemical vapour deposition at high temperatures. J. Nanosci. Nanotechnol. 2008, 8, 2442-9.

[24] Conroy D, Moisala A, Cardoso S, Windle A, Davidson J. Carbon nanotube reactor: Ferrocene decomposition, iron particle growth, nanotube aggregation and scale-up. Chem. Eng. Sci. 2010, 65, 2965-77.

[25] Lee S-H, Park J, Kim H-R, Lee J, Lee K-H. Synthesis of high-quality carbon nanotube fibers by controlling the effects of sulfur on the catalyst agglomeration during the direct spinning process. RSC Adv. 2015, 5, 41894-900.

[26] Gspann TS, Smail FR, Windle AH. FD173: Spinning of carbon nanotube fibres using the floating catalyst high temperature route: purity issues and the critical role of sulphur. Faraday Discuss. 2014, 173, 47-65.

[27] Tibbetts GG, Bernardo CA, Gorkiewicz DW, Alig RL. Role of sulfur in the production of carbon fibers in the vapor phase. Carbon 1994, 32, 569-76.

[28] Ci L, Rao Z, Zhou Z, Tang D, Yan X, Liang Y, et al. Double wall carbon nanotubes promoted by sulfur in a floating iron catalyst CVD system. Chem. Phys. Lett. 2002, 359, 63-7.

[29] Reguero V, Alemán B, Mas B, Vilatela JJ. Controlling carbon nanotube type in macroscopic fibers synthesized by the direct spinning process. Chem. Mater. 2014, 26, 3550-7.

[30] Dresselhaus MS, Dresselhaus G, Saito R, Jorio A. Raman spectroscopy of carbon nanotubes. Phys. Rep. 2005, 409, 47-99.

[31] Heller DA, Barone PW, Swanson JP, Mayrhofer RM, Strano MS. Using Raman spectroscopy to elucidate the aggregation state of single-walled carbon nanotubes. J. Phys. Chem. B 2004, 108, 6905-9.

[32] Tsentalovich DE, Headrick RJ, Mirri F, Hao J, Behabtu N, Young CC, et al. Influence of carbon nanotube characteristics on macroscopic fiber properties. ACS Appl. Mater. Interfaces 2017, 9, 36189-98.

[33] Liu K, Sun Y, Lin X, Zhou R, Wang J, Fan S, et al. Scratch-resistant, highly conductive, and high-strength carbon nanotube-based composite yarns. ACS Nano 2010, 4, 5827-34.

[34] Lee S-H, Kim H-R, Lee T, Lee H, Lee J, Lee J, et al. Synthesis of carbon nanotube fibers from carbon precursors with low decomposition temperatures using a direct spinning process. Carbon 2017, 124, 219-27.

[35] Jung Y, Jeong YC, Kim JH, Kim YS, Kim T, Cho YS, et al. One step preparation and excellent performance of CNT yarn based flexible micro lithium ion batteries. Energy Storage Mater. 2016, 5, 1-7.

[36] Vilatela JJ, Elliott JA, Windle AH. A model for the strength of yarn-like carbon nanotube fibers. ACS Nano 2011, 5, 1921-7.

[37] Sundaram RM, Koziol KKK, Windle AH. Continuous direct spinning of fibers of single-walled carbon nanotubes with metallic chirality. Adv. Mater. 2011, 23, 5064-8.

Chapter 4 Empirical Approach 2: Effect of the Bundling Behavior of Individual Component CNTs on the CNTY Strength

4.1 Introduction

Carbon nanotubes (CNTs) and CNT yarns (CNTYs) have drawn considerable attention due to their excellent mechanical and electrical properties and their potential utility [1-3]. CNTYs with a high electrical conductivity and strength are thought to require void-free and defect-free materials with a high degree of CNT alignment; however, CNTYs produced through a variety of methods have exhibited significantly poorer mechanical and electrical properties [2, 4-9] than individual CNTs, which exhibit moduli as high as 1 TPa, strengths as high as 50 GPa [10, 11], and electrical conductivities on the order of 10^6 S m^{-1} [3, 12, 13]. Over the last decade, several papers have described the manufacture and improvement of CNTY properties through nanostructural control, including the number of walls, diameters, and lengths of the CNTs [14, 15], as well as microstructural control, including the twist angle and CNT alignment along the yarn axis [1, 9, 16]. Long and highly aligned CNTs tend to produce high-performance CNTYs [1, 17]. Despite the variety of structural approaches tested thus far, raw CNTYs still show poor properties due to the interfacial slippage among bundles or CNTs [7, 8]. Recent studies have modified the CNT surfaces using chemical reactions to introduce covalent or hydrogen bonds, which are stronger than the van der Waals interactions, in an effort to enhance the interfacial strength [18-20].

The functional groups introduced onto the CNT surfaces are essential for inducing bonding sites [21], and they provide a powerful approach to improving the interfacial strength; however, functionalization necessarily introduces defects. The conversion of sp^2 into sp^3 carbon atoms on the CNT surfaces decreases the inherent mechanical and electrical properties of the CNTs [12, 13]. Additionally, it is difficult to attach functional groups uniformly onto the CNT surfaces because additional procedures, such as re-dispersing closely packed CNTs for chemical reactions after CNTY formation, are required.

Physical interactions may potentially ameliorate interfacial slippage. One such method of enhancing the physical interactions involves polymer infiltration. This method does not require the re-dispersion of CNTs or chemical modification. The amount of additive infiltrated into the CNTY may be easily controlled. Polymer infiltration, therefore, provides a simple and promising method of fabricating high-performance CNTYs without destroying the unique CNT structures or properties. Only a few polymers, including epoxy [22, 23] or PVA [2, 14, 22, 24-26], are effective in improving the CNTY load transfer efficiency, although it has not previously been understood how these polymers act in the CNTY/polymer composite materials.

The architectures of CNTs are important not only in CNT/polymer composite materials, but also in CNTYs. Raw CNTY or CNTY/polymer materials deformed differently under tensile stress, depending on the CNT architecture, which influenced the load delivery efficiency and provided very different properties [1, 6, 14, 22, 27, 28]. Although the CNTs present in the CNTYs were linked to one another through weak van der Waals interactions, the total interaction energy depended strongly on the CNT bundle structure, including the contact area. Closely packed CNT bundles tended to

show better mechanical properties [9, 25, 26]. Solvent densification provides one approach to improving both the mechanical and electrical properties of the CNTYs by reducing the number and size of the pores in the CNTYs, thereby changing the bundle structure without incorporating supporting materials [9, 25]. The structure of a CNT is of crucial importance to determining both the mechanical properties and the electrical properties of a CNTY and a CNTY/polymer composite material [1, 16, 22]. For these reasons, conventional composite theory, which has focused mainly on the interfacial strength between the matrix and the CNTs without considering the CNT architectures, has not been able to explain CNTY strengthening via polymer infiltration [22, 29, 30].

In this work, we explored the effects of polymer infiltration into CNTYs and measured the structural and property changes that took place throughout the process. A variety of polymers with different Hansen affinity parameters (HAPs) toward CNTs were infiltrated into the CNTYs in an effort to characterize the effects of the interactions between the CNTs and the polymer. The structural changes that took place during the process and the properties of the polymer-infiltrated CNTY were strongly related to the interactions determined by the HAP. The mechanical and electrical properties were simultaneously improved by polymer infiltration into the CNTY. The deformations of the CNTYs could be predicted based on the relationship between the properties and the structures of the polymers infiltrated into the CNTYs.

4.2 Experimental

Spinning the CNTYs

Continuous CNTYs were prepared using aerogel spinning methods involving chemical vapor deposition (CVD) in a vertical furnace at 1200 °C [29, 30]. The carrier gas and reactants, hydrogen, ferrocene, thiophene, and methane, were supplied at the top of furnace, and the CNT assemblies were transformed into the yarn through a water bath at the bottom of the furnace. Adsorbed water was removed by heating at 100 °C in a vacuum dry oven.

Solvent and polymer infiltration into the CNTY

The solvent- and polymer-infiltrated CNTYs were obtained by passing the CNTY through a second bath, as shown in Fig. 4.1a, at room temperature. One-third of the winder was submerged in the second bath filled with the solvent or polymer solution. The CNTY was soaked in the second bath solution for an hour to prepare the fully solvent- or polymer-absorbed CNTYs to eliminate the kinetic effect because the polymer infiltration into CNTYs is a kinetic limited process. The CNTY was then dried in a vacuum oven at 100 °C for more than 6 hours. The densification and polymer infiltration agents dimethyl sulfoxide (DMSO), PS (MW 280000, Sigma Aldrich), PAN (MW 150000, Sigma Aldrich), and PVA (MW 130000, Sigma Aldrich) were purchased and used as received. The polymer infiltration bath was prepared using polymer solutions (0.05~1.0 wt%). The polymers were dissolved in the solvents (PS in dimethylformamide (DMF), PAN and PVA in DMSO) at 80 °C.

Polymer/CNT composite

CNT (CM250, Hanwha Chemical : 0.5, 3 and 5 w/w%) were dispersed in 5 wt% each polymer solution, using a horn-type ultrasonicator (SONOPLUS UW-3200, Bandelin Electric) for 30 min. Optical microscope (BX-52, Olympus) was use to analyze CNT dispersion state and the PS solution showed the highest dispersibility among three polymers. Also, CNT/PS had the lowest resistivity among three 3 w/w% CNT/polymer composite films and percolation threshold.

Characterization of CNTYs

The linear densities (tex, g/km) of the raw and polymer-infiltrated CNTYs were measured by weighing 50 m of each sample. Thermal gravimetric analysis (TGA, SDT-Q600, TA Instruments) was used to measure the purity of the CNTs, between room temperature and 950 °C in an air atmosphere. The number of walls and diameters of the synthesized CNTs were analyzed using TEM methods (JEM-2100F, JEOL). The crystallinity, alignment of CNTs along the yarn axis, and chemical characteristics of the CNTs were evaluated using X-ray photoelectron spectroscopy (XPS) (AXIS-His, KRATOS) and polarized Raman spectroscopy using a 532 nm laser (RAMANplus, Nanophoton) integrated with a tensile stage (TST350, Linkam). The surface morphologies and internal structures of the CNTY were measured before and after cutting with a focused ion beam (FIB) (Helios 650, FEI) using SEM methods (JSM-6700F, JEOL). The mechanical and electrical properties were measured using a 10 mm length of CNTY at a strain rate of 3 mm/min on an INSTRON 5543 instrument equipped with a 50 N load cell and a Keithley 2634B unit.

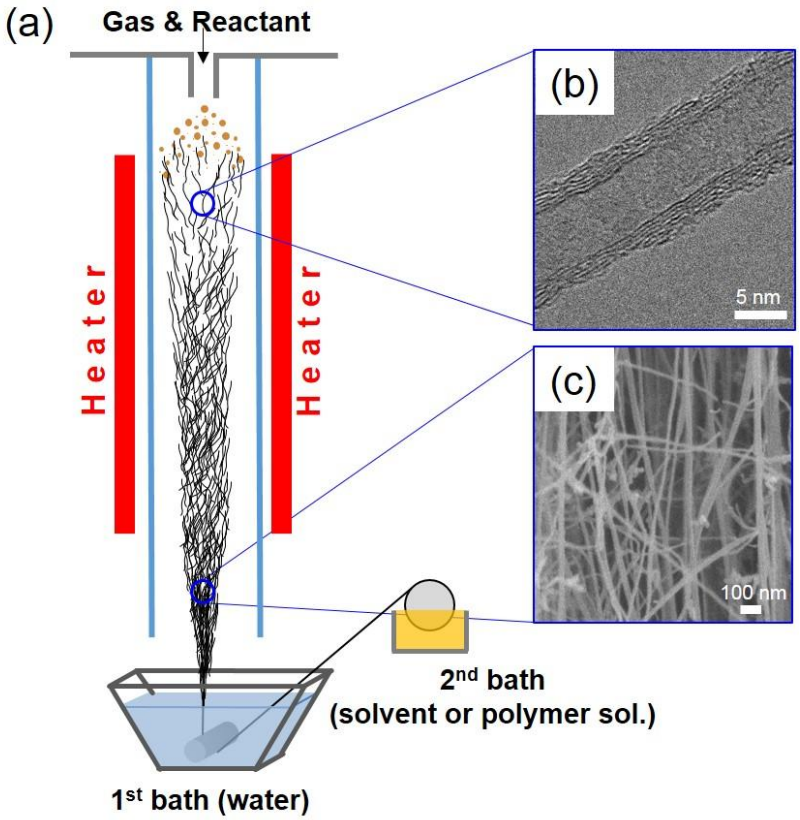

Fig. 4.1. (a) Schematic diagram showing the CNTY spinning process using the aerogel method. (b) TEM image of the synthesized CNTs that composed the CNTY. (c) SEM image of the CNT assemblies prior to passage through the water bath.

4.3 Results and discussion

The CNTYs were fabricated continuously without a substrate using the floating catalyst CVD method [31, 32] in which a first water bath and a winder were placed below the vertical furnace (Fig. 4.1a). CNTs were synthesized in the heating zone in which carbon source gas and the catalyst precursor decomposed in a H_2 gas flow. CNTs synthesized in the heating zone then descended along the direction of gas flow and under the force of gravity in a continuous stream to permit continuous spinning. CNTs having 6-8 walls were grown on the catalyst nanoparticles having inner and outer diameters of 5 and 10 nm, as shown in Fig. 4.1b.

The synthesized CNTs were composed of ~15 wt% carbonaceous material and ~12 wt% catalyst impurities (Fig. 4.2a). Few functional groups were present to enable chemical bond formation among the CNTs or with other additives, as shown in the X-ray photoelectron spectroscopy (XPS) spectrum (Fig. 4.2b). The assemblies (Fig. 4.1c) were transformed into fiber-like shapes due to the hydrophobic surface characteristics, and a meniscus appeared at the interface between the CNT assemblies and water. Partially bundled CNT structures were observed due to volume contraction (Fig. 4.3a). The surfaces of the raw CNTYs revealed highly aligned bundles that were linked with the CNTs through van der Waals interactions, and many pores and spaces were present between the bundles and the CNTs. Raw CNTYs formed a reticulate structure, as the bundles were highly linked with the individual CNTs (Fig. 4.3b). The aerogel spun CNTYs typically provide better mechanical properties than CNTYs produced through liquid-state spinning methods [1, 2, 5, 7, 25]. Although the aerogel spun CNTYs tend to have loose packing structures, the loads are transferred efficiently through the inter-bundle network, thereby evenly distributing a load.

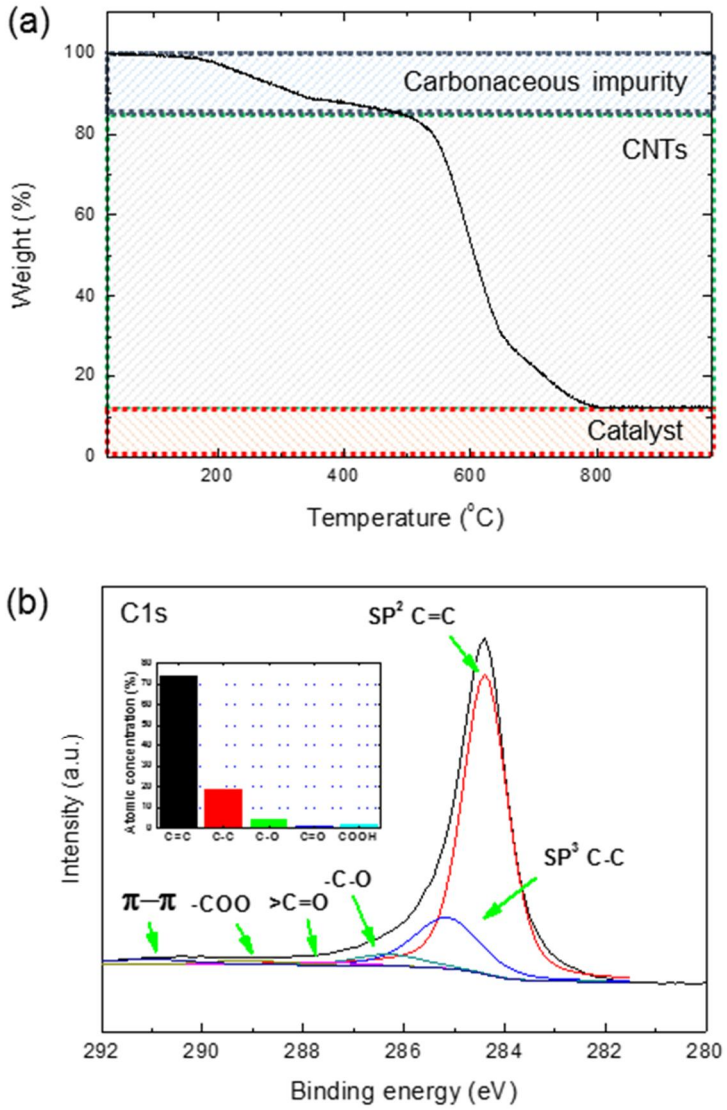

Fig. 4.2. Quantitative analysis of various carbon and catalyst impurities present in the CNTs, evaluated using (a) TGA measurements and (b) C1s spectrum deconvolution.

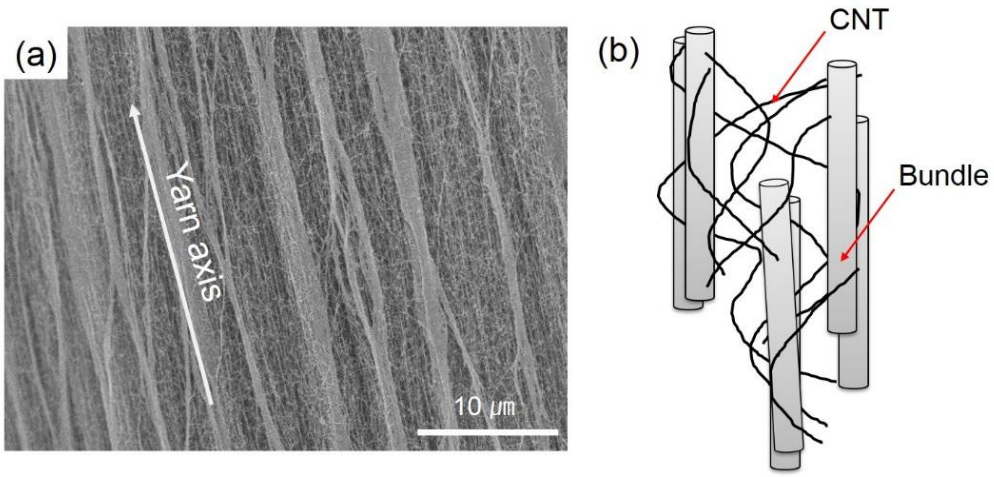

Fig. 4.3. (a) SEM micrographs of the surface of a raw CNTY, and (b) schematic diagram of the reticulate CNTY.

Despite the network structure of the CNTYs, the highly porous structure prevented the full transfer of loads to neighboring bundles. Solvent densification is widely used to minimize the presence of empty spaces [1, 9, 25]. Solvent densification works by closing the gap between CNTs and bundles due to capillary forces during solvent evaporation. DMSO is well known as a good solvent for CNTY densification because it is easily penetrated into CNTY [25]. After solvent densification by DMSO, the diameter of the CNTY decreased dramatically and a closely packed internal CNTY structure was observed in spite of a reduction in CNT alignment. The number of junctions in this closely packed structure increased after the densification process compared to the raw CNTYs. As the contact area among CNTs increased, the load could be more efficiently transferred to neighboring bundles, and the mechanical and electrical properties of the CNTYs improved significantly (Fig. 4.4 and Table 4.1). The polymer infiltration process was performed using the procedure used for solvent infiltration, except that the second bath was replaced with a polymer solution instead of a solvent. Previous reports and our preliminary tests suggested that a small amount of polymer infiltration improved both the mechanical and electrical properties of the CNTYs [18, 25]. The polymers used in this study were much weaker than the CNTs and acted as electrical insulators. The polymer chains increased the linear density of the CNTY/polymer rather than bearing the actual load, which would have lowered the theoretical strength. Three different polymers were tested in this study to better understand the polymer's role in the CNTY/polymer system. Polymers were selected according to the theoretically and experimentally well-defined HAP value of the CNTs [33-36], which was calculated according to the following equation based on the Hansen solubility parameter (HSP), which is the value of the cohesive energy density of the material.

$$\Delta\bar{\delta} = \sqrt{(\delta_{d.P} - \delta_{d.CNT})^2 + (\delta_{p.P} - \delta_{p.CNT})^2 + (\delta_{h.P} - \delta_{h.CNT})^2} \qquad (4.1)$$

Table 4.2 lists the three components that contributed to the HSP: the dispersive (δ_d), polar (δ_p), and hydrogen bonding (δ_h) terms [35], and the affinity parameter between the polymers (P) and the CNTs. CNTs are characterized as having a dispersive term that is much higher than the polar or hydrogen bonding terms because no functional groups are present on the basal planes of CNTs. The low affinity parameter ($\Delta\bar{\delta}$) indicated that the PS and CNTs had similar characteristics.

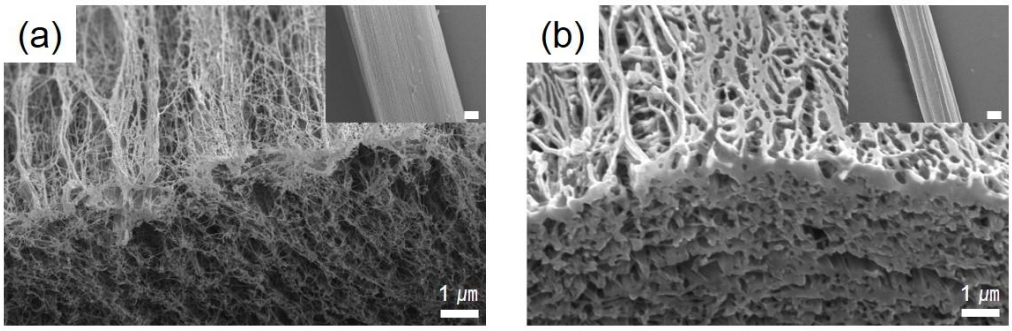

Fig. 4.4. SEM images of the cross-sectional cuts produced using focused ion beam (FIB) from (a, b) raw CNTYs or DMSO-infiltrated CNTYs (inset: scale bar indicates 10 μm).

Table 4.1. Summary of the raw and solvent-infiltrated CNTY properties.

	Raw CNTY	CNTY (solvent)
Alignment ($I_{G\,//}/\,I_{G\perp}$)	1.93 ± 0.39	1.51 ± 0.33
Specific stiffness (GPa/(g cm^{-3}), N/tex)	12.8 ± 1.6	28.5 ± 3.3
Specific strength (GPa/(g cm^{-3}), N/tex)	0.79 ± 0.04	1.15 ± 0.10
Toughness (J/g)	39 ± 4	80 ± 15
Electrical conductivity (×10^5 S/m)	0.15 ± 0.01	3.1 ± 0.20

Table 4.2. Hansen solubility and affinity parameters of the CNTs [36] and polymers [35].

	Hansen solubility parameter (MPa$^{1/2}$)			Hansen affinity parameter with CNT (MPa$^{1/2}$)
	δ_d	δ_p	δ_h	
CNT	19.7	6.2	4.2	-
PS	18.5	4.5	2.9	2.5
PAN	21.7	14.1	9.1	9.5
PVA	15.0	17.2	17.8	18.1

To confirm the validity of HAP for estimation of affinity between CNT and polymers, CNT/polymer composite films were prepared to compare the dispersibility of each polymer. Resistivity and optical microscope (OM) images of the composite films were obtained to evaluate the dispersibility (Fig. 4.5 and Table 4.3). CNT/PS composite film showed the lowest resistivity especially at low concentration, indicating that the CNTs were well dispersed in PS matrix and formed a percolation pathway at low concentration. It is also observed in the OM images showing less aggregated CNTs in the polymer matrix. In addition, PS was always more infiltrated into CNTY than the other two polymers with the same concentration solution because of its higher affinity with CNT (Fig. 4.6b). These results support the fact that HSP and HAP are appropriate concepts to estimate the dispersion of CNTs in polymer matrix and the affinity of CNT-polymer.

The mechanical properties (specific strength and stiffness) of the samples were compared in units of GPa/(g cm^{-3}) that is numerically equivalent to N/tex. The specific strength and stiffness provided an accurate comparison of the yarn's mechanical properties, given the pores present in the yarn and the practical difficulties associated with measuring the real cross-sectional area of the graphitic layers (walls of CNT). The specific stiffness of the CNTY/polymer material displayed remarkable variability, as shown in Fig. 4.7. Regardless of the type of polymer used, the stiffness of the polymer-infiltrated CNTYs improved compared to the corresponding properties of the raw or solvent-infiltrated CNTYs.

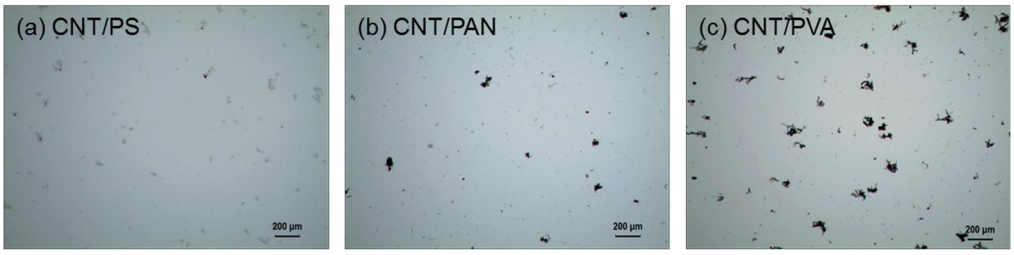

Fig. 4.5. Optical microscope images of 0.5 w/w% CNT dispersed in (a) PS, (b)PAN and (c) PVA solution (5wt%).

Table 4.3. Electrical resistivity of CNT/polymer composite films.

k·Ω/㎝	PS	PAN	PVA
CNT 0.5 w/w%	52.9 ± 14.4	NA	NA
CNT 3 w/w%	1.32 ± 1.03	9.89 ± 4.41	NA
CNT 5 w/w%	0.018 ± 0.002	0.014 ± 0.005	12.8 ± 4.98

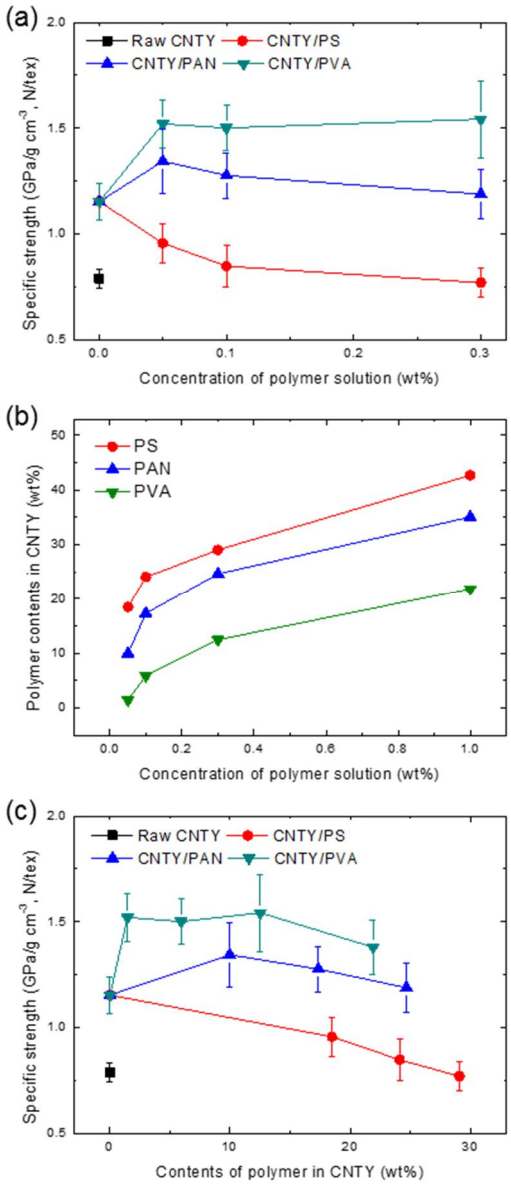

Fig. 4.6. (a) Specific strength of the various polymer-infiltrated CNTYs as a function of the polymer solution concentration (2nd bath). Infiltrated polymer contents into the CNTY according to polymer solution concentration and (c) specific strength as a function of the polymer contents in the CNTY.

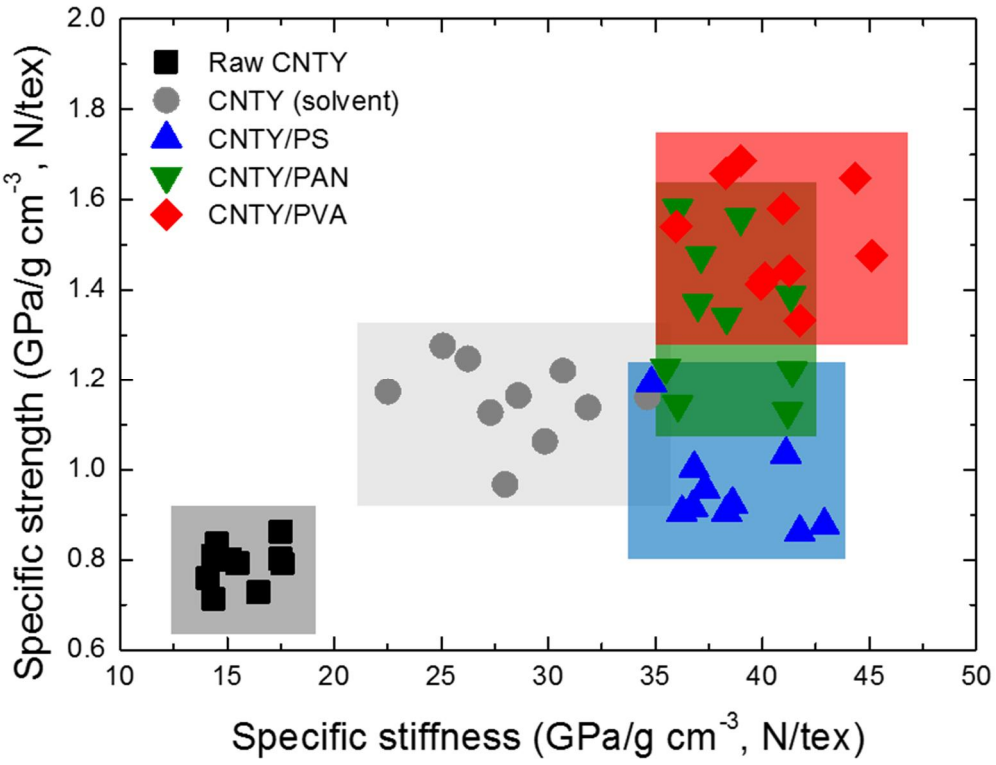

Fig. 4.7. Plot showing the specific stiffness and strength values measured from the raw CNTYs and polymer-infiltrated CNTYs.

The strength of the network junctions determined the stiffness in the reticulated materials because the initial load was transferred from one bundle to the other bundles [22, 37]. The alignment among CNTs was of crucial importance to the mechanical and electrical properties [1]. The CNT alignment did not change significantly as a result of polymer infiltration. The polymer chains were deposited on the surfaces of the CNTs. The molecular-level coupling of bundles and junctions was further confined by the wrapping of the polymer chains, which improved the lateral interactions between CNTs and enhanced the resistance to stress [6, 37, 38].

The alignment in the polymer-infiltrated CNTYs was slightly higher than the alignment in the solvent-treated CNTYs (1.51 ± 0.33) and was lower than the alignment in the raw CNTYs (1.93 ± 0.39). The orientations of the CNTY/polymers were 1.89 ± 0.63 (CNTY/PS), 1.87 ± 0.69 (CNTY/PAN), and 1.83 ± 0.30 (CNTY/PVA), as determined by polarized Raman spectroscopy. Although the CNT alignment, a key factor for stiffness, in the CNTYs could be controlled through a combination of the synthesis conditions and the speed of the winder during pre-drawing [1, 39], the highly networked and partially orientated CNTYs were prepared in this study to eliminate, as much as possible, the effects of alignment on the mechanical properties; the reason to why the CNTY in this study showed relatively low stiffness compared to the other currently reported CNTYs.

The PVA-infiltrated CNTY displayed a specific strength that was higher than the value measured for any other CNTY. All three polymer-infiltrated CNTYs displayed similar stiffness values (Fig. 4.7). These observations could not be explained using conventional composite theory. The conventional composite theory predicts that CNTs behave as fillers incorporated into a polymer matrix. The mechanical properties of the

CNTY/polymer would, then, decrease compared to the raw CNTYs because the polymers are generally much weaker than the CNTs; however, the CNTY/polymers displayed much better mechanical properties than the raw CNTYs.

The theory of fiber-reinforced composites (FRCs) predicts that fibers (CNTs) should be longer than a critical length (l_c), and the interactions between the polymer matrix and the fiber should be strong to enable full utilization of the fiber as a reinforcement means, as described in equation (4.2) [29, 30]. σ_f and τ_m are the ultimate strength of the fiber and the shear strength between the matrix and the fiber.

$$l_c = \frac{\sigma_f d}{2\tau_m} \quad (4.2)$$

As shown in Fig. 4.4a–c, PS satisfied the FRC requirements by producing small bundle sizes (high aspect ratio) and strong interactions with the CNTs. PS is, therefore, the best candidate among the three polymers for use in FRC. The PS-infiltrated CNTYs, however, showed the lowest specific strength and stiffness (Fig. 4.7). In contrast, PVA-infiltrated CNTYs showed better specific strengths than any other polymer-infiltrated CNTYs regardless of the solution concentration and the amount of infiltrated polymer into CNTY (Fig. 4.6). It provides new physical insights; first, the type of polymer is the key factor for enhancing the mechanical properties of CNTY rather than the amount of polymer. Second, this discrepancy between the theoretical predictions and experimental results suggests that factors outside of the FRC theory should be considered in the design of polymer-infiltrated CNTY. The internal

structures and deformation behaviors of the CNTYs appeared to explain the inconsistent trends displayed by the different polymers in the CNTY/polymer and CNT/polymer FRC composites [26, 29, 30].

The internal structures of three polymer-infiltrated CNTYs were imaged to explore how the polymers strengthened the composite and how the affinity between the polymer and the CNTs affected this strengthening process. Although PS had the highest affinity toward CNTs, the bundle size in the PS-infiltrated CNTYs was the smallest among the CNTY/polymer composites. The bundle size in the PVA-infiltrated CNTYs, on the other hand, was the largest among the polymers, as shown in Fig. 4.8a–c. As the bundle size increased, the contact area between the CNTs in the bundle increased, thereby increasing the intra-bundle shear strength and electrical conducting paths, PVA infiltrated CNTY showed the lowest relative resistance and the highest conductivity [1, 9, 25].

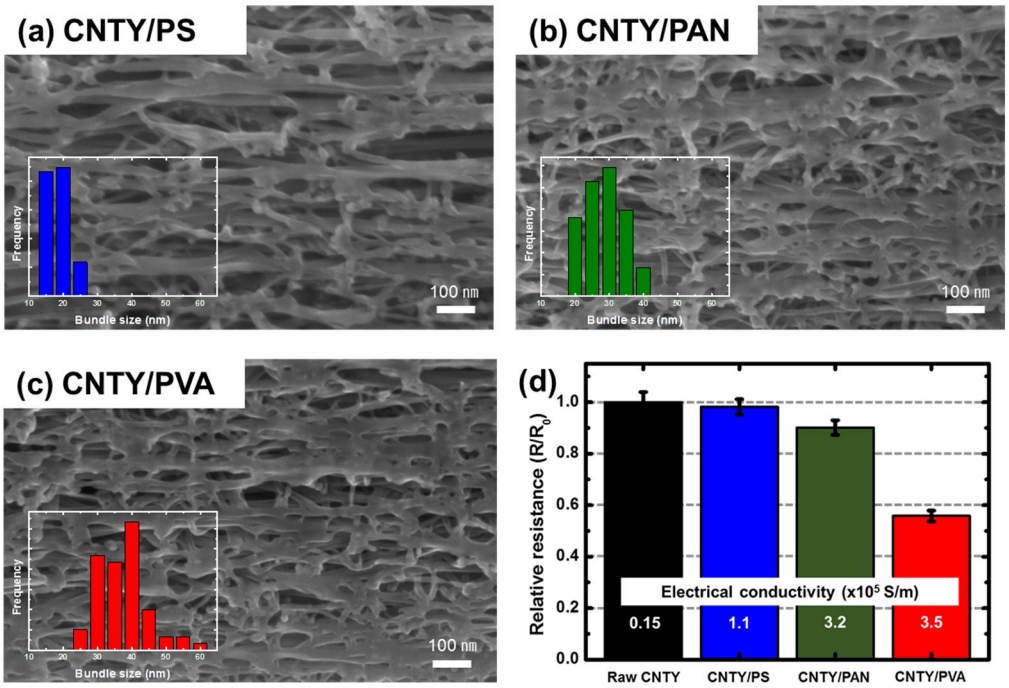

Fig. 4.8. SEM images of the internal structures along longitudinal cross-sections, cut using FIB, of the (a) PS-, (b) PAN- and (c) PVA-infiltrated CNTYs (the bundle size distribution is represented in the image). (d) The relative electrical resistance of each polymer infiltrated CNTY (the conductivity is represented in the graph).

The bundle sizes in a CNT solution or dispersion depend strongly on the CNT dispersion state. In other words, smaller CNT bundles are formed in a solution or matrix, which has better dispersibility of CNT. The dispersion state of a CNT is affected by the affinity between the CNTs and the solvent; therefore, the bundle size should be affected by the affinity between the CNTs and the polymer. PS, which had the highest affinity for CNTs, yielded the smallest CNT bundle size because the PS chains efficiently dispersed and segregated the CNTs (Fig. 4.5) [21].

The stress–strain curves revealed an inflection point that corresponded to the change in the deformation behavior from elastic to plastic. The inflection points of the PS-, PAN-, and PVA-infiltrated CNTYs appeared at 1.44 %, 1.95 %, and 2.01 % of the tensile strain, respectively (Fig. 4.9). This ordering was correlated with the intra-bundle shear strength. Larger bundles had a higher interfacial strength, therefore, the CNTY deformations changed later than they did in the smaller bundles. The CNTY performance depended on the type of polymer used for infiltration, which, in turn, affected the bundle size. Higher-affinity polymers produced smaller bundle sizes (Fig. 4.8). The PVA-infiltrated CNTY relied only on physical bonding, which spontaneously occurred during deformations via intermolecular coupling. The CNTY/PVA stored and dissipated energy efficiently until failure [6]. The PVA-infiltrated CNTY showed a high specific strength with a high electrical conductivity and toughness. The properties were better than those of other CNTYs, CNTY/polymer materials, and commercially available polymer fibers or yarns (the right upper corner corresponds to a better performance), as shown in Fig. 4.10a and b. Most of the CNTYs and commercial fibers tested previously were biased toward a high strength, a high electrical conductivity, or a high toughness. The polymer-infiltrated CNTYs explored in this study showed

multifunctional properties and superior performance over both mechanical and electrical properties.

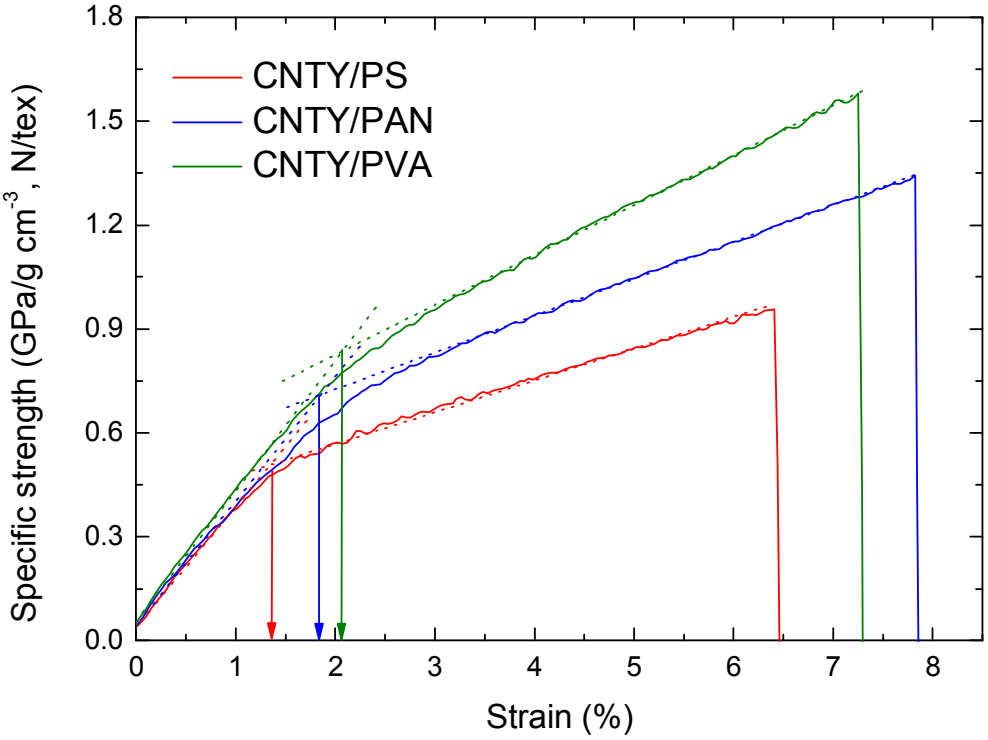

Fig. 4.9. Stress–strain curves of the PS-, PAN-, and PVA-infiltrated CNTYs (the arrows indicate the inflection points).

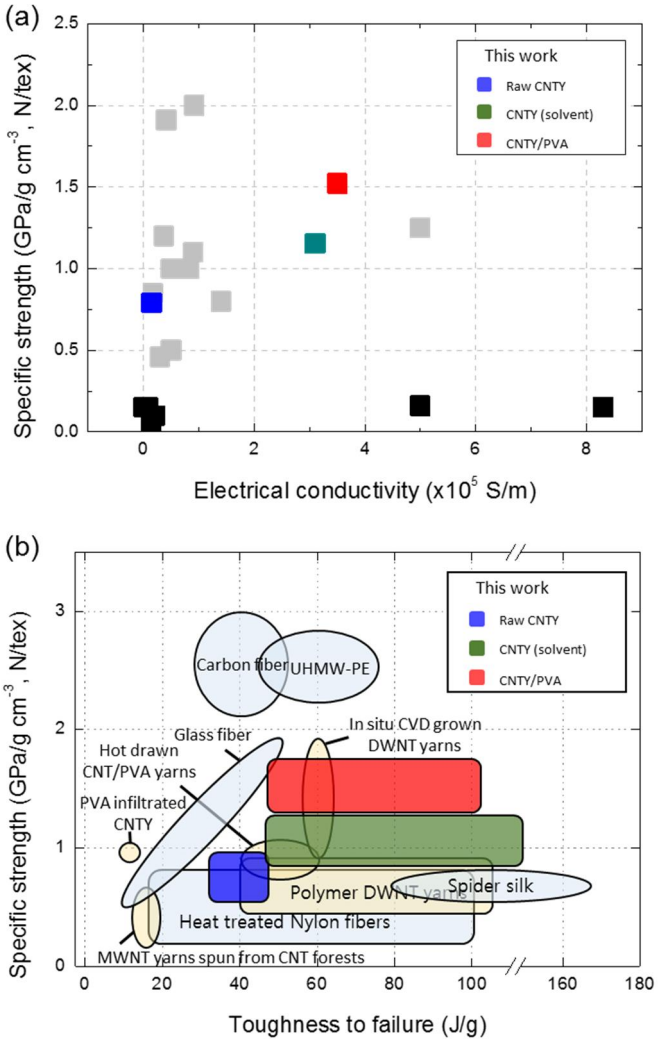

Fig. 4.10. Specific strength as a function of (a) the electrical conductivity (black and gray squares indicate CNTYs produced by liquid [2, 4, 5, 40, 41]- or solid [7-9, 17, 25, 31, 42-46]-state spinning; the other GPa values assumed to be equivalent to the GPa/(g cm^{-3}) values) and (b) toughness. Adapted from ref 6. Copyright 2010 American Chemical Society. Colored squares indicate raw (blue), solvent-infiltrated (olive), and PVA-infiltrated (red) CNTYs examined in this work.

PVA efficiently enhanced not one but both of the mechanical and electrical properties of CNTYs. PVA was used previously as a binder due to its good adhesion properties, although the HAP value, which indicates the affinity between the PVA and CNTs, was poor. The chemical and physical properties of CNT and PVA are very different, as the CNT surfaces display strong hydrophobic characteristics whereas PVA displays very hydrophilic characteristics in that it can be dissolved in water. The increase in the shear strength, therefore, did not arise from the adhesion properties of PVA, but rather from the poor affinity between PVA and the CNTs, which increased the bundle size. Our theory was further supported by the PS-infiltrated CNTY measurements. This composite should have shown better mechanical and electrical properties than the others, according to previous rationalizations, because PS has an HSP similar to that of CNTs. However, PS was the most ineffective polymer at improving the properties of the CNTYs because the HAP value was higher than that of CNTs, thereby producing small CNT bundles.

The deformation behaviors of the composite materials were further analyzed based on the G' Raman spectrum peak shift at around 2700 cm^{-1}. A down-shift in the G' peak indicated elongation of the CNTs and indicated that the load was transferred more efficiently. Down-shifted G' values are closer to those obtained from single CNTs (–37.5 cm^{-1}/%) [47, 48]. Fig. 4.11 shows that the CNTs were elongated under a tensile stress of about 10 cm^{-1}/% of the down-shift until reaching 2 % of tensile strain, which coincided with the deformation inflection point of the CNTYs (Fig. 4.9). The G' peak did not shift further beyond this point. Individual CNTs were elongated to only 0.53 % until the CNTYs failure and the load was dissipated by the shear strength of the intra- or inter-bundle interactions. Although the down-shifted G' values of the CNTY/polymer were far lower than those of individual CNTs, these values were better

than those of the raw and solvent-infiltrated CNTYs, which had G' down-shift values of 5.1 and 7.8 cm^{-1}/%, respectively (Fig. 4.12).

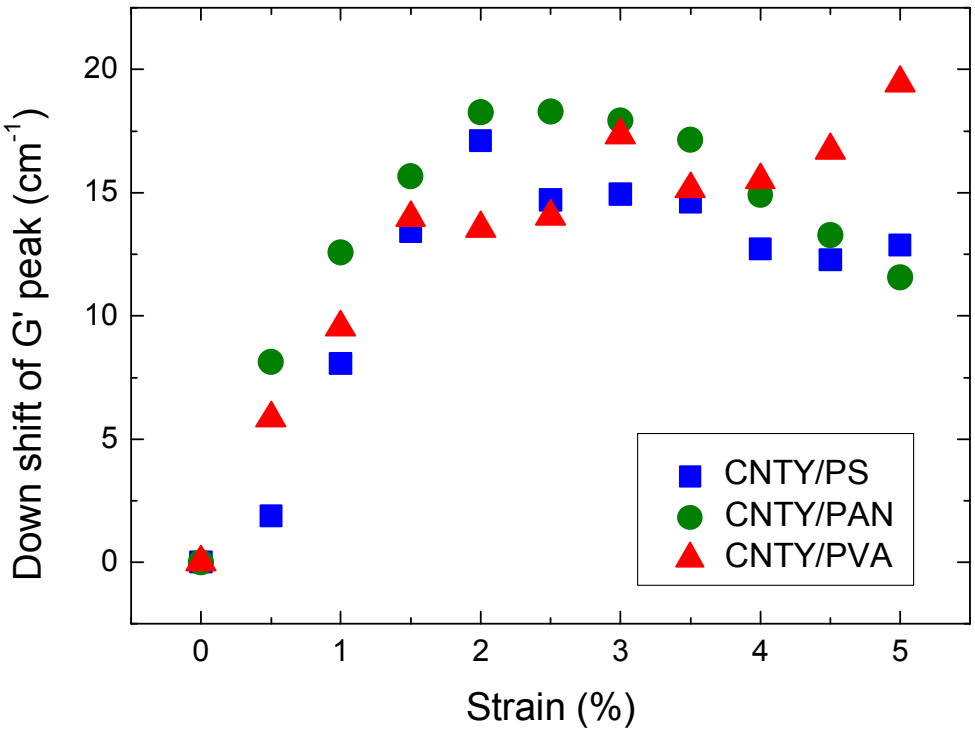

Fig. 4.11. G' peak shift in the CNT/polymer Raman spectrum.

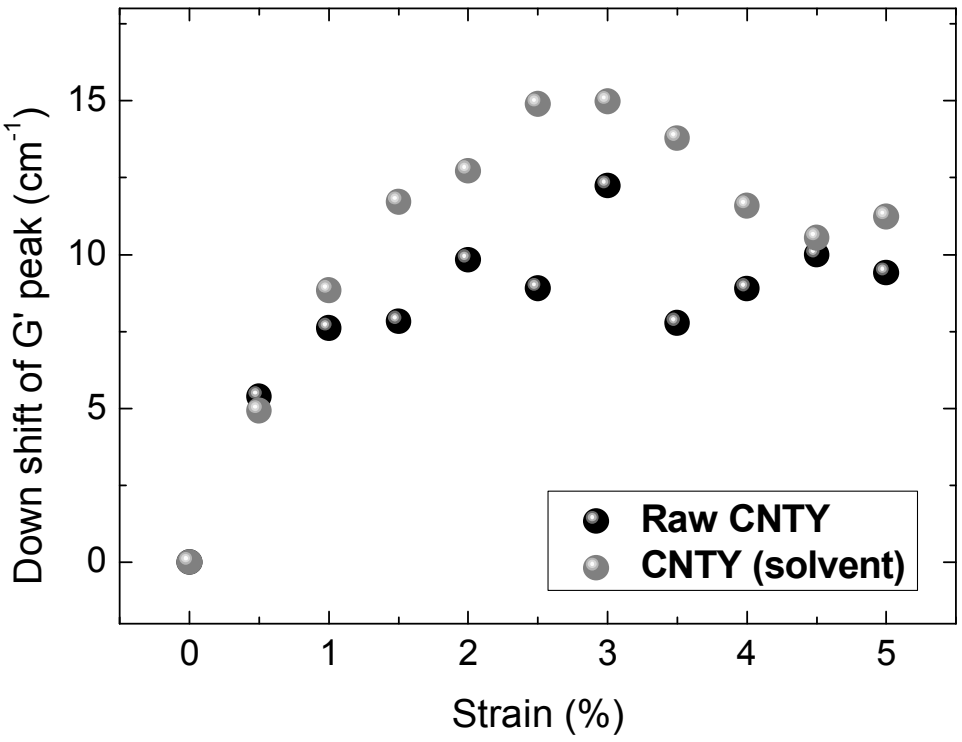

Fig. 4.12. G' peak shift in the Raman spectra of the raw and solvent-infiltrated CNTYs.

The full potential of CNTs may be realized through performance optimization based on a better understanding of the deformation behaviors of CNTYs. Reporting composite performances without understanding the origin of these values does not inform an optimization process. The deformation behaviors of the CNTY could be inferred based on an investigation of the structural changes displayed during polymer infiltration, as well as the Raman spectral results obtained from the CNTY/polymer (Fig. 4.11).The deformation states could be proposed to pass through three stages, as shown in Fig. 4.13. In the first stage, elastic region, the G' peak was down-shifted and increased the load transfer efficiency as a result of polymer infiltration, regardless of the type of polymer, producing elongated CNTYs due to a combination of CNT elongation and straightening, which was fully recovered after removing tensile stress. The second stage, plastic region, of permanent deformation was a result of CNT slippage, as it could explain the difference between the specific strengths of the three different polymer-infiltrated CNTYs. Larger bundle sizes associated with a poor HAP value between the polymer and the CNTs shifted the deformation behavior later in the process since larger bundles dissipated energy more efficiently by intra-bundle slippage. The CNTYs finally pulled out under the tensile stress. The ideal structure of CNTY for full utilization of CNTs' unique properties is provided by having all CNTs in a single yarn to possess a high aspect ratio, to form a perfect bundle without pores and other impurities, and willing to be completely fractured rather than showing pull-out failure by CNT slippage [49, 50].

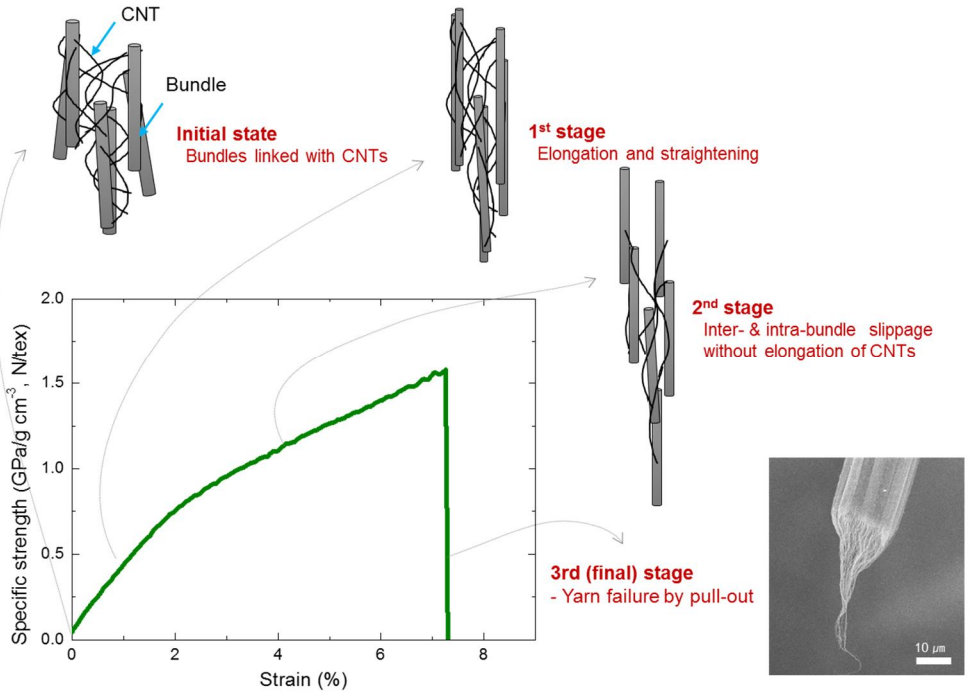

Fig. 4.13. Suggested deformation behaviors of the polymer-infiltrated CNTYs.

Despite that the real deformation behavior might be more complicated than our suggestion and other CNTYs can deform differently depending on their structure, this deformed state provides guidelines for the design of CNTY structures for use as lightweight materials, super-strong fibers, highly conductive cables, or in other sensor applications. Also, changes in the microstructures of the CNTYs must be considered during the design process to allow for the preparation of tailor-fitted materials.

4.4 Conclusion

Polymers were infiltrated into reticulate CNTYs produced using an aerogel method. The polymer chains enhanced the junction strength through molecular-level coupling, regardless of the affinity of the polymer for the CNTs. The CNTY bundle size in the presence of the polymer depended strongly on the affinity of the polymer for the CNTs. Larger bundles and larger contact areas due to the poor affinity and poor infiltration of the polymer favored the formation of structures that more efficiently dissipated and stored energy. A model for the deformation behavior of the CNTYs and the role of the polymer in the polymer-infiltrated CNTYs was suggested. Several mechanical and electrical properties of the CNTY/polymer improved simultaneously to values as high as 40 GPa/(g cm^{-3}) for the specific stiffness, 1.52 GPa/(g cm^{-3}) for the specific strength, 75 J/g for the toughness, and 3.5×105 S/m for the electrical conductivity, through adequate polymer infiltration. Further improvements in the CNT orientations along the yarn axis and appropriate modulation of the molecular-level coupling agent may potentially improve the CNTY properties toward the values obtained from individual CNTs.

4.5 References

[1] Koziol K, Vilatela J, Moisala A, Motta M, Cunniff P, Sennett M, et al. High-performance carbon nanotube fiber. Science 2007, 318, 1892-5.

[2] Vigolo B, Pénicaud A, Coulon C, Sauder C, Pailler R, Journet C, et al. Macroscopic fibers and ribbons of oriented carbon nanotubes. Science 2000, 290, 1331-4.

[3] Li QW, Li Y, Zhang XF, Chikkannanavar SB, Zhao YH, Dangelewicz AM, et al. Structure-dependent electrical properties of carbon nanotube fibers. Adv. Mater. 2007, 19, 3358-63.

[4] Kozlov ME, Capps RC, Sampson WM, Ebron VH, Ferraris JP, Baughman RH. Spinning solid and hollow polymer-free carbon nanotube fibers. Adv. Mater. 2005, 17, 614-7.

[5] Zhang S, Koziol KKK, Kinloch IA, Windle AH. Macroscopic fibers of well-aligned carbon nanotubes by wet spinning. Small 2008, 4, 1217-22.

[6] Naraghi M, Filleter T, Moravsky A, Locascio M, Loutfy RO, Espinosa HD. A multiscale study of high performance double-walled nanotube–polymer fibers. ACS Nano 2010, 4, 6463-76.

[7] Zhang X, Li Q, Tu Y, Li Y, Coulter JY, Zheng L, et al. Strong carbon-nanotube fibers spun from long carbon-nanotube arrays. Small 2007, 3, 244-8.

[8] Tran CD, Humphries W, Smith SM, Huynh C, Lucas S. Improving the tensile strength of carbon nanotube spun yarns using a modified spinning process. Carbon 2009, 47, 2662-70.

[9] Liu K, Sun Y, Zhou R, Zhu H, Wang J, Liu L, et al. Carbon nanotube yarns with high tensile strength made by a twisting and shrinking method. Nanotechnology 2010, 21, 045708.

[10] Yu MF, Files BS, Arepalli S, Ruoff RS. Tensile loading of ropes of single wall carbon nanotubes and their mechanical properties. Phys. Rev. Lett. 2000, 84, 5552-5.

[11] Yu M-F, Lourie O, Dyer MJ, Moloni K, Kelly TF, Ruoff RS. Strength and breaking mechanism of multiwalled carbon nanotubes under tensile load. Science 2000, 287, 637-40.

[12] Dai H, Wong EW, Lieber CM. Probing Electrical transport in nanomaterials: conductivity of individual carbon nanotubes. Science 1996, 272, 523-6.

[13] Wang, Liu, Yu G, Xu, Zhang, Zhu. Anisotropic Electrical transport properties of aligned carbon nanotube films. J. Phys. Chem. B 2001, 105, 9422-5.

[14] Jia J, Zhao J, Xu G, Di J, Yong Z, Tao Y, et al. A comparison of the mechanical properties of fibers spun from different carbon nanotubes. Carbon 2011, 49, 1333-9.

[15] Reguero V, Alemán B, Mas B, Vilatela JJ. Controlling carbon nanotube type in macroscopic fibers synthesized by the direct spinning process. Chem. Mater. 2014, 26, 3550-7.

[16] Zhao J, Zhang X, Di J, Xu G, Yang X, Liu X, et al. Double-peak mechanical properties of carbon-nanotube fibers. Small 2010, 6, 2612-7.

[17] Zhang S, Zhu L, Minus M, Chae H, Jagannathan S, Wong C-P, et al. Solid-state spun fibers and yarns from 1-mm long carbon nanotube forests synthesized by water-assisted chemical vapor deposition. J. Mater. Sci. 2008, 43, 4356-62.

[18] Beese AM, Sarkar S, Nair A, Naraghi M, An Z, Moravsky A, et al. Bio-inspired carbon nanotube–polymer composite yarns with hydrogen bond-mediated lateral interactions. ACS Nano 2013, 7, 3434-46.

[19] Boncel S, Sundaram RM, Windle AH, Koziol KKK. Enhancement of the mechanical properties of directly spun CNT fibers by chemical treatment. ACS Nano 2011, 5, 9339-44.

[20] Min J, Cai JY, Sridhar M, Easton CD, R. Gengenbach T, McDonnell J, et al. High performance carbon nanotube spun yarns from a crosslinked network. Carbon 2013, 52, 520-7.

[21] Kim SW, Kim T, Kim YS, Choi HS, Lim HJ, Yang SJ, et al. Surface modifications for the effective dispersion of carbon nanotubes in solvents and polymers. Carbon 2012, 50, 3-33.

[22] Ma W, Liu L, Zhang Z, Yang R, Liu G, Zhang T, et al. High-strength composite fibers: Realizing true potential of carbon nanotubes in polymer matrix through continuous reticulate architecture and molecular level couplings. Nano Lett. 2009, 9, 2855-61.

[23] Zu M, Li Q, Zhu Y, Dey M, Wang G, Lu W, et al. The effective interfacial shear strength of carbon nanotube fibers in an epoxy matrix characterized by a microdroplet test. Carbon 2012, 50, 1271-9.

[24] Miaudet P, Badaire S, Maugey M, Derré A, Pichot V, Launois P, et al. Hot-drawing of single and multiwall carbon nanotube fibers for high toughness and alignment. Nano Lett. 2005, 5, 2212-5.

[25] Liu K, Sun Y, Lin X, Zhou R, Wang J, Fan S, et al. Scratch-resistant, highly conductive, and high-strength carbon nanotube-based composite yarns. ACS Nano 2010, 4, 5827-34.

[26] Li S, Zhang X, Zhao J, Meng F, Xu G, Yong Z, et al. Enhancement of carbon nanotube fibres using different solvents and polymers. Compos. Sci. Technol. 2012, 72, 1402-7.

[27] Vilatela JJ, Elliott JA, Windle AH. A Model for the strength of yarn-like carbon nanotube fibers. ACS Nano 2011, 5, 1921-7.

[28] Liu X, Lu W, Ayala OM, Wang L-P, Karlsson AM, Yang Q, et al. Microstructural evolution of carbon nanotube fibers: deformation and strength mechanism. Nanoscale 2013, 5, 2002-8.

[29] Fu S-Y, Lauke B. Effects of fiber length and fiber orientation distributions on the tensile strength of short-fiber-reinforced polymers. Compos. Sci. Technol. 1996, 56, 1179-90.

[30] Kelly A, Tyson WR. Tensile properties of fibre-reinforced metals: Copper/tungsten and copper/molybdenum. J. Mech. Phys. Solids 1965, 13, 329-50.

[31] Li Y-L, Kinloch IA, Windle AH. Direct spinning of carbon nanotube fibers from chemical vapor deposition synthesis. Science 2004, 304, 276-8.

[32] Jung Y, Song J, Huh W, Cho D, Jeong Y. Controlling the crystalline quality of carbon nanotubes with processing parameters from chemical vapor deposition synthesis. Chem. Eng. J. 2013, 228, 1050-6.

[33] Lee K, Lim HJ, Yang SJ, Kim YS, Park CR. Determination of solubility parameters of single-walled and double-walled carbon nanotubes using a finite-length model. RSC Adv. 2013, 3, 4814-20.

[34] Lim HJ, Lee K, Cho YS, Kim YS, Kim T, Park CR. Experimental consideration of the Hansen solubility parameters of as-produced multi-walled carbon nanotubes by inverse gas chromatography. Phys. Chem. Chem. Phys. 2014, 16, 17466-72.

[35] Hansen CM. Hansen Solubility Parameters: A User's Handbook. 2nd ed. Boca Raton, FL: CRCPress by Taylor&Francis Group; 2007.

[36] Ha H, Ha K, Kim SC. An empirical equation for electrical resistivity of thermoplastic polymer/multi-walled carbon nanotube composites. Carbon 2010, 48, 1939-44.

[37] Liu X, He X-Q, Yang Q-S, Mai Y-W. Overall behavior and microstructural deformation of R-CNT/polymer composites. Compos. Part. B 2011, 42, 2123-9.

[38] Liu L, Ma W, Zhang Z. Macroscopic carbon nanotube assemblies: Preparation, properties, and potential Applications. Small 2011, 7, 1504-20.

[39] Motta M, Kinloch I, Moisala A, Premnath V, Pick M, Windle A. The parameter space for the direct spinning of fibres and films of carbon nanotubes. Physica E 2007, 37, 40-3.

[40] Muñoz E, Suh DS, Collins S, Selvidge M, Dalton AB, Kim BG, et al. Highly conducting carbon nanotube/polyethyleneimine composite fibers. Adv. Mater. 2005, 17, 1064-7.

[41] Davis VA, Parra-Vasquez ANG, Green MJ, Rai PK, Behabtu N, Prieto V, et al. True solutions of single-walled carbon nanotubes for assembly into macroscopic materials. Nat. Nanotechnol. 2009, 4, 830-4.

[42] Zhu HW, Xu CL, Wu DH, Wei BQ, Vajtai R, Ajayan PM. Direct synthesis of long single-walled carbon nanotube strands. Science 2002, 296, 884-6.

[43] Zhang M, Atkinson KR, Baughman RH. Multifunctional carbon nanotube yarns by downsizing an ancient technology. Science 2004, 306, 1358-61.

[44] Randeniya LK, Bendavid A, Martin PJ, Tran C-D. Composite yarns of multiwalled carbon nanotubes with metallic electrical conductivity. Small 2010, 6, 1806-11.

[45] Zhong X-H, Li Y-L, Liu Y-K, Qiao X-H, Feng Y, Liang J, et al. Continuous multilayered carbon nanotube yarns. Adv. Mater. 2010, 22, 692-6.

[46] Miao M. Electrical conductivity of pure carbon nanotube yarns. Carbon 2011, 49, 3755-61.

[47] Cronin SB, Swan AK, Ünlü MS, Goldberg BB, Dresselhaus MS, Tinkham M. Resonant Raman spectroscopy of individual metallic and semiconducting single-wall carbon nanotubes under uniaxial strain. Phys. Rev. B 2005, 72, 035425.

[48] Dresselhaus MS, Dresselhaus G, Saito R, Jorio A. Raman spectroscopy of carbon nanotubes. Phys. Rep. 2005, 409, 47-99.

[49] Yakobson BI, Samsonidze G, Samsonidze GG. Atomistic theory of mechanical relaxation in fullerene nanotubes. Carbon 2000, 38, 1675-80.

[50] Behabtu N, Green MJ, Pasquali M. Carbon nanotube-based neat fibers. Nano Today 2008, 3, 24-34.

Chapter 5 Empirical Approach 3: Strength Improvement by Controlling the Bundling Behavior and Chemical Crosslinking

5.1 Introduction

Due to developments within the aerospace engineering industry fueled by the enormous interest in space, the revolutionary idea of a space elevator has attracted significant attention. The concept of a space elevator as a transportation system from earth to space was initially proposed in 1895 by Konstantin Tsiolkovsky [1]. A cable connecting the earth to a station in space is regarded as the most critical component in order to realize the idea. Due to the very long length of the cable given the great distance from earth to space, the constituents of the cable should be lightweight and should have very high strength (a high specific strength) to endure the weight of the cable itself. Among the various candidates, such as Kevlar and carbon fibers, carbon nanotube (CNT) has been considered the most promising material because it has an extraordinary theoretical modulus of 1 TPa and strength as high as 60 GPa with a low density level (1.3 g/cm^3), which is approximately six times lower than that of steel (density of 7.9 g/cm^3; assumed strength of 5 GPa) [2-5].

Despite the outstanding mechanical properties of individual CNTs, the highest potential of this material has not yet been manifested in macroscopically assembled CNT yarn (CNTY), as failures in CNTY are mainly pull-out failures due to the weak van der Waals interaction rather than CNT breakage. Various attempts have been made

to date in an effort to minimize discrepancies in the mechanical properties between individual CNTs and the assembled structures of CNTYs [6-10]. The most promising approach to overcome the CNTY failure mechanism is to synthesize infinitely long CNTs so that fiber failure would arise from CNT breakage instead of slippage between the CNTs. A few research groups have reported the growth of CNT with centimeter-scale lengths created by controlling the catalyst lifetime and by optimizing the synthesis conditions [11-13]. Unfortunately, a very long synthesis time is an essential prerequisite; thus, these methods are not practical when attempting to develop commercially feasible CNTYs.

Accordingly, recent advances in CNTYs have been directed toward finding alternatives to the weak van der Waals interactions. In this respect, many researchers have adopted strong covalent bonds in their CNTYs, as these bonds are up to ten times stronger than van der Waals interactions. These advances are realized through chemical modifications of CNTs or through the use of binding materials to avoid pull-out failures, but the performances of the resultant materials have been disappointing and have not met expectations [7, 14-16]. We assumed that this phenomenon was attributed to a lack of a deeper understanding of the assembled structure, which have multiple effects on the mechanical properties of CNTY. Taken together, the development of reliable CNT bundling (assembly) engineering processes which eventually lead to robust CNTY is highly desirable.

Herein, we suggest a design method which provides an efficient load transfer network within CNTY by considering the CNT assembled structure. This method significantly improves the specific strength without sacrificing toughness. In general, the CNT-based structural material can potentially offer a stronger load transfer network

structure when the surfaces of individual CNTs are homogenously functionalized to maximize the number of reaction sites, which is related to the crosslinking density. Unlike earlier concepts, however, in the present study, preferentially grafted polymeric materials surrounding only the outside of the CNT bundle are demonstrated to be the most efficient strategy to realize an efficient load transfer network and to suppress intra-CNT bundling slippage. This approach, along with a highly aligned double walled-CNT (DWNT) synthesis process, can produce exceptionally high mechanical strength and modulus values as well as high electrical conductivity without a loss of toughness, exceeding the values of benchmark materials.

5.2 Experimental

CNTY preparation

CNTYs were fabricated through a direct spinning method with ferrocene, thiophene and methane at 1200 °C, as described in our previous report [2].

Chemical modification of CNTYs

CNTYs were oxidized by a mixture of sulfuric acid and nitric acid (v/v = 3:1) at 60 °C for 1 h. Polymeric materials were grafted onto the surfaces of the CNTs by soaking CNTYs in PABA (0.1 M) and sodium nitrite (0.1 M) dissolved in 150 ml of 1 M HCl or a 98% H2SO4 solution at 60 °C for 24 h. They were further crosslinked with PPD in DMF at 100 °C for 24 h. The CNTYs were then washed with DMF and DI water several times to remove unreacted reagents after each chemical reaction.

Characterization and analysis

The CNTs were characterized with HR-TEM (JEM-2100F, JEOL) and Raman spectroscopy (RAMANplus, Nanophoton) using a 532 nm laser. The chemical characteristics were evaluated by X-ray photoelectron spectroscopy (XPS; Sigma Probe, Thermo Fisher Scientific) and Fourier-transform infrared spectroscopy (FT-IR). Contact angle measurements (Krüss) were used to measure the wettability. The internal structures of the CNTY were observed after cutting the material with a focused ion beam (FIB; Helios 650, FEI). The size distribution of the dispersed CNTs was studied by a dynamic light scattering (DLS) analysis using an ELSZ 1000ZS size analyzer by

Otsuka. The specific strength was calculated according to the linear density, which was determined by weighing 15 m long-CNTY and then dividing this value into the measured load of a single yarn with a tensile stage (TST350, Linkam) at a gauge length of 10 mm and strain rate of 3 mm/min. The synthesized polymer was characterized by gel permeation chromatography (GPC; Ultimate 3000, Thermo).

5.3 Results and discussion

CNTs, mainly composed of DWNT, were synthesized by floating catalyst chemical vapor deposition (FCCVD) and formed a unique reticulated structure. The CNTs are closely connected to each other in the form of a network structure possessing numerous junctions (Fig. 5.1). This network structure and the hydrophobic characteristics of CNTs enable continuous spinning (via the aerogel-like CNT intermediate assembly) in water.

The as-synthesized raw CNTYs (R-CNTY) were functionalized with monomolecular functional groups and polymeric materials based on three different routes (Fig. 5.2) to investigate the importance of bundle engineering to achieve optimum mechanical properties of the CNTY. First, oxidized CNTY (denoted as O-CNTY) was prepared by a commonly used method with a mixed acid (H_2SO_4/HNO_3), as described in the experimental section. Oxidation disrupts the sp^2 hybridization of carbon and allows the homogeneous introduction of oxygen units to produce sp^3 carbon-based functional groups, including carboxylic acid or hydroxyl, on the walls of individual CNTs within the CNTY (Fig. 5.2b) [17]. The prepared CNTs were then modified with aryl diazonium salts, a well-known reagent for covalent functionalization, in 98% H_2SO_4 [16, 18]. Whereas oxidization generates monomolecular functional groups on the surfaces of CNTs, the diazotization reaction enables the surfaces of CNTs to be decorated with polymeric materials. PABA may also react with the phenyl groups of PABA covalently linked on the CNTs. Consequently, the polymerized PABA (p-PABA) structure polyene was produced with grafting onto the CNTs [18].

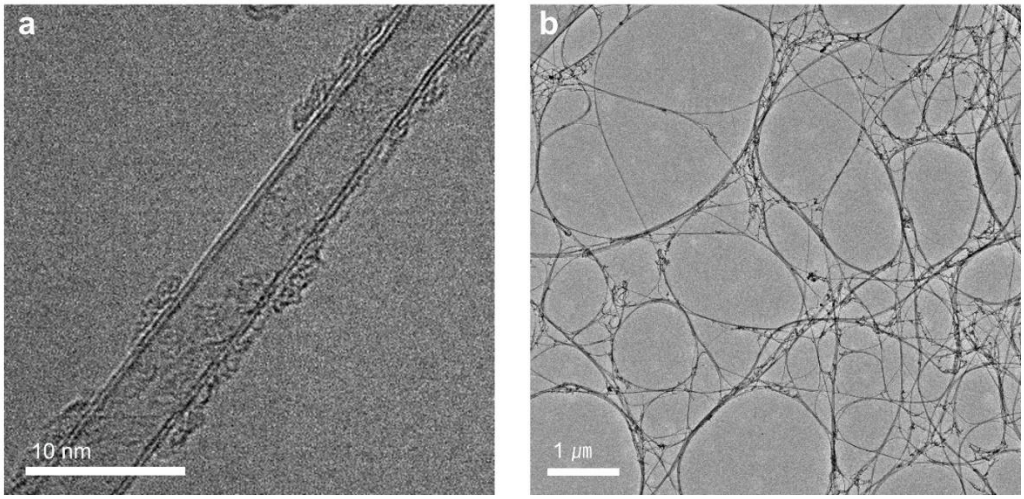

Fig. 5.1. TEM images of (a) as-synthesized individual double-walled CNT, and (b) the network structure of the DWNTs.

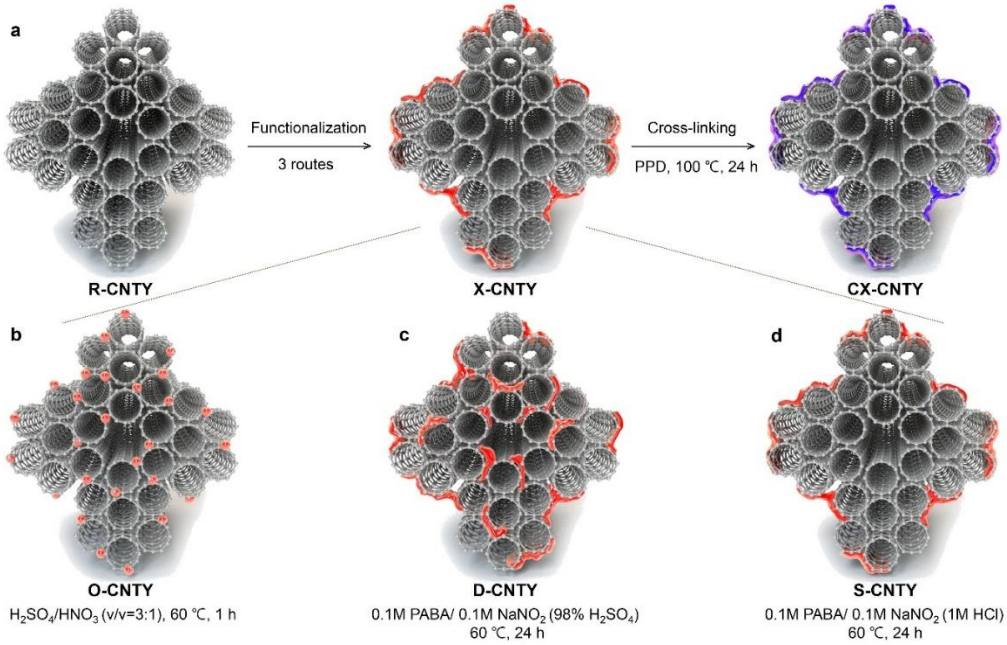

Fig. 5.2. (a) Schematic illustration of the fabrication process from raw CNTY (R-CNTY) to crosslinked CNTY (CX-CNTY). (b) Chemically oxidized CNTY (O-CNTY) by mixed acids. (c) Polymeric materials grafted onto CNTY (D-CNTY) by a diazotization reaction in a reaction medium with good wettability. (d) CNTY selectively polymer grafted (S-CNTY) by diazotization in a reaction medium with poor wettability.

Polymeric materials which contain functional sites to be crosslinked were grafted onto both the outside and inside of the CNT bundle due to the very high wettability of the used medium (H2SO4), thereby forming a functionalization shape similar to that of O-CNTY (denoted as D-CNTY). The diazotization reaction was subsequently carried out in a different medium of 1M HCl (aq) for site-specific CNT bundle engineering. With this method, p-PABA could be selectively grafted around the outside of the CNT bundles, as illustrated in Fig. 5.2d, owing to the poor wettability of CNTs with the 1M HCl aqueous solution (denoted as S-CNTY). The detailed site-specific reaction mechanisms of diazotization and polymeric material formation with CNTs are described in Fig. 5.3a. Highly reactive diazonium salts were generated from PABA with sodium nitrite in an acidic medium, and the diazotization reaction readily occurred by means of the radical coupling between the CNT and the diazonium salts.

To realize the site-specific functionalization of CNTY, the wettability differences in reaction media toward CNTs were utilized in this study. The as-synthesized CNTs showed high affinity with both 98% H_2SO_4 and the mixed acid of H_2SO_4/HNO_3. Sulfuric acid was immediately spread across the surface, and the contact angle was measured and found to be 32˚, as shown in Fig. 5.3b. This high wettability unties the CNT-CNT physical junctions in the CNT bundle upon the ingress of the solvent. Therefore, functional groups would be randomly attached to both the inside and outside surfaces of the CNT bundles, similar to O- and D-CNTYs. On the other hand, the poor wettability of the 1M HCl aqueous solution, confirmed by the very high contact angle of 115˚ (see Fig. 5.3c), can provide a different option for CNT bundle engineering. In such a reaction medium, p-PABA can be dominantly grafted onto a specific region, in this case the outside surfaces of the CNT bundles, as illustrated in Fig. 5.2d.

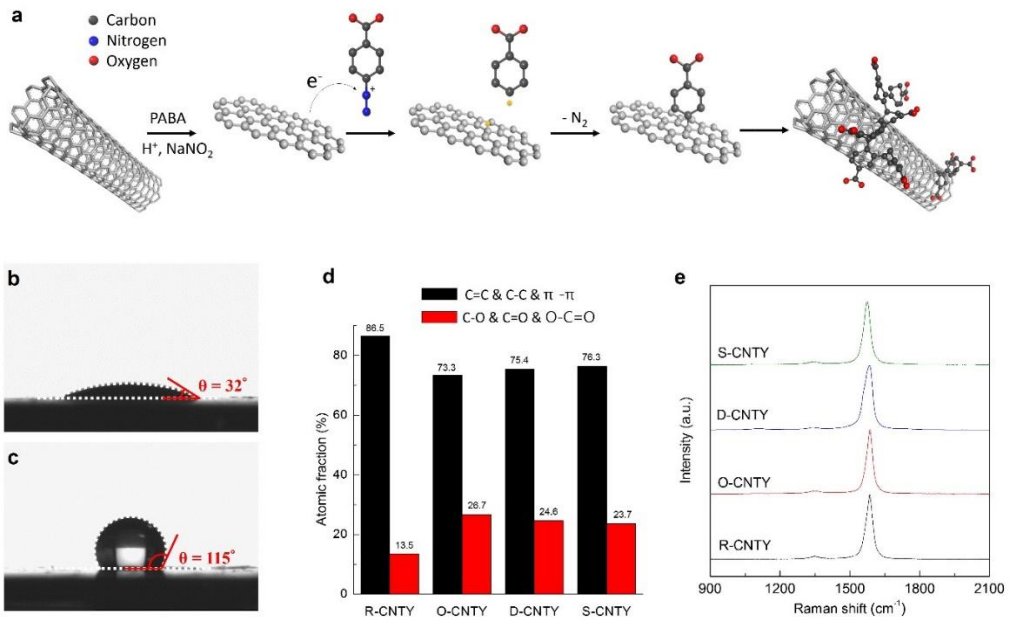

Fig. 5.3. (a) Mechanism of the diazotization reaction on the surfaces of CNTs with PABA and the grafting of polymerized PABA (p-PABA). (b) Contact angle of the 98 % H_2SO_4 with R-CNTs. (c) Contact angle of the 1M HCl with R-CNTs. (d) Quantitative analysis of the carbon forms by XPS. (e) Raman spectra of each CNTY.

An XPS analysis was conducted to obtain information about the chemical nature of the CNTYs. The various functional groups of the CNTYs were quantitatively calculated from the C1s spectral deconvolution provided in Fig. 5.4. The numbers of carbon atoms related to oxidation, C-O, C=O, and O-C=O, were found to have nearly doubled relative to that of R-CNTY after the functionalization step. All functionalized CNTYs showed similar numbers of oxidized carbon atoms regardless of the functionalization method used, as shown in Fig. 5.3d. From the Raman spectroscopy results, the degrees of disorder carbons in the CNTYs were indirectly investigated. The D- and G-band correspondingly appeared around at 1340 cm^{-1} and 1580 cm^{-1}, representing disordered and graphitic carbons. The intensity ratio of two representative peaks, I_D/I_G, provides information about the quality of the CNT, and all CNTYs have similar values of about 0.04 both before and after the chemical reactions (Fig. 5.3e). These results indicate that all chemical reactions used for CNTY modification in this study have only minor effects on the intrinsic mechanical properties of the CNTs. Thus, we can reasonably exclude additional factors which may have originated from the change of the intrinsic mechanical properties depending on the functionalization method used in this study.

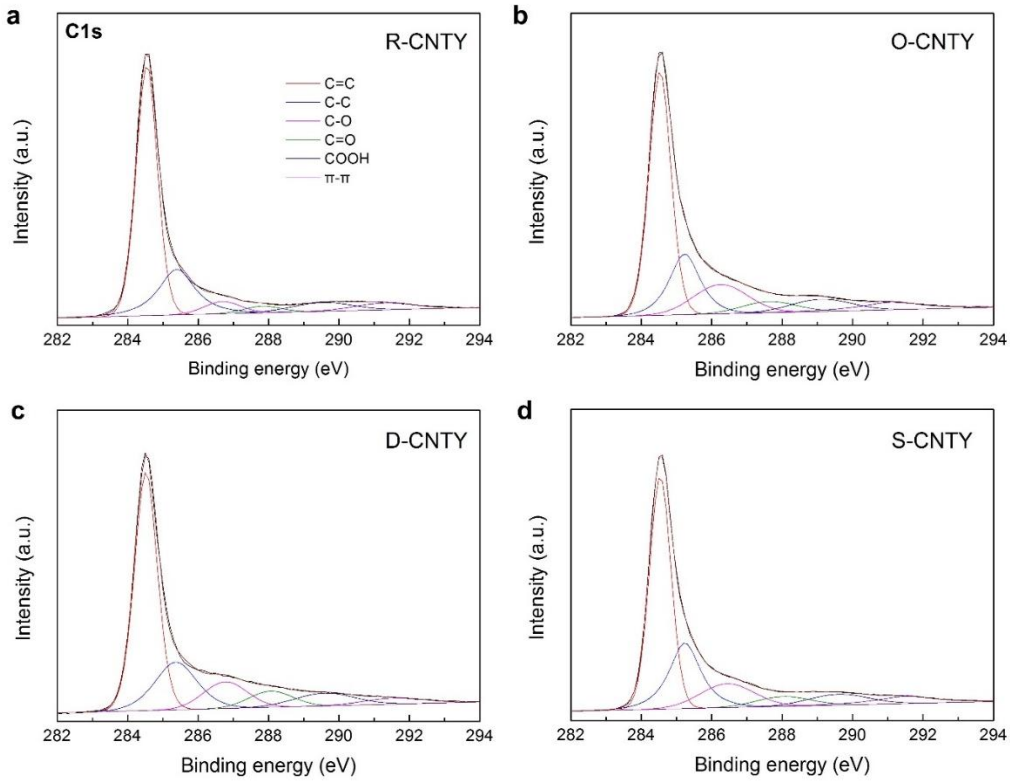

Fig. 5.4. Deconvoluted XPS C1s spectra of (a) R-CNTY, (b) O-CNTY, (c) D-CNTY and (d) S-CNTY.

Structural characterization of CNTYs was also conducted. The walls of the CNTs were clearly observed without noticeable defects regardless of the method used, as denoted by the white dotted lines along the walls of the tubes in the TEM images, as shown in Figs. 5.5a-d before and after the chemical modification step. These results indicate that the graphitic carbon of the CNTs is well preserved even after the attachment of the functional groups onto the surfaces of the CNTs, a finding which is also consistent with the identical I_D/I_G ratio of the samples shown in Fig. 5.3e. R- and O-CNTs show relatively smooth surface characteristics compared to the D- and S-CNTs. The O-CNT have the cleanest surfaces among them because the oxidation chemistry in this case removed the unfavorable non-graphitic carbonaceous materials from the CNTs, known as the CNT purification process. Non-graphitic carbonaceous materials tend to be easily oxidized by a mixture of nitric and sulfuric acids and then become detached from the surfaces of the CNTs. On the other hand, for both the D- and S-CNT samples, a rough surface was observed, indicating that layers of polyene a few nanometers thick were successfully deposited around the CNTs and junctions. Synthesized polymeric materials are indicated by the white arrows in the TEM images, as shown in Figs. 5.5c and d. The relative weight-average molecular weight (Mw) and polydispersity index (PDI) of p-PABA as measured by GPC were 29203 and 1.63, respectively (Fig. 5.6). After chemical modification, all CNTYs showed a much more compact structure compared to R-CNTY on the macroscopic scale, as shown in the SEM images of the longitudinal and radial cross-section of the FIB-cut CNTYs (Figs. 5.5e-l).

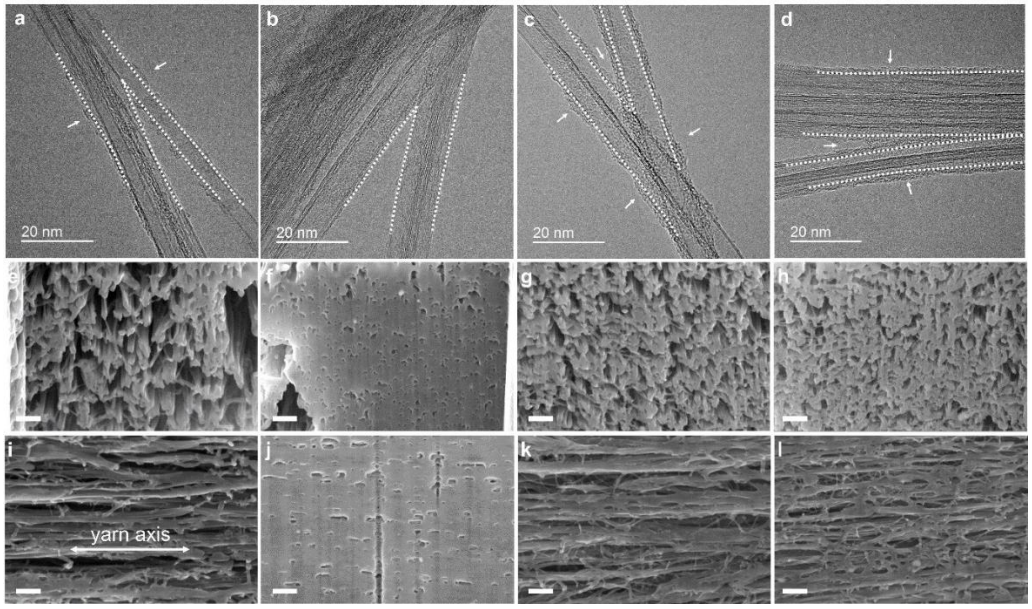

Fig. 5.5. TEM images of CNTs and SEM images of the cross-sections and longitudinal sections of (a, e, i) R-CNTY, (b, f, j) O-CNTY, (c, g, k) D-CNTY and (d, h, l) S-CNTY. White dotted lines and arrows indicate the outer walls of the CNT and polymeric materials in a-d. The scale bar is 200 nm in e-l.

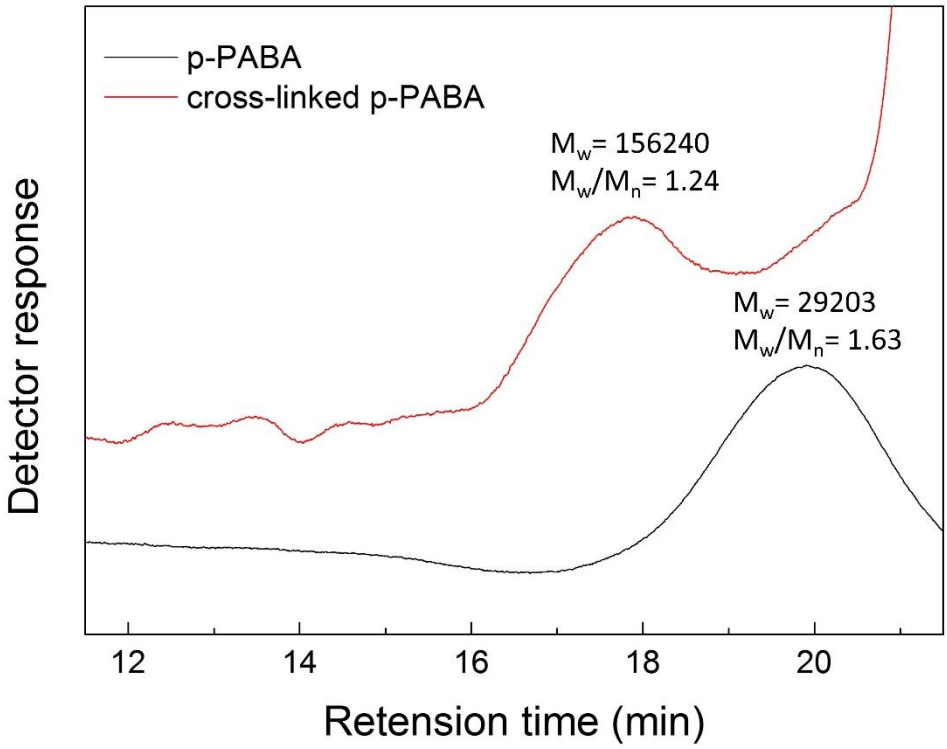

Fig. 5.6. GPC spectra of p-PABA and crosslinked p-PABA with PPD molecules.

The mechanical performance of the CNTYs was then assessed. In general, a compact and tightly assembled structure of CNTY is strongly preferred because it implies a higher fraction of the surface in contact with neighboring CNTs, thereby enabling higher load-transfer efficiency rates [2, 19, 20]. We determined the Raman peak shift values of the samples to elucidate the effects of the designed architecture of CNTY on the formation of load-transfer pathways. The Raman peak shift reflects the extent of the inter-nanotube interaction and contact area depending on the magnitude of the bundle organization. Orthogonal electronic dispersion occurs when CNTs are in contact with each other, leading to a shift of the peak to a lower value.

Although O-CNTY clearly has the most closely packed structure, oxidized CNTs are expected to have ineffective assembled structure due to the repulsion between the functional groups of CNTs originating from the overly close assembled structure. Despite the higher packing density of O-CNTY, this sample exhibited a much lower Raman peak shift value compared to those of the D- and S-CNTY samples, from 2688.9 cm^{-1} to 2683.0 cm^{-1} for R-CNTY. The G' peak shift of the Raman spectra indicated that the D- and S-CNTY samples have much tighter junctions [21] which are downshifted by up to -13.1 and -19.8 cm^{-1}, respectively, as shown in Fig. 5.7a. Grafting of p-PABA surrounding the CNT bundles effectively encouraged stronger lateral interaction and tightly roped CNTs. This was also confirmed through an examination of the dispersed state of the CNTYs in DMF (5 mg/l) by means of ultrasonication for 10 min. The size of each CNTY was measured, and the S-CNTYs were found to have the largest aggregated particles. The average sizes of the O-, D- and S-CNTY dispersions as measured by DLS were 536, 1076 and 1476 nm, respectively, and the O-CNTYs exhibited the most stable dispersion state, as shown in the insets of Fig. 5.7b-d. We assumed that the dispersion stability and size of the

samples under the given sonication energy indirectly implied the tightness of CNT bundling within the CNTY. In this regard, the poor dispersion and larger aggregate size of the S-CNTY may lead to the tightest CNT bundling among the tested samples.

In order to investigate the yarn architecture effect of CNTYs on the stress transfer efficiency, we conducted in situ Raman analysis during tensile loading was also performed. Raman band is strongly resonant under deformation of CNTs, and it is suggested that the downshift rate of G' peak implies load transfer efficiency between CNT with neighboring CNTs [10, 22, 23]. Load transfer efficiency is an important index to determine the strength of CNTY. The higher value means the more effective dissipation of the applied stress, leading to the deterred CNTY breakage by relieving the stress concentration. The small downshift rate in O-CNTY implies that O-CNTY has unfavorable chemical nature and microstructure for ensuring the efficient load-transfer pathway. On the other hands, the evident downshift of -32.3 cm^{-1}/% in S-CNTY indicates the highest load transfer efficiency among them, implying homogeneous stress distribution in CNTYs during tensile loading (Fig. 5.7e-h). We simplified the load-transfer system according to the bundling engineering as shown in Fig. 5.7i and j. While a CNT in the middle of CNT bundling is easily pulled out from the CNTs bundle in case of poor load transfer, a CNT within a CNT bundle, having a good load transfer efficiency, is pulled out with extension of neighboring CNTs by sharing applied load. Such evident difference in the Raman shift value depending on the CNTY architecture highlights the importance of bundling engineering for facilitating the substantial stress transfer to the overall CNTY.

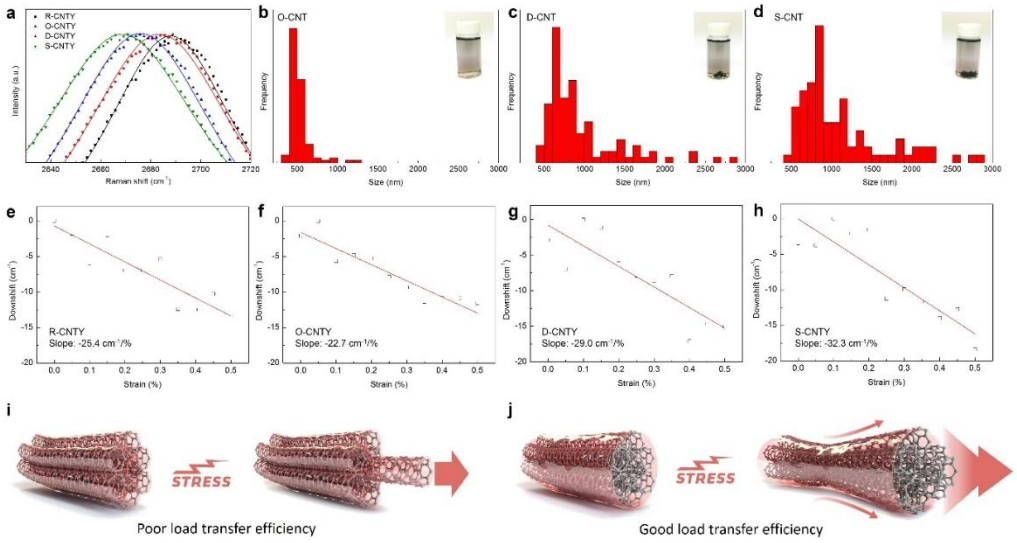

Fig. 5.7. (a) Raman spectra of G' peaks (symbols) with fitting using a Lorentzian function (solid lines) for raw and chemically modified CNTYs. (b-d) Size distribution of CNT aggregations depending on the functionalization method used. (e-h) Downshift rate of the G' peak of each CNTY during tensile loading according to an in-situ Raman analysis. Symbols and solid lines are the raw data and linear fittings, respectively. (i,j) Schematic representation of the deformation behavior of CNTYs exhibiting poor and good load transfer efficiency.

Fig. 5.8a shows representative specific-strength-strain curves of raw and functionalized CNTYs, and the average values of the mechanical properties are summarized in Table 5.1. O-CNTY shows slightly lower mechanical performance than R-CNTY, although O-CNTY has a much denser structure. With regard to the sliding mechanisms at the interface of the CNT-CNT junctions during deformation, the seemingly contradictory results can be explained by a lubricant effect by which the functional groups may act as a lubricant during the deformation process. Functional groups at the interfaces hampered the van der Waals interactions between the CNTs, weakening the tensile strength. The negative effect of functional groups on the mechanical performance of CNTYs was also demonstrated in other experimental and computational studies. Filleter et al. investigated the effects of functional groups on CNTs through MM and PBE/DZP simulations [24], and Im et al. [14] reported experimental results in which oxidized CNTY displayed lower mechanical performance than as-spun CNTY. Both results support the contention that non-crosslinked functional groups are disadvantageous for CNTY strengthening. On the other hand, for CNTYs densified by polyene grafting, D- and S-CNTY displayed higher mechanical performance levels above a specific strength of 2.0 GPa/(g cm^{-3}), with specific stiffness values as high as 90 GPa/(g cm^{-3}) as a result of the improved load transfer efficiency.

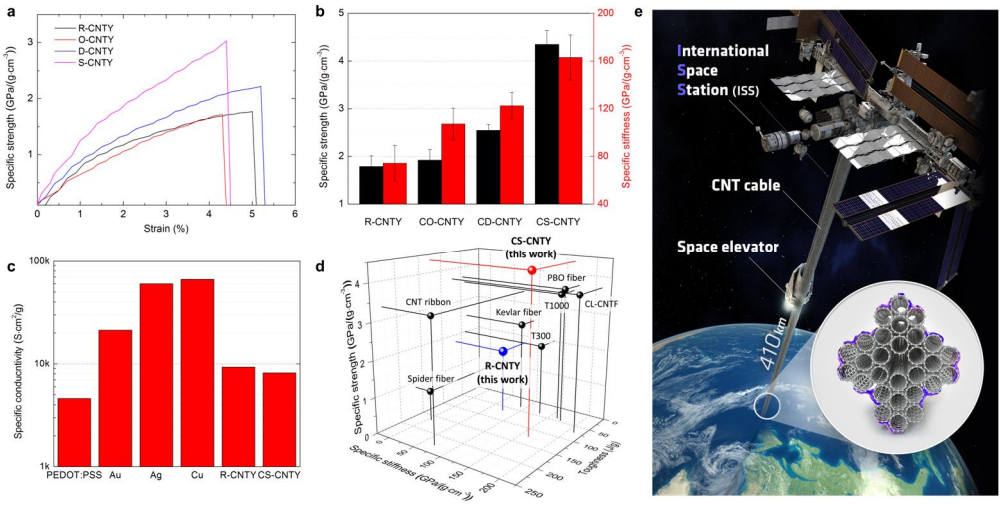

Fig. 5.8. (a) Specific strength and strain curves of raw and functionalized CNTYs. (b) Mechanical properties of each functionalized CNTY sample after crosslinking. (c, d) Comparison of the specific conductivity and mechanical properties with conducting polymer, metals and high-performance fibers. The carbon fiber data were obtained from www.torayca.com, and the toughness of each fiber was estimated using typical values. (e) Conceptual image of a CNT-cable-based space elevator from the earth to the ISS.

Table 5.1. Comparison of the specific strength, stiffness and toughness before and after the chemical modification process.

Sample	Specific strength (GPa/(g cm^{-3}))	Specific stiffness (GPa/(g cm^{-3}))	Toughness (J/g)
R-CNTY	1.79 ± 0.22	74.2 ± 15.0	65.2 ± 11.8
O-CNTY	1.74 ± 0.15	66.9 ± 7.3	50.9 ± 5.1
D-CNTY	2.23 ± 0.30	93.5 ± 11.4	77.5 ± 14.4
S-CNTY	2.98 ± 0.22	128.9 ± 14.4	87.7 ± 8.2

The crosslinking of the modified CNTYs was accessed. To examine the possibility of realizing a further improvement, CNTYs were subsequently crosslinked with PPD molecules (as denoted by the capital letter, C, added before the sample name for the crosslinked CNTYs). Crosslinking generally restricts the slippage between CNTs and improves the mechanical performance of CNTYs. To confirm the chemical crosslinking, XPS, FT-IR and GPC analyses were conducted. The N 1s peak was found in the XPS wide scan spectrum, and the atomic percentage of nitrogen tripled after crosslinking (Fig. 5.9). Furthermore, as clearly indicated from the FT-IR spectra, the representative peaks of imide bonds appeared at ~3340 cm^{-1}, ~1510 cm^{-1}, and 1610 cm^{-1}; these are assigned to -NH, -C-N, and N-C=O, respectively, after p-PABA crosslinking with PPD molecules, as shown in Fig. 5.10. The relative molecular weight of p-PABA increased nearly fivefold from 29203 to 156240 with a PDI of 1.24 as a result of the PPD crosslinking (Fig. 5.6).

As shown in Fig. 5.8b, crosslinking with PPD could very effectively enhance the strength and stiffness to 4.35 GPa/(g cm^{-3}) and 163 GPa/(g cm^{-3}), respectively. This superior result is even beyond the performance of commercialized high-performance fibers. The mechanical performance outcomes of other crosslinked CNTY, CO- and CD-CNTY are also presented in Fig. 5.8b. In addition, CS-CNTY has specific conductivity and toughness which are competitive with those of other conductive polymers, metals and commercial fibers (Figs. 5.8c-d). The internal structure of the junction as a basic component of the load-bearing elements consisted of tightly packed CNTs, and the outer layer of the CNT junction was chemically crosslinked through covalently grafted polymers, as illustrated in Fig. 5.2a. The unique structure with the chemically crosslinked polymer layer played a crucial role in disturbing the intra-CNT

bundle slippage which was governed by physical interaction via the van der Waals force.

This enable CS-CNTYs with a specific strength of 4.35 GPa/(g cm^{-3}) to endure weights equal to that of CNTY up to 440 km long. Therefore, CS-CNTY has sufficient potential to be used as a cable, a core part, of a space elevator traveling from the earth to the International Space Station (ISS), of which the altitude is about 410 km, as shown in Fig. 5.8e.

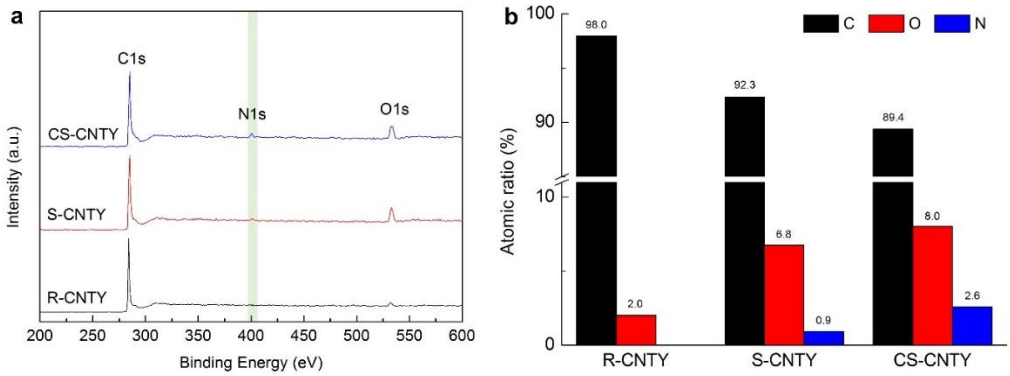

Fig. 5.9. (a) XPS wide spectra and (b) quantitative analyses resu신 of the R-, S- and CS-CNTYs.

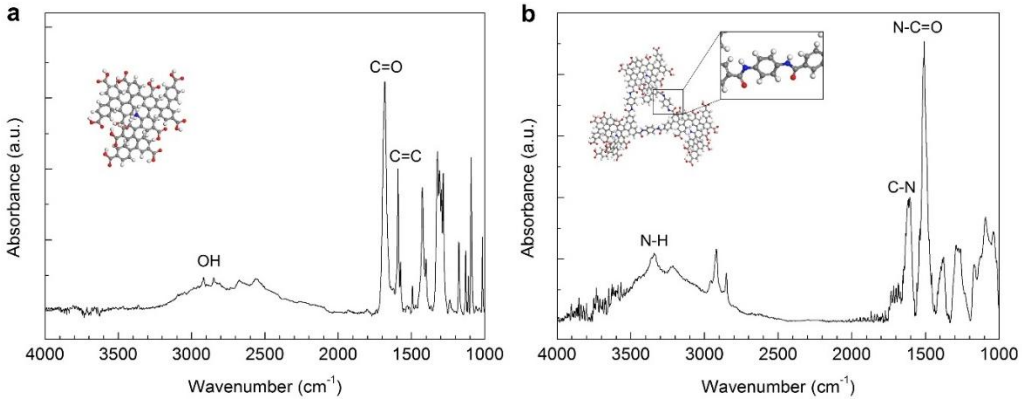

Fig. 5.10. FT-IR absorbance spectra of (a) p-PABA and (b) crosslinked p-PABA.

5.4 Conclusion

We readily fabricated structure-controlled CNTYs by utilizing a chemical reaction condition and the affinity differences of reaction media toward CNTs. DLS and in situ Raman peak shift results revealed that covalently grafted polymer chains on CNT junctions effectively enhanced the intra-CNT bundle interaction, and a further improvement of the load transfer efficiency was achieved by the crosslinking of polymers surrounding the CNT bundles. In comparison with commercial fibers such as carbon fiber and Kevlar, the resultant CS-CNTY showed remarkable mechanical performance. We expect that our unique approach to CNTY architecture engineering will enhance our understanding of the mechanical behavior of CNTY and extend its areas of application not only to high-strength materials but also to other applications such as conducting wire, sensors and wearable devices.

5.5 References

[1] Tsiolkovsky KE. Speculations between earth and sky. Moscow: Isd-vo AN-SSSR; 1895.

[2] Jung Y, Kim T, Park CR. Effect of polymer infiltration on structure and properties of carbon nanotube yarns. Carbon 2015, 88, 60-9.

[3] Li Y-L, Kinloch IA, Windle AH. Direct spinning of carbon nanotube fibers from chemical vapor deposition synthesis. Science 2004, 304, 276-8.

[4] Yu M-F, Lourie O, Dyer MJ, Moloni K, Kelly TF, Ruoff RS. Strength and breaking mechanism of multiwalled carbon nanotubes under tensile load. Science 2000, 287, 637-40.

[5] Yu MF, Files BS, Arepalli S, Ruoff RS. Tensile loading of ropes of single wall carbon nanotubes and their mechanical properties. Phys. Rev. Lett. 2000, 84, 5552-5.

[6] Wang JN, Luo XG, Wu T, Chen Y. High-strength carbon nanotube fibre-like ribbon with high ductility and high electrical conductivity. Nat. Commun. 2014, 5, 3848.

[7] Min J, Cai JY, Sridhar M, Easton CD, R. Gengenbach T, McDonnell J, et al. High performance carbon nanotube spun yarns from a crosslinked network. Carbon 2013, 52, 520-7.

[8] Behabtu N, Young CC, Tsentalovich DE, Kleinerman O, Wang X, Ma AWK, et al. Strong, light, multifunctional fibers of carbon nanotubes with ultrahigh conductivity. Science 2013, 339, 182-6.

[9] Di J, Hu D, Chen H, Yong Z, Chen M, Feng Z, et al. Ultrastrong, foldable, and highly conductive carbon nanotube film. ACS Nano 2012, 6, 5457-64.

[10] Ma W, Liu L, Zhang Z, Yang R, Liu G, Zhang T, et al. High-strength composite fibers: realizing true potential of carbon nanotubes in polymer matrix through continuous reticulate architecture and molecular level couplings. Nano Lett. 2009, 9, 2855-61.

[11] Lee J, Oh E, Kim T, Sa J-H, Lee S-H, Park J, et al. The influence of boundary layer on the growth kinetics of carbon nanotube forests. Carbon 2015, 93, 217-25.

[12] Zhang Q, Wang D-G, Huang J-Q, Zhou W-P, Luo G-H, Qian W-Z, et al. Dry spinning yarns from vertically aligned carbon nanotube arrays produced by an improved floating catalyst chemical vapor deposition method. Carbon 2010, 48, 2855-61.

[13] Ghemes A, Minami Y, Muramatsu J, Okada M, Mimura H, Inoue Y. Fabrication and mechanical properties of carbon nanotube yarns spun from ultra-long multi-walled carbon nanotube arrays. Carbon 2012, 50, 4579-87.

[14] Im Y-O, Lee S-H, Kim T, Park J, Lee J, Lee K-H. Utilization of carboxylic functional groups generated during purification of carbon nanotube fiber for its strength improvement. Appl. Surf. Sci. 2017, 392, 342-9.

[15] O'Brien NP, McCarthy MA, Curtin WA. Improved inter-tube coupling in CNT bundles through carbon ion irradiation. Carbon 2013, 51, 173-84.

[16] Park O-K, Choi H, Jeong H, Jung Y, Yu J, Lee JK, et al. High-modulus and strength carbon nanotube fibers using molecular cross-linking. Carbon 2017, 118 413-21.

[17] Kim SW, Kim T, Kim YS, Choi HS, Lim HJ, Yang SJ, et al. Surface modifications for the effective dispersion of carbon nanotubes in solvents and polymers. Carbon 2012, 50, 3-33.

[18] Cai JY, Min J, McDonnell J, Church JS, Easton CD, Humphries W, et al. An improved method for functionalisation of carbon nanotube spun yarns with aryldiazonium compounds. Carbon 2012, 50, 4655-62.

[19] Beese AM, Wei X, Sarkar S, Ramachandramoorthy R, Roenbeck MR, Moravsky A, et al. Key factors limiting carbon nanotube yarn strength: exploring processing-structure-property relationships. ACS Nano 2014, 8, 11454-66.

[20] Liu K, Sun Y, Lin X, Zhou R, Wang J, Fan S, et al. Scratch-resistant, highly conductive, and high-strength carbon nanotube-based composite yarns. ACS Nano 2010, 4, 5827-34.

[21] Heller DA, Barone PW, Swanson JP, Mayrhofer RM, Strano MS. Using Raman spectroscopy to elucidate the aggregation state of single-walled carbon nanotubes. J. Phys. Chem. B 2004, 108, 6905-9.

[22] Liu Z, Zhang J, Gao B. Raman spectroscopy of strained single-walled carbon nanotubes. Chem. Commun. 2009, 6902-18.

[23] Venkateswaran UD, Rao AM, Richter E, Menon M, Rinzler A, Smalley RE, et al. Probing the single-wall carbon nanotube bundle: Raman scattering under high pressure. Phys. Rev. B 1999, 59, 10928-34.

[24] Filleter T, Yockel S, Naraghi M, Paci JT, Compton OC, Mayes ML, et al. Experimental-computational study of shear interactions within double-walled carbon nanotube bundles. Nano Lett. 2012, 12, 732-42.

[25] Motta M, Moisala A, Kinloch IA, Windle AH. High performance fibres from 'Dog Bone' carbon nanotubes. Adv. Mater. 2007, 19, 1-3726.

[26] Naraghi M, Filleter T, Moravsky A, Locascio M, Loutfy RO, Espinosa HD. A multiscale study of high performance double-walled nanotube–polymer fibers. ACS Nano 2010, 4, 63-6476.

[27] Vollrath F, Knight DP. Liquid crystalline spinning of spider silk. Nature 2001, 410, 541.

Abstract in Korean

본 연구는 고강도 탄소나노튜브 섬유 제조를 위한 이론 및 실험적 접근을 통하여 기존의 고강도 섬유의 역학적 물성을 넘어서는 초고강도 탄소나노튜브 섬유 제조를 목적으로 하였다. 탄소나노튜브 고유의 높은 역학적 성질과 종횡비로 인하여 탄소섬유와 같은 기존의 고강도 섬유 물성을 넘어서는 초고강도 탄소나노튜브 섬유를 제조하고자 하는 노력이 지난 수십년 동안 지속되어왔다. 그 결과 2000년대 초반부터 지금까지 다양한 탄소나노튜브 섬유 제조방법이 소개되었으며, 현재 이러한 방법을 통해 탄소나노튜브 섬유의 연속적 생산이 가능하게 되었다. 그럼에도 불구하고 여전히 탄소나노튜브 섬유에서 탄소나노튜브 한 가닥이 갖는 우수한 역학적 특성이 발현되지 못하고있다. 이러한 한계를 극복하고자 최근에 탄소나노튜브 섬유의 역학적 강도를 향상시키는 다양한 방법들이 제안되어왔다. 탄소나노튜브는 나노튜브의 길이, 벽수, 직경 등의 나노구조에 따라서 다양한 물성을 갖는다. 또한 집합체 내에서 탄소나노튜브 미세구조는 집합체의 역학적, 전기적 성질 등에 밀접하게 연관되어있다. 따라서 초고강도 탄소나노튜브 섬유를 제조하기 위해서는

탄소나노튜브의 나노구조와 집합체 내에서의 탄소나노튜브 미세구조를 제어하는 것이 가장 큰 이슈이다.

1장에서는 탄소나노튜브 섬유의 간략한 설명과 섬유의 역학적 성질에 영향을 미치는 관련 인자들을 도출하였으며, 역학적 성질을 향상시키고자 진행된 최근의 연구들을 종합하고 아직 해결되지 못한 이슈들과 해결방법을 모색하여 본 연구의 목적을 설명하였다.

2장에서는 탄소나노튜브 섬유의 파단 메커니즘을 바탕으로 이론적으로 나노구조 및 미세구조와 탄소나노튜브 섬유 강도의 상관관계를 도출하였다. 먼저 섬유를 구성하는 가장 기본 구성요소인 탄소나노튜브의 나노구조와 역학적 물성 간의 상관관계를 연구하고, 다음 단계에서는 개별의 탄소나노튜브가 집합체를 형성할 때 미세구조가 섬유의 강도에 미치는 상관관계를 이론적으로 도출하였다.

3장과 4장에서는 2장에서 도출된 탄소나노튜브의 나노구조와 미세구조의 구조적 인자가 섬유의 강도에 미치는 영향을 실험적으로 확인하였으며, 실제 다른 나노구조를 갖는 탄소나노튜브로 이루어진 섬유를 제조하여 탄소나노튜브의 나노구조가 탄소나노튜브 섬유의 역학적 성질이 미치는

영향을 실험적으로 확인하였다. 또한 고분자 사슬이 탄소나노튜브 섬유의 내부구조에 미치는 영향과 탄소나노튜브 섬유 강도 향상에 미치는 영향을 실험적으로 관찰하였다.

마지막으로 5장에서는 앞선 장에서 도출된 이론과 실험적 접근을 바탕으로 나노 구조 및 미세구조가 최적화된 탄소나노튜브 섬유를 기반으로 가교결합을 통해서 최종적으로 기존의 고강도 섬유의 역학적 성질을 능가하는 초고강도 탄소나노튜브 섬유를 성공적으로 제조하였다. 차후 연구에서 탄소나노튜브의 합성법을 개선함으로써 더 높은 역학적 성능을 갖는 탄소나노튜브 섬유의 제조가 가능 할 것으로 예측된다.

주요어: 탄소나노튜브, 섬유, 초고강도, 미세구조, 나노구조, 역학적 성질, 구조재료, 가교결합

학번: 2013-30186